AN EXPERIMENTAL INVESTIGATION INTO RESPONSE DISTRIBUTION IN COUPLED PLATES SYSTEMS.

BY

Uri Shapiro D.I.C.

Dissertation submitted to the
University of Warwick
for the award of the degree of
Doctor of Philosophy.

Coventry 1971

ABSTRACT.

In this thesis, response distribution in a class of conservatively coupled plates system is investigated experimentally. The ratio of the space-average, time-maximum response of the coupled plates is shown to be proportional to an empiric expression of the space-average time-maximum rotary and transverse receptances, and the time-maximum receptance of the point where the disturbing force is applied, which are parameters open to measurement.

The amount of error of estimating response ratio through applying the expression is analysed and found to be small.

A brief survey of potential applications of the results of this project to practical structures follows, together with proposed additional work to extend the validity and applicability of the findings.

Experimental techniques and apparatus are discussed and described in great detail. An innovation in the experimental set-up is associated with the construction of non-contacting transducer, fitted to a scanning rig, employed to detect response distribution in panel type vibrating elements. Since the experimental apparatus proved useful for the purpose of the project, further work is suggested in order to improve its versatility and develop the rig into an industrial tool, to fulfil a much needed function in dynamic testing.

It is suggested that the methods developed in the thesis to estimate response distribution experimentally, have some advantages over present day methods, which is demonstrated by comparing the procedures and some of the basic assumptions involved.

Acknowledgement.

I take pleasure to acknowledge the guidance and assistance given to me by Dr. V. Marples of the University of Warwick.

Thanks are due to the technical staff of the School of Engineering Science for their help whenever requested.

The financial contribution of the Science Research council towards the construction of the rig and purchase of the instrumentation is acknowledged with gratitude.

I wish to thank my wife Ophira for her encouragement and for typing the thesis.

Table of contents.

DESCRIPTION OF THESIS WORK.

The work reported in this thesis is primarily concerned with the transmission of structure-borne vibrational energy. The investigation is mainly experimental, centering on the response distribution in a pair of conservatively coupled structural elements.

The ultimate gaol is to establish the response distribution in a system of 2 coupled elements, to show that the distribution is proportional to a coupling parameter which is open to measurement, and to obtain the characteristics of that relationship. Determination of the relationship between the coupling parameter and response ratio facilitates assessment of energy distribution in a practical situation by using comparatively simple means.

The thesis opens in section 1 with an introduction of the problem of the flow of vibrational energy in complex structures. A short review of previous investigations related to that topic follows. The review tends to focus on the part of work which is directly related to the topic of this thesis, namely the flow of vibrational energy through the coupling. The second part of the section presents the mathematical formulation of the flow and sharing of energy which form the basis for this research.

In section 2 of the thesis, experimental techniques are discussed. A chart is drawn to aid the planning (Fig 2) and the ways to attain the parameters outlined. A scheme to detect and appreciate errors which may be introduced into the results is worked out.

Section 3 is a self-contained part of the thesis which deals with the experimental apparatus. An experimental rig, essentially a measuring device, was constructed to detect response distribution in a plate element.

A plate was chosen for a specimen because it is of distributed mass and elasticity, yet which lends itself to both prediction and measurement of the dynamic parameters.
The experimental set-up is specified, the mechanical construction and signal network described and evaluated in the light of preliminary results.

Records obtained in a series of experiments are presented and discussed in section 4.
The analysis is greatly aided by an analog 2-degree-of-freedom model developed in appendix 6 I. Errors in the records of the response parameters are examined.
Energy distribution is computed from the experimental data for some selected normal modes.

In section 5, conclusions are presented, which fall into two main categories. Those related to response (and hence energy) distribution, and those related to the experimental set-up.

It was shown that response ratio of a conservatively coupled plate system, sinusoidally excited, is proportional to an empiric expression of coupling and input receptance.
Finding and techniques employed in this work are compared to previous work in the field, and some further research is suggested.

Several different items are contained in the appendix, (section 6), some of which are off the main interest of the thesis.
A discussion of plate vibration with particular reference to experimental data on coupled modes and the 2 types of coupling tested in the course of the work.
The scanning rig usefulness is reviewed in connection with the variety of applications it had for the purpose of the project.

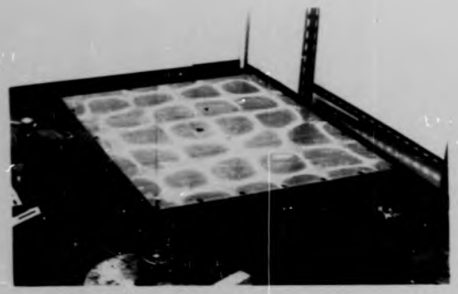

b) Nodal pattern

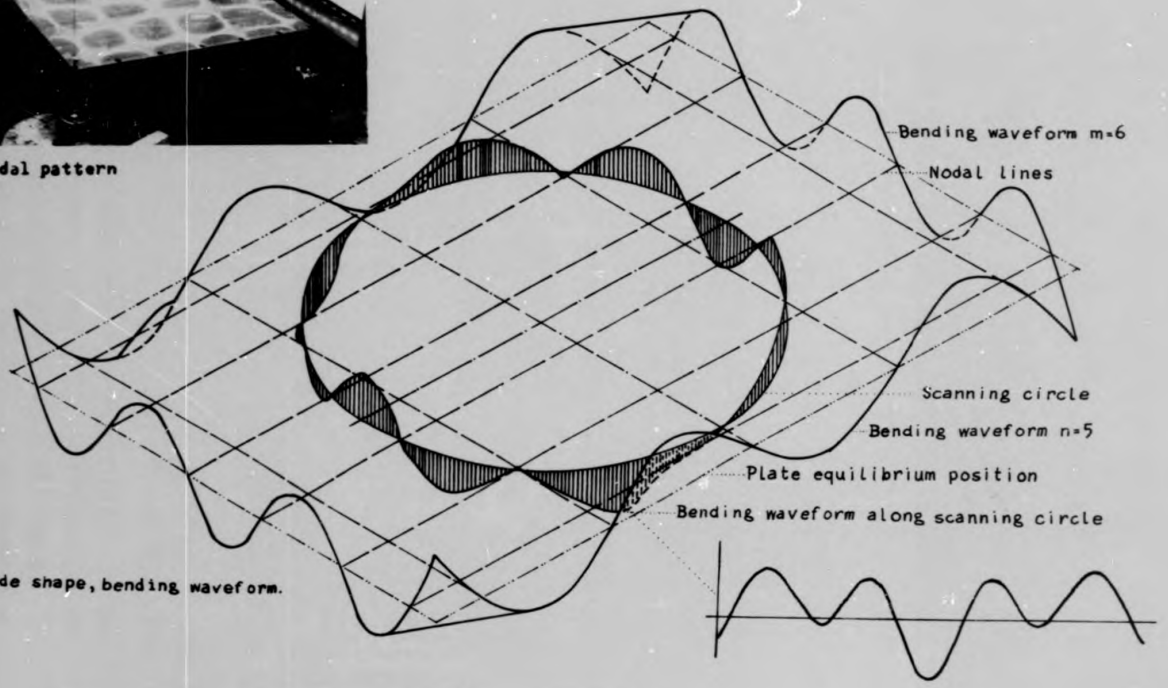

a) Mode shape, bending waveform.

Fig 1. A display of mode 6x5 showing mode shape, nodal pattern, and the bending waveform along the circle of scanning.

1. INTRODUCTION.

The trend in recent engineering development towards lighter, more complex and rigid structures, together with more powerful propulsion systems has resulted in increased noise and vibration. This is due to the combined effect of reduced damping in structural members and joints and to higher levels of vibration excitation.

Dynamically a structure can be described as consisting of a chain of structural elements of different types linked together in various ways forming a path for the transmission of vibrational energy. Some components receive their excitation directly from a mechanical source or from the environment, others indirectly through transmission, refferred to as structure-borne sound.

Hence all parts of the structure can be excited, even those remote from the sources. Panels and plate elements play a particularly important role in that when excited, they couple well with the surrounding fluid, radiate noise and conversly are relatively highly susceptible to excitation to vibration by incident waves.

I.Review of previous work.

One way to tackle this problem is to reduce the flow of vibrational energy through the structure in order to isolate the source of energy from the receiving parts. Several techniques have been attempted. Here we mention a few of them. Mizutani (1) used small vibration generators to supress some of the vertical modes of vibration of a ships' hull. In his theoretical study he assumed the hull and superstructure to have dynamic characteristics similar to that of a beam. Adams investigated the effect of inserting parts made of a

damping material, of the appropriate mechanical properties, on the dynamics of a steel plate (2). The effectiveness of the treatment depends entirely on the position of the inserts relative to the vibrational mode shape.

Another method is to reduce the flow of the structure-borne sound through the coupling which links together constituent elements. This involves a study of energy-sharing between coupled subsystems.

The simplest subsystem to study comprises a pair of coupled structural components, one of which is directly excited, energy passing through the coupling to the other one, it thus being set into vibration.

This concept was utilized (3) to estimate vibration transmission of the spacecraft Mariner '69'. The craft was assumed to be divided into 4 subsystems coupled together. A set of 2 coupled subsystems was studied in turn.

The methods used in the investigation, which have been developed during the last decade, were derived from the theory of room acoustics, and became known as the statistical energy approach. In this approach modal energy is taken as the primary variable, and then coupled oscillator theory is applied to calculate the flow of energy between coupled structures. For the latter step to hold, it was assumed that the vibration characteristics of each substructure are quite similar to the vibration characteristics of the substructure when it is isolated from the other substructure.

Lyon and Eichler first used the statistical energy method to study the response of coupled structures to random excitation (5). They computed the energy flow in a system connected by a small linear conservative coupling.(i.e. That neither generates nor dissipates energy). They showed that the time-average flow is proportional to the difference in the time-

average energy stored in the subsystems, and that energy flows in the direction of the energy gradient. They concluded that such a coupling tends to equipart the energy.
In this approach, the flow of energy from one subsystem to the other is governed by two kinds of loss factors.

In a study of absorption of energy in plates, Heckl suggested to group losses of energy into distributed and localized damping (4).
Distributed damping is related to losses of the separate subsystem through hysteresis in the material, sound emission, and air pumping. Localized damping is associated with losses of energy through the boundary owing to coupling to another element - the coupling loss factor.

Scharton (6) proved the time-average power flow between randomly excited coupled oscillators is proportional to the time-average energy difference of the oscillators even for strong coupling.
But this proof was not extended to coupled structures.
He focused on the conceptual difficulty to devise a technique to divide an elastic system into coupled subsystems in such a manner that the motion of the coupled structures can be described in terms of the coupled structure modes.
One of the great difficulties in applying the statistical energy method to predict response levels of coupled structural elements is to determine the loss factors.

Lyon and Scharton reported detailed investigations of the ways to compute the coupling loss factor (7) and Ungar reviewed the state of art (8) in 1966.
Scharton computed a proportionality factor, the coupling rate factor, in terms of 9 parameters. 3 represent each subsystem in the coupled but blocked situation (i.e. such that one subsystem is allowed to vibrate, while the other is held fixed), and 3 coupling parameters.

It is shown analytically and experimentally, that for sine excitation the coupling can be negative and energy does not always flow in the direction of the energy gradient. Thus the tendency towards equipartitioning of energy does not exist in this case. Ungar stated categorically that the coupling loss factor can be determined only by experiment, through testing the structures in the coupled and uncoupled situations.

Rosselli attempted to measure the transmission of random vibration between conservatively coupled aluminium plates (10). Measured values were compared with a theoretical prediction, using the statistical energy approach. Loss factors were determined in experiment by decay rate technique.
The poor agreement between computed and measured energy flow seemed to stem partly from errors inherent in the experimental techniques.

Experimental work carried out alongside the analysis show a significant amount of divergence from the theoretical predictions of energy, or response, distribution. This was attributed mainly to the drawbacks associated with an assessment of the coupling loss factor in particular.
To ease the problem, it was suggested by Ungar (8) to define loss factors in terms of quantities of energy instead of viscous damping. The loss factor being defined in relation to energy dissipated in an element, and the coupling loss factor, to energy flowing to the other element through the coupling.

This problem was tackled recently by Newland (9) from a different angle. A different coupling rate factor was proposed which is related to a new parameter, the rate of shift of the modal frequency of an oscillator as a result of the presence of a coupling. Hence power flow is proportional to the difference in the time-average modal

energies, the average modal densities, and the average shift of the natural frequencies of the oscillators.
Among other conditions, this derivation is valid for lightly damped oscillators, loosely coupled, where the bandwidth of interest is small as compared to the centre frequency, but still contains many oscillators.
In ordinary metal structures this is likely to occur in the region of the higher frequencies.
As yet this theoretical development has not been substantiated experimentally to examine its usefulness.

II. Energy distribution.

When sinusoidal excitation is applied to a pair of coupled elements at a natural frequency of the coupled system, the elements vibrate in a normal mode of motion. In the steady state each element stores energy, kinetic and potential, in relative proportions varying with time, their maxima occuring at 90 degrees phase difference, are equal.
We define stored energy as that associated with the position and velocity coordinates of motion of a particle.
Then the kinetic and potential energies can be expressed in terms of the generalized coordinates of position q and velocity q,

$$(1.1)\quad T_{kin} = {}^1/_2\, M(\dot{q})^2 \qquad T_{pot} = {}^1/_2\, kq^2$$

The motion of the particle is associated with losses of energy through dissipation in the material, sound radiation, and air pumping. We group those kinds of losses into the damping coefficient C, as proposed by Heckl. Then, the energy lost in the element is,

$$(1.2)\quad \Delta T = {}^1/_2\, C(\dot{q})^2$$

The amount of energy stored in an element depends, therefore, upon the quantity of energy $T_{in} = \Delta T$ being generated at the source and delivered to that element.
When another element is coupled to that element, it can receive the energy to maintain its motion through the directly excited element and the coupling only.
Now the amount of energy generated in the source and passed to the conservatively coupled system, in the steady state, becomes

$$(1.3)\quad T_{in} = \Delta T_1 + \Delta T_2$$

This amount is fed into the element which is directly excited, henceforth called the primary element, of which an amount ΔT_2 flows through the coupling to the receiving element.
From the view-point of the primary element ΔT_2 is lost by the provision of a coupling.

Now one can think of "balance of energy" where the sum total of energy needed to maintain the motion of a set of coupled elements, in the steady state, is that flowing from the generator into the vibrating system,

$$T_{in} = \sum_{i=1}^{n} \Delta T_i$$

where losses in joints are included through being counted as elements. From eq'n 1.2 it is apparent that the losses are proportional to velocity, so we prefer to deal with kinetic energy which is proportional to the same parameter.

Sharing of energy is defined as the ratio of modal kinetic energy stored in the 2 coupled elements,

$$T_1/T_2 = \frac{M_1(\dot{q}_1)^2}{M_2(\dot{q}_2)^2}$$

Setting (1.4) $\mu = M_1/M_2$ and bearing in mind that $q = q\omega$ we have,

$$T_1/T_2 = \mu \frac{(q_1\omega_1)^2}{(q_2\omega_2)^2}$$

and since both elements in the coupled system oscillate at the same frequency we finally end up with,

$$(1.5) \quad T_1/T_2 = \mu (q_1/q_2)^2$$

The energy flowing from the generator via the primary element and the coupling into the receiving element ΔT_2 is referred to as the flow of energy and is the only quantity of energy passing through the coupling

$$(1.6) \quad \Delta T_2 = {}^1/_2 \, C_2(q_2\omega)^2$$

From the aforesaid it is clear that the loss of energy in each element is proportional to the motion of that element. So we may express the flow of energy as a function of quantities of energy in ratio form, which may prove more practical in experimental work. Rearranging eq'n 1.3 we have,

$$(1.7) \quad \Delta T_2 = \frac{T_{in}}{1+\Delta T_1/\Delta T_2}$$

For practical reasons we wish to express the ratio $\Delta T_1/\Delta T_2$ in terms of measurable parameters.

$$(1.8) \quad \Delta T_1/\Delta T_2 = \frac{C_1(q_1)^2}{C_2(q_2)^2}$$

Substituting eq'n 1.8 into 1.7, the energy flow becomes,

$$(1.9) \quad \Delta T_2 = \frac{T_{in}}{1+C_1q_1^2/C_2q_2^2}$$

2. EXPERIMENTAL TECHNIQUES DISCUSSION.

Planning of experimental techniques is guided by the requirement of parameters to compute eq'ns 1.5 and 1.9 governing energy distribution, by the search for parameters representing coupling response, and by the methods adopted to detect and assess errors in the results.

I. Normal modes

A plate, being of distributed mass and elasticity, is a multi-mode system. Mode shapes and modal parameters depend on material properties, body geometry, boundary conditions and frequency of excitation.

A plate element subjected to transverse sinusoidal excitation at a natural frequency, vibrates in a normal mode. The motion of each particle of the element consists of a rotary component and a displacement component perpendicular to the plane of the plate which are associated with bending waves in the plate. Points of zero perpendicular motion, are of maximum rotary motion, and are referred to as Nodes.

Mapping nodes of a normal mode yields a pattern related to the mode which is uniquely representative of that particular mode. Hence a nodal pattern can serve to identify modes.

Fig 1b exhibits a nodal pattern of a normal mode. The pattern was obtained by sprinkling dry sand on a rectangular plate, freely suspended, sinusoidally excited at a modal frequency. Since nodes are points of no transverse motion, (In practice it would be more precise to say: least motion) the sand tends to accumulate along the nodes. The nodal pattern thus obtained is known as Chladni Pattern.

To a first approximation bending waveforms of vibrating plates can be assumed to be similar to those of vibrating beams.

The waveform of a vibrating plate will be the product of the characteristic beam functions for two vibrating beams with the appropriate end conditions. Thus for a rectangular plate having 4 free edges the approximate waveform assumed will be the product of the characteristic functions of two beams with free ends. This is illustrated in Fig 1a by a drawing of the mode of vibration showing the waveforms of the characteristic beam functions along the edges. Opposite edges have the same waveform.

Assuming a vibrational mode shape for a given plate and the boundary conditions, it is possible to calculate the modal frequency and predict response distribution in nondimensional units as has been described by Warburton (11) .

A description of an elastic, multi-mode element essentially incorporates information on the modal density. A metal specimen possesses a comparatively high modal density. Hence modes are often close together (see Fig 12) causing an off resonance excitation of modes adjacent to the normal mode of interest. In the vibrational mode shape this results in extraneous motion being superimposed on the normal mode motion and consequently in a nodal pattern, different from that predicted.

In normal resonance testing to determine natural frequencies and other modal parameters the method suggested by Kennedy and Pancu (12) and evaluated by Bishop and Pendered (13) is admirable. This method requires accurate measurement of the phase between the disturbing force and the vibrational point-response and leads to separate the pure mode part of the motion from the off-resonant contribution. For the purpose of studying energy distribution separation of modal components is not necessary. Moreover, such a separation will introduce an appreciable error into the results because the off-resonant motion stores and dissipates energy as well as pure mode motion.

However it is then necessary to speak in terms of the resonant

state and frequency being defined as that state and frequency at which maximum displacement response per unit force input occurs .

Modal parameters are defined in such a manner that the peak amplitude plot yields damping ratio and resonant frequency.

It has been assumed by investigators of energy distribution in coupled structures that the mode of vibration of each substructure is similar to the mode of vibration of that substructure when it is not coupled. Hence it is possible to divide any structure into isolated substructures and then to couple together modes of these substructures to obtain formulation of the systems' dynamics (e.g. see ref. 6 p. 53).

Coupled-mode representation of coupled structure vibration is a crucial question in this work since the philosophy of planning the experimental techniques is strongly based on the presence of coupled normal modes in the coupled plate specimen. Evidently, identifying pairs of modes, coupled together in the vibrating coupled plates is essentially the basis of our technique through being employed to determine response distribution in each plate.

In view of the aforesaid and because the coupled-mode assumption has never been verified, we prove its validity by experiment as described in section 3 and analysed in section 6 II. The record displayed in Fig 23 is an explicit indication to that effect.

The procedure to obtain the dynamic mass and damping coefficient of the subsystems' modes involves testing each of the coupled plates being uncoupled in order to determine those parameters without interference owing to interaction with the coupled element. Validity of this process is subject to the assumption that the modal damping and mass of the uncoupled modes remain approximately unchanged by the provision of the coupling.

This is true if the mode shapes and bending waveforms of the coupled and uncoupled subsystems are similar, however distorted. Clearly, while the stiffness, and hence resonant frequency, are changed due to edge restraint applied by the impedance of the other plate owing to the coupling - damping and mass distribution are expected to change only slightly, and only in the immediate vicinity of the coupling. Unless the condition of similar mode shape is met, error is introduced into this latter statement about damping and mass distribution.

Ways and means to detect and assess the error are dealt with later in this section.

II. Response distribution

Next, we examine the plate response distribution. In section 1, stored energy was defined in relation to transverse motion. The effect of rotary motion on the calculation of modal frequencies of beams is given by Timoshenko (p. 334 of ref. 14). A similar calculation provides an idea of the orders of magnitudes of errors involved in energy considerations, by ignoring rotary inertia effects. Thus the correction of a calculated natural frequency of the 10th mode of a beam, 26" long and 1/8" x1" cross section, is .63%, which is insignificant. Although the 10th beam mode is well above the frequency region of our interest, it is important to bear in mind that the errors due to neglecting that effect become significant in higher modes when the element is subdivided by the nodal pattern into comparatively small portions. Then not only the error grows but the nodal lines become closer and closer, until it invalidates the assumption that the length of the element is large as compared to the thickness dimension.

For a plate vibration where transverse response is distributed in a manner described by a product of the characteristic beam

functions and rotary motion neglected, the energy is stored and dissipated unevenly over the plate area. Thus we shall refer henceforth to time-maximum, space-average energy distribution. Consequently the generalized coordinate q is replaced by the coordinate of transverse position X, and velocity $\dot{X}$.

This step greatly simplifies the task to obtain response parameters, at the cost of a small amount of error.

The time-maximum displacement response at a point (x,y) on a plate vibrating in a normal mode is given by,

$$(2.1)\quad X(x,y) = \theta(x)\phi(y)$$

where $\theta(x)$ and $\phi(y)$ are the characteristic beam functions in x and y directions respectively.

Now the space-average time-maximum plate displacement per nondimensional unit response can be obtained,

$$(2.2)\quad \tilde{X} = Xrms = \left[\frac{1}{hl}\int_0^h\int_0^l X^2\,(x,y)\,dx\,dy\right]^{1/2}$$

where h and l are width and length of the plate.

III. Modal parameters.

Damping coeficient of vibrating systems can be determined from a record of the exponential decay. But it is difficult if not impossible to use free decay rate technique to determine the damping factor of multi-mode systems such as plates, because many modes would be excited and it would be extremely difficult to determine the response in any single mode and to identify that mode. The extent of the problem can be estimated from the modal density of the plot in Fig 12.

It was decided therefore to employ steady state techniques.

For an uncoupled plate, vibrating in a normal mode, the amount

of the space-average, time-maximum energy dissipated in the mode, is the time-maximum energy input from the vibration generator. namely,

$$FX_{in}\omega = {}^1/_2 CX^2 = {}^1/_2 C(\bar{X}\omega)^2$$

The modal damping, in terms of f_n the resonant frequency,

$$(2.3)\quad C = \frac{F\,X_{in}}{\pi f_n \bar{X}^2}$$

which is an approximation, defining modal damping in a plate element. The ratio of modal damping as required for eq'n 1.9 can be obtained from the response of the separate plates, each vibrating in the same normal mode as that of the respective coupled plate. This statement amounts to $C_1/C_2 = C_a/C_b$ where the subscripts 1 and 2 denoting the coupled plates, correspond to a and b denoting the same plates in the uncoupled state. Then modal damping ratio becomes,

$$(2.4)\quad C_1/C_2 = \frac{F_a X_{in,a}}{f_{n,a}} \quad \frac{f_{n,b}}{F_b X_{in,b}} \quad \left(\frac{\bar{X}_b}{\bar{X}_a}\right)^2$$

A plate vibrating in a normal mode can be represented by a spring-mass-dashpot system where the coordinate of motion of the mass represents an equivalent of the response distribution of the plate element $\bar{X}$. Similarly the distributed mass, stiffness and damping are represented by equivalent M,k and C respectively, of the single-degree-of-freedom damped system. Thus modal mass can be expressed in terms of modal damping, resonant frequency, and the magnification factor Q. The ratio of the modal mass of the coupled modes is given by,

$$(2.5)\quad \mu = \frac{C_a f_{n,b}}{C_b f_{n,a}} \left[\frac{4Q_a^2-1}{4Q_b^2-1}\right]^{1/2}$$

A straightforward implication of eq'n 2.2 in that $\bar{X}$ is obtained by integrating the plate response point by point. This would be an impractical proposition, and costly. So a technique was devised, consisting of measurement and computation, which is based on the concept of plates vibrating in normal modes.
In this technique we record the bending waveform of the plate vibrating in a normal mode, along an arbitrarily pre-determined part of the plate, a circle of a fixed diameter and centre. Such a record is uniquely representative of the vibrational mode. The mode shape, nodal pattern, and the bending waveform along the circle of a given mode are shown in Fig 1.
The use of the record is twofold, as outlined below. As stated earlier, given the situation and the mode shape, it is possible to construct the bending waveform theoretically. In this work we used the charactristic beam functions given by Warburton (11), to construct the bending waveforms along a circle for the same conditions (plate, radius, centre, boundaries) for all the modes included in the frequency band of interest.
Thus we had a catalogue of bending waveforms for each of the plates. Comparing the recorded bending waveform to the appropriate catalogue yields the identification of the mode.
A space-average displacement of the complete plate $\bar{X}_p$ per unit nondimensional response, is calculated from eq'n 2.2.
Further, a similar average of the displacement along the circle $\bar{X}_t$ being the average of the displacement of the theoretical bending waveform, obtained. (See Fig 29).
Since it is possible to measure the rms value of the recorded bending waveform mentioned above, an experimental parameter $\bar{X}_m$, corresponding to the theoretical parameter $\bar{X}_t$ was determined.

The recorded and the theoretically constructed bending waveforms of the respective normal modes are expected to appear identical in their shape, differing in scale only. This is

illustrated in Fig 11.
It follows that the ratio of the recorded and the computed averages, yields a factor N, referred to in the thesis as the normalizing factor.

$$(2.6)\quad N = \bar{X}_m / \bar{X}_t$$

The factor N when accommodating a difference in scale only, that is when there appears to be a good agreement between the waveforms, can be thought of as a dimensional factor used to apply dimensions to the factor $\bar{X}_p$.

Now the expression for the space-average time-maximum displacement response of a plate, used in eq'n 2.3 and 2.4,

$$(2.7)\quad \bar{X} = \bar{X}_p N = \bar{X}_p(\bar{X}_m/\bar{X}_t)$$

IV. Coupling parameters

For any given set of 2 subsystems which are subsequently coupled, the dynamic behaviour of the coupled system is governed by the coupling conditions.
An assessment of the response distribution in that system, other than by direct measurement, requires that coupling conditions be known.
In elastic systems it would be extremely difficult and experimentally impossible to determine the coupling stiffness, in the case of an elastic coupling, owing to the interaction between the constituent coupled modes.
The method suggested hitherto, described in section 1, suffers from various drawbacks and need to decouple a given coupled system to obtain the necessary parameters.

It seems that, as an experimental technique, a more practical proposition would be to represent coupling conditions through

its motion parameters which are open to measurement.
We choose to observe the motion associated with those bending waves at right angles to the centre line of the coupling. Bending waves of the 2 coupled modes are joined at the point of coupling, resulting in superposition of their motion at that point. Hence the motion at the coupling, represented by the amplitude and slope of the bending wave, at that point, varies along the coupling, with the variation of the waves superimposed on each other.
Exception occurs, in the particular case, when the spacing between nodal lines on both sides of the coupling (measured along the centre line of the coupling), is identical, as in Fig 23.
This particular case is illustrated in Fig 13b.
Hence slope and amplitude at any point in the coupling are representative of the coupling motion.
A corrected and somewhat more detailed analysis of the dynamics of the coupling, derived from experimental data is given in section 6 III.

Coupling response is measured at a pre-determined set of points along its centre line. Amplitude X_c and slope ϕ_c are recorded simultaneously at each point.
Records of parameters of the coupling response of the normal modes that are tested, are subsequently compared against the recorded parameters of response distribution of the respective modes.

V. Errors

Several 'watch-dog' measures are taken in this project, to ensure good control over possible sources of errors.

The validity of eq'n 2.6 and hence 2.7 was subject to an acceptable agreement between the recorded and theoretically constructed bending waveforms along the given circle. This implies that the vibrational mode shape, present in the plate

A	Area under bending waveform.
a,b	Subscript denoting the separate plates 1 and 2 respectively.
c	Subscript denoting coupling.
C	Damping coefficient.
F	Amplitude of disturbing force.
f	Circular frequency.
h,l	Higher and lower frequencies corresponding to half power point.
in	Subscript denoting point of forcing.
m,t	Subscript denoting measured and theoretical values.
n	Subscript denoting resonant.
M	Mass.
N	Normalising factor.
Q	Magnification factor.
r	Radius, or subscript denoting radius of scanning.
(r,θ)	Notation of a bending waveform.
S_d	Factor of error due to drift.
S_{fr}	Factor of error due to flanking energy.
S_m	Factor of difference between measured and calculated response ratio.
S_r	Factor of error due to poor agreement between bending waveforms.
T	Energy stored in a vibrating element.
ΔT	Energy dissipated in a vibrating element.

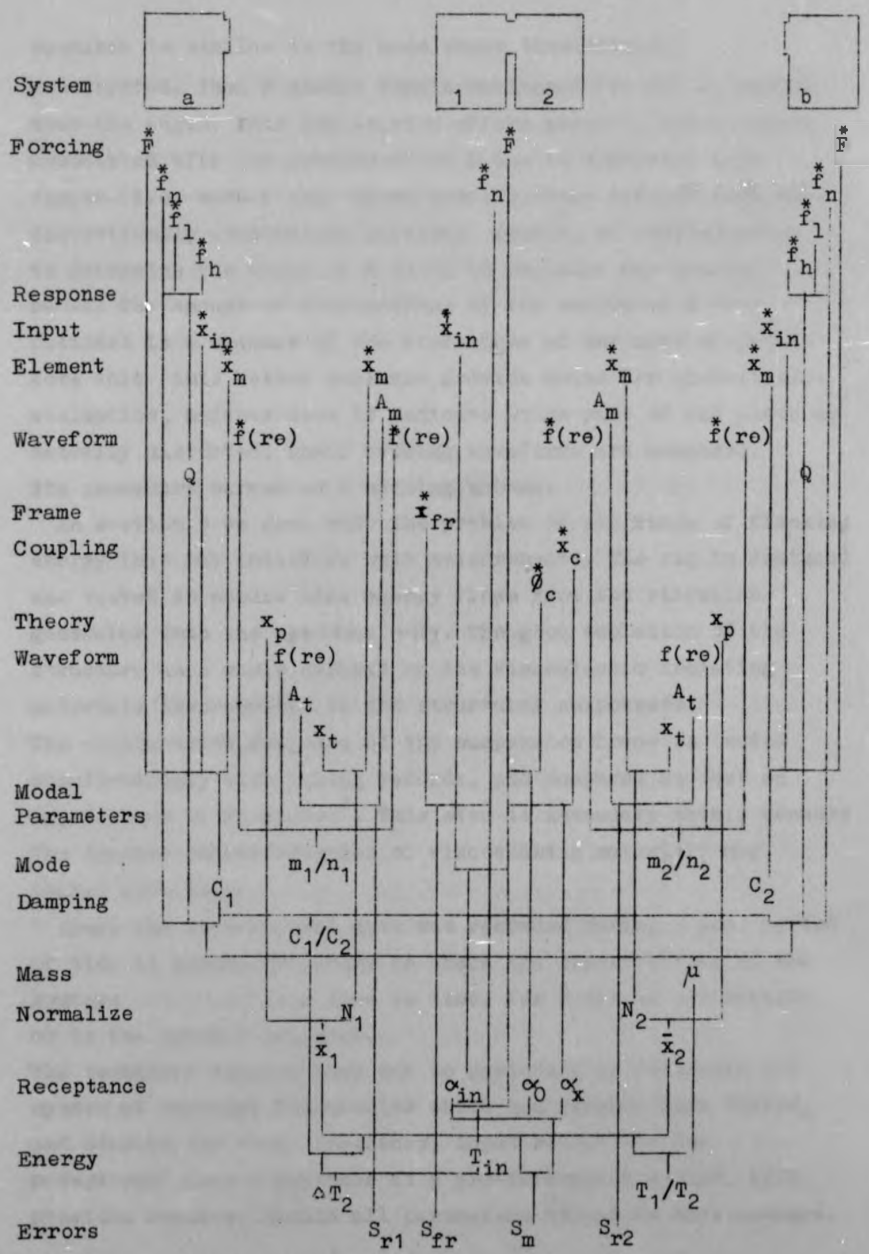

Fig 2. Chart of planning experimental techniques.

specimen is similar to the mode shape theoretically constructed. Then N should remain unchanged for all r, except near the edges. This implication offers means to detect error associated with the assessment of N due to distorted mode shapes.(i.e. such a mode whose nodal pattern differs from the theoretically constructed pattern). Testing of coupled-modes to determine the value of N is to be repeated for several radii. The amount of fluctuations of the values of N thus obtained is a measure of the distortion of the mode shape. Note that this method does not provide means for quantitative evaluation, neither does it indicate which part of the plate is actually distorted, until bending waveforms are compared. The procedure serves as a warning scheme.

In section 3 we deal with the problem of all kinds of flanking energy that may interfere with measurements. The rig is designed and tested to ensure that energy flows from the vibration generator into the specimen only. The good isolation of the structure as a whole depends on the viscoelastic isolating materials incorporated in the structural components.
The acceleration response of the suspension frame is tested simultaneously with taking records, and compared against an upper limit of 25 cm/sec^2. This step is necessary mainly because the dynamic characteristics of viscoelastic materials may change with time.

Since the experimental data was recorded during a long period of time it became necessary to check the repeatability of the systems behaviour from time to time, for drift in calibration or in the dynamic response.
The technique adopted here was to periodically re-excite the system at resonant frequencies which had already been tested, and compare the modal frequency, input receptance and subsystems' mean receptance at a pre-determined radius, with previous records. Should all parameters appear to have changed,

it indicates drift in the calibration, which could be checked.

In the event that some of the parameters, only, appeared different then the systems' response has changed.

Ways and means to detect error or failure, related to the apparatus are discussed in section 3.

Section 2 was summarized into the chart of planning experimental techniques, Fig 2.

The chart is combined of 3 divisions. The centre part for the coupled plates, system and a part for each of the uncoupled plates, on both sides.

The flow of the chart follows the sequence of the process to obtain the parameters, down to the ultimately sought parameters at the bottom of the chart. The 2 sets of parameters at the bottom of the chart are those required to accommodate eq'n 1.5 and 1.9, and those required to assess and detect errors.

It is possible to pick a parameter at the final stage, S_{fr} say, and follow back (upward) the process by which the parameter was obtained , thus revealing the parameters which are an essential part of the process. In the present example we see that an expression of X_{fr}, X_{in} and f_n yields X_{fr}. One sees straightaway that this parameter can be determined from the coupled plates system.

The chart facilitates a quick general appreciation of the effort involved to obtain a given parameter.

Observing the chart it becomes apparent that the techniques employed to obtain modal parameters fall into two categories. While amplitude response distribution $\bar{X}$ is obtained by testing the coupled system, determination of modal damping, mass and stiffness involved testing the subsystems being uncoupled. As suggested earlier, this is a serious drawback in practical situations. Hence the main effort in this work is directed to establish the relationship between the response ratio of the

coupled plates and coupling parameters.

Some of the parameters in the chart are marked with an asterisk. Those are the parameters obtained directly from measurement involving no computation.

The aim of such a presentation is to give an overall appreciation of the amount of experimental data as compared to the process of analysing systems' dynamics, and the sharing of each specimen in the data.

3. AN APPARATUS FOR STUDYING RESPONSE DISTRIBUTION IN COUPLED VIBRATING FLAT PLATES.

I. Specifications.
II. Experimental rig.
III. Calibration.
IV. Preliminary results.
V. Discussion.
VI. Conclusions.

a) General arrangement

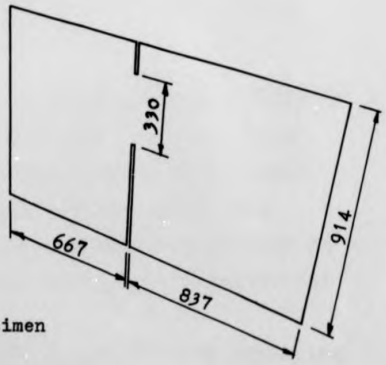

b) The specimen

Fig 3. Experimental rig for studying response distibution in coupled flat plates systems.

The purpose of this section is to describe a research rig which has been devised and constructed to provide the essential tool for the study of energy distribution in transversly vibrating plates.
The experimental apparatus has been designed to meet the requirements of the experimental techniques outlined in the preceding section and presented in the form of a chart in Fig 2.

The reader will appreciate that the experimental apparatus introduced in this section is an outcome of the necessity to compromise between the desirable, more expensive equipment and a limited financial grant.
Although this gave rise to some time-consuming procedures, it did not cripple the work as a whole.
The value of the rig for the project is demonstrated by some typical results, the validity of which is established by a series of subsidary tests.
Additional laboratory applications and further development of the rig for specific industrial applications, beyond the scope of the thesis, are described in section 6 IV.

I. Specification.

The parameters marked with an asterisk in the chart of Fig 2 can be classified into those measured at a point, such as frequency and force of excitation, input point response, and a group of the distributed parameters comprising coupling and plates response measured over an area. This classification is evident in the experimental set up.

The first group of parameters is attained by employing

transducers fitted at a fixed position, whereas the latter group is obtained from transducers which change their position, assisted by mechanical means, in a pre-planned part of the plate system.

For the determination of mode shapes and response distribution the transducer used should be a non-contacting one to avoid loading the plate and interfering with the mode shape by an additional mass. The transducer is made to move along a circle of constant diameter and pre-determined centre.

The plot of displacement response of the plate vibrating in a normal mode thus obtained exhibits a representation of the plate b nding waveform, of the kind shown in Fig 1, and yields the identification of that mode.

In considering possible structures of a coupling, we distinguish between three different types, a point coupling (Fig 26b), an elastic distributed coupling (Fig 26a), and a sort of a combination of both, i.e. a series of point couplings, such as spot welding.

The first 2 cases were tested in the course of the work, although the elastic one was used in the study of energy distribution.

The response of an elastic coupling, consisting of the components of the constituent coupled modes, as described in Fig 13b is distibuted over the border line between the two plates and needs to be detected along that line, referred to as the coupling centre line. As in the case of measuring plate response, non-contacting transducers are desirable here for the reasons mentioned. But in order to describe the dynamic situation at a point of the coupling

in sufficient detail, it is necessary to record the slope and amplitude response. The amplitude can be obtained from a transducer placed at the coupling centre line. In order to record the slope, the amplitude must be measured at the points marked in Fig 13b as those related to the measurement of $\emptyset_c$. This procedure amounts to recording the bending waveform in the Y-Z plane for amplitude,and in the X-Z plane to measure the slope.

Since some of the modes displayed amount of instability in the response, it was necessary to perform simultaneous measurements of both coupling parameters, to ensure that they were obtained for the same conditions. This required a minimum of 3 transducers arranged in the form of an equilateral triangle.

The procedure of taking records was repeated at each of 15 points, equally spaced along the coupling centre line.

The schematic reconstruction of coupling response shown in Fig 13b could be derived from such records obtained at 6 points and provided that the constituent coupled modes were identified.

Any vibrating system is described by its modal densities and by the modal parameters such as frequency, mass, stiffness and damping. These depend not only on the material properties and body geometry but also on subsystem coupling and on boundary conditions.

In considering coupled rectangular plates there are basically three possible boundary conditions: clamped, supported, free, and their 12 combinations, which can be applied to a part or a whole edge.

The provision of a supported edge restraint involves

considerable difficulty in providing sufficient inertia to keep the edge at rest while introducing no bending moment. Similarly the provision of a clamped edge restraint is equally difficult in ensuring zero slope at the edge. Completely free boundaries also present a difficulty in a situation where the body must be supported in some way. Nevertheless, despite the fact that suspension and excitation at some points of a multi-mode element is bound to interfere with the shape of the modes due to the manner of suspension, free boundary condition appears to be the easiest to meet.

In the transverse vibration of plates, points in the plate undergo small time-dependent displacements in the direction perpendicular to the plane of the plate. For any normal mode of vibration, this motion can be described by a pattern of nodal lines. They are approximately parallel to the edges in most cases of vibration of rectangular plates, so that a mode can be identified by the number of nodal lines m and n in the x and y directions respectively.

It would seem that points of nodes in the plate offer the most suitable dynamic characteristics for suspension attachment. But as the location of nodes varies with modes, and since for practical reasons it is not feasible to shift the points of suspension attachment according to the excited mode, this alternative was discarded.

In the case of free boundaries, the corners of a rectangular plate are of maximum displacement, for all normal modes.
Yet it was found that the least amount of distortion due to suspension attachment occurs when the corners are attached. In order to understand the reason for this to happen we compare the space-average stiffness of a plate

having 2 adjacent sides freely supported (pinned) and the 2 other sides free, to that of a plate having all sides freely supported.
The first case is analogous to suspension at the corner of a free plate and the latter one to suspension elsewhere away from the edges at an arbitrary mode. Our assumption that a nodal line is approximated by a pinned boundary is implied.

It is common knowledge that the space-average stiffness of the former case (2 sides free, 2 pinned) is lower than the stiffness of the other case. Hence the fixed point of suspension being attached to the corner of the plate, accommodates the mode motion in the (comparatively) greater flexibility of the vicinity of the corner., thus being the region where mode shape is distorted, as described by Shapiro (17).

By 'distorted mode' we mean a mode shape, different from that approximated to by a product of the appropriate characteristic beam functions.

For a square plate the nodal pattern can be a circle of a centre matching with the middle of the square, as can be seen for example in mode 4/2 - 2/4 in p. 373 of reference 11. In this case concentric circles are of displacement contours. Then waveforms of such circles around a circular path, are represented by plots of straight lines, parallel to the x axis, bearing no significance to a particular mode and consequently yielding no identification.

To prevent the crippling effect of a transducer detecting a response of the type described, and to facilitate a concurrent theoretical treatment in terms of normal modes of vibration - a rectangular plate was chosen for the specimen.

There are several reasons for a plate to display a distorted mode shape. Distortion of mode shape owing to constructional design of the rig, such as attachments location and type of forcing, misalignment, and the like, may be of a localized nature.

It is possible that in this situation, the method designed to identify normal modes through the bending waveform along a circle becomes incapacitated as the distortion, however localized, interferes with part of the circle.

The overall nodal pattern of the mode may still remain identifyable in terms of m x n nodal lines, which is the case shown in plate 1 of Fig 24.

The solution appears to be in the technique of mapping the nodal pattern applying the phenomenon that the phase angle between the disturbing force and a signal of a displacement transducer, changes through 180 degrees (approximately) when the transducer crosses a nodal line (18).

Another reason for distortion, which is inherent in the specimen and the boundary conditions, can be expressed in terms of the modal density.

A high modal density as compared to the modal bandwidth may cause an off-resonant excitation of adjacent modes. Normally this is likely to result in the motion of one or more normal modes being superimposed on the mode of interest. Consequently any point response is the vectorial sum of the components, at that point, of all the modes being excited. This is a distributed effect, whose extent depends on the relative modification factors and resonant frequencies of the modes involved.

Naturally, in cases where natural frequencies are so close together that resonant modes are distorted beyond

recognition these states cannot usefully be treated on the basis of peak amplitude testing and these have been ignored both in tests reported here and in subsequent testing to be reported later.
This is no disadvantage since the purpose is to study power flow and not the modes of vibrating plates.
Similarly those resonant conditions having adjacent anti-resonances above the half-power points have been excluded from consideration, because the peak amplitude plot does not yield the damping ratio with any accuracy.

From this description it is evident that sinusoidal forcing of the system at constant force amplitude is undertaken.
But in specifying the details of the excitation system it is necessary to give some consideration to the point at which the excitation is applied. The ideal point at which to excite a particular mode is its anti-node.
This is, as shown by both Plunkett (15) and Dunn (16), where the source of excitation encounters the least mechanical impedance.
At any other point the impedance is greater, reaching a maximum at a node. Exciting the plate at any point other than an anti-node requires higher force input per unit displacement response since it can give rise to deflection of points which would otherwise be nodes, to superposition of rigid body motion on the mode of vibration, to local distortion in the vicinity of the force input point or to highly distorted modes due to off-resonant excitation of adjacent modes, (see p. 379 of ref.13).

All these effects are easily detectable. Readings of force level and displacement response can be corrected in respect of the first two effects but where the latter occurs

a) Transducer scanning unit.

b) Plotter driven proportional to scanning.

c) Transducers measuring coupling.

d) Suspension attachment of specimen.

Fig 4. Components of experimental rig for studying response distribution in coupled flat plates.

the only course of action is to alter the position of application of the source, which is a laborious procedure involving precautions to avoid misalignment.

In a rectangular plate which is freely suspended, all points along the edges have the maximum displacement for that beam function for all modes. Hence if the disturbing force is located close to a corner of the plate, the lowest mode in which it can be located in a node is that having a bending wavelength of four times the distance from the forcing point to the edge.
So, if the location of the force is close enough to the edge the frequency at which this bending wavelength could be established will be so high as to be beyond the range of interest in the investigation.

For the determination of the mode shape the transducer used should be a non-contacting one to avoid loading the plate and interfering with the mode shape.

II. Experimental rig.

The rig consists of a steel base frame isolated from the floor by anti-vibrat ; mountings. The base carries a vertical steel frame supporting the specimen , an aluminium plate 1/8" thick and about 3'x 5' in size, cut partially to form a system of two rectangular plates coupled together by an integral bridge. Fig 3a shows a general view of the rig and Fig 3b the specimen. It is suspended from steel wires in tension within the frame, being connected at each corner of the plates by means of flexible rubber mountings shown in Fig 4d. This approximates, as closely as it is possible to do so, the condition of free boundaries. Furthermore this kind of mounting is vital if transmission

of energy to the specimen through a flanking path is to be avoided. Each plate element faces a scanning unit mounted on the base frame and insulated from it by anti-vibration mounts.

The scanning unit, shown in Fig 4a, comprises an arm carrying the transducer which may be rotated in a plane parallel to the plate, and mounted on a shaft. The shaft is made in two parts joined by a soft rubber coupling and mounted in a pair of air bearings. Both units are driven by a common electric motor. The selection of air bearings is dictated by the need to avoid noise generation in, and transmission through the bearings, and to insulate the part of the shaft carrying the transducer from the part driven by the motor.

Coupling response is measured by the set of 3 proximity transducers mounted as shown in Fig 4c, facing the coupled plate system its centre line against the coupling centre line. (The centre line of the unit is marked C.L. above the top transducer).
This unit is fitted to slide up and down on a steel stem in a plane parallel to the plane of the plate. A spring loaded catch, built in the transducer holder unit, locates the unit, in each of the 15 pre-determined points of measurement. So that a repeatability of those positions is ensured. The stem is bolted to a steel base plate which rests on a soft rubber pad on the floor, thus satisfatory insulation from floor vibration is achieved.

The insulation using a soft rubber mounting constitutes a danger of permitting the transducers mounted on the stem to float relative to the plate surface. In preliminary tests of building vibration it was found that door slamming and

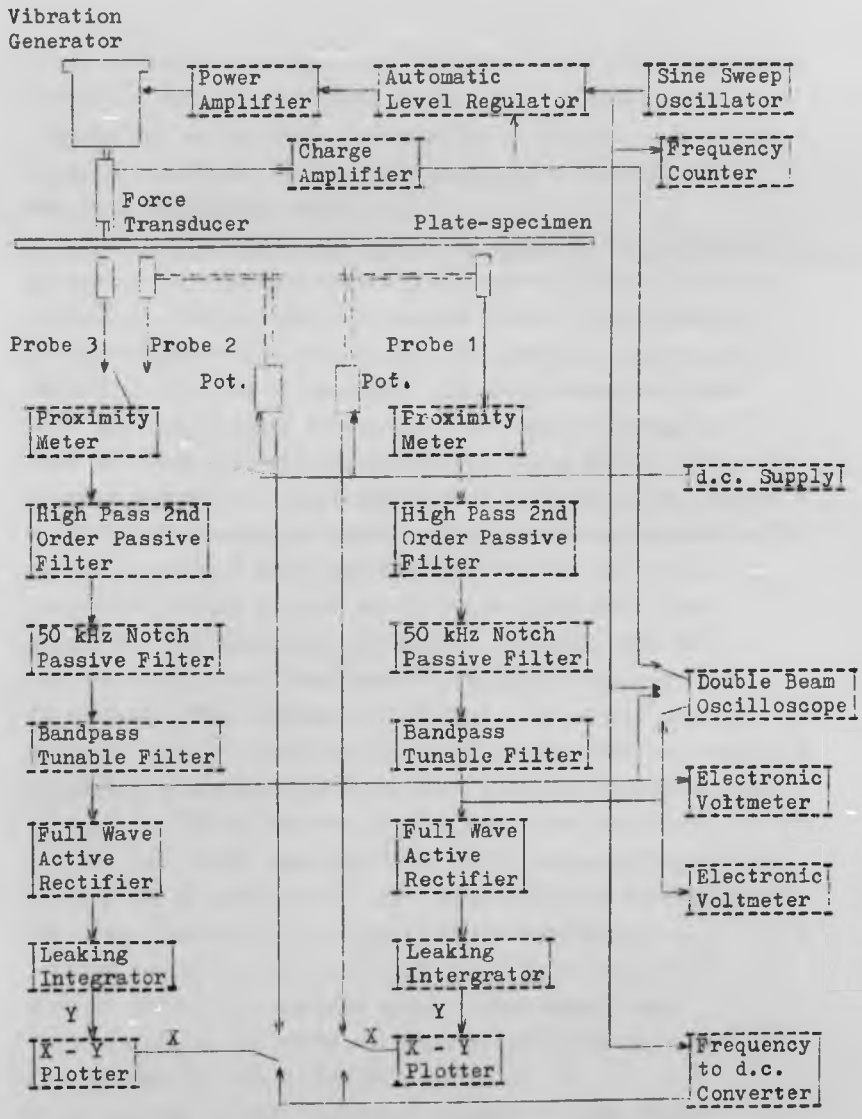

Fig 5. Block diagram of the instrumentation.

heavy workshop equipment were the only factors of significant effect on results. With soft rubber pad insulation this problem was solved and repeatability of records of coupling response confirmed if the transducers were floating, it was in a negligible amount only.

A separate stand supports the electromagnetic vibration generator in a seismic manner with respect to the direction of forcing. The generator is bolted to the plate through a piezo-electric force transducer. The physical connection is made while the arm is scanning care being taken to ensure that the displacement transducer indicates no change of mean position while the connection is being made. It is thereby ensured that no constraint is applied to the plate.

The instrumentation system employed is shown schematically in Fig 5. A sweep sine oscillator drives the vibration generator through a power amplifier and automatic level regulator. The regulator is fed with a signal from the piezoelectric force transducer to maintain constant input force level. The response of the plate, the input point response, and the coupling response are detected by capacitive proximity transducers with variable air gap. The vibration modulates a 50 kHz carrier. The signal contains mains hum and d.c. drift caused by the bodily swing of the plate. A set of high pass, notch, and tunable filters discriminates the signal which is then rectified and smoothed by a leaking integrator and fed to an x-y plotter to give a plot of vibration amplitude against transducer scan. The waveform in the plate is thereby described in a rectified form as can be seen in Fig 11.
If an average of that waveform is needed a time domain analyser is used, connected in parallel with the plotter.

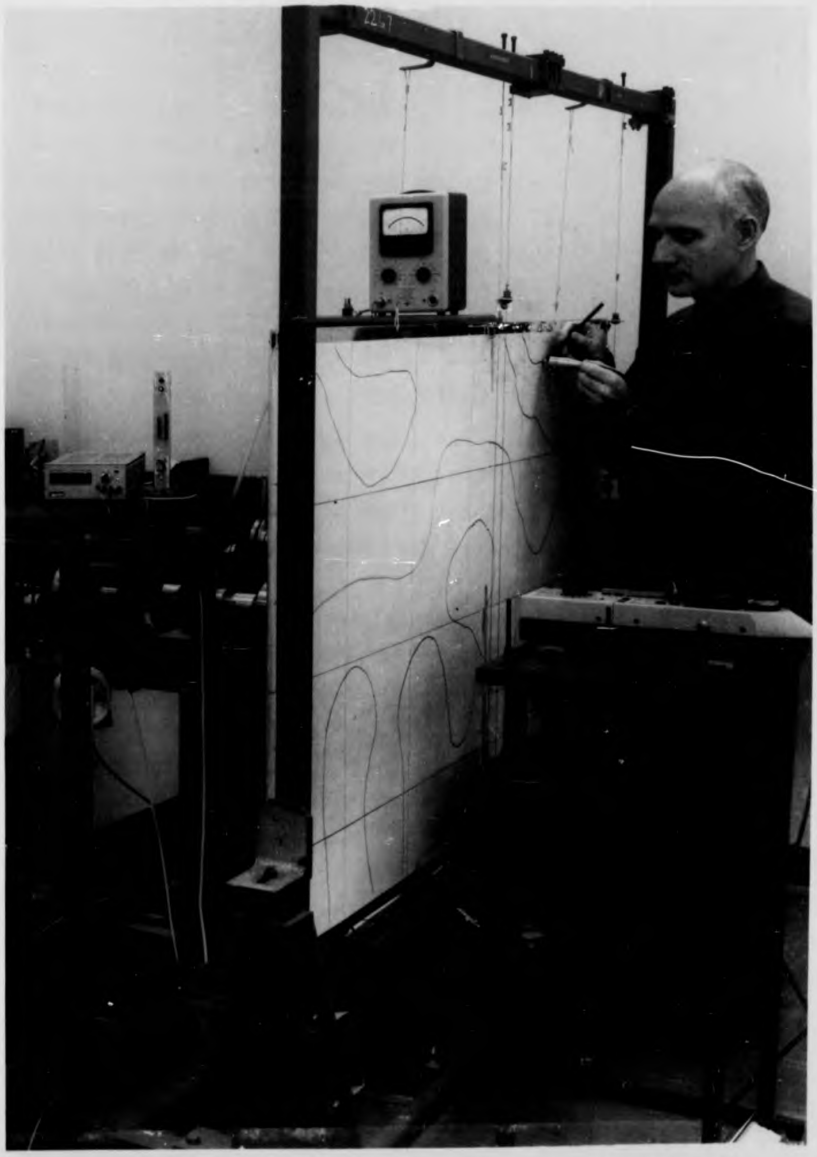

Fig 6. Mapping of the nodal pattern of a coupled vibrational mode using an acoustical technique.

The filter set attenuates both the 50 kHz carrier of the proximity meter and mains hum by 52 db. This is 25 db more than the signal attenuation at the lower mode frequencies of interest and 57db more than the attenuation of higher mode frequencies.

To plot the bending waveform the horizontal sweep of the plotter is driven from a d.c. supply through a potentiometer fitted to the shaft of the scanning rig (Fig 4b), thereby yielding a plot with abscissa proportional to angle of rotation of transducer scan.

This whole system of scanning rig and instrumentation, is duplicated as shown in Fig's 3 and 5 so that simultaneous records of the waveforms on both plate elements can be made.

To record peak-amplitude plots such as Fig 12, the x axis of the plotter is driven from the oscillator through a frequency-to-d.c. voltage converter. The horizontal sweep is then proportional to frequency of excitation on a linear scale.

Response and force signals are measured by digital voltmeters and displayed simultaneously on an oscilloscope in order to have a continous display of the level of signal distortion. The oscilloscope can also be used to record vibration decay rates.

Mapping the nodal pattern of the vibrational mode, using acoustical technique is shown in Fig 6. A condenser microphone is held facing the plate at a distance of about 1cm from the surface. The signal is fed into the sound level meter, and then compared against a signal from the force transducer both on a phase meter and an oscilloscope. A change through 180 degrees in phase difference between

the signals indicates that the microphone has crossed a nodal line.

Apart from this manual technique being laborious, a drawback is inherent in the method, in that when a node or another point of low displacement response is detected, the signal generated is neither enough to drive the phase meter, nor to display the situation clearly on the oscilloscope. Hence it was necessary to increase and decrease the gain alternately. It could engage up to a day's work to map a mode.

The strategic component to check flanking energy is the frame of suspension of the specimen . Vibrational energy being detected in the frame indicates that either part of the energy flows from the generator through the primary plate and the frame to the driven plate, avoiding the coupling or that the specimen is excited by extraneous source such as the motor, or the building, through the frame. This is monitored by an accelerometer fitted to the frame at the point of attachment of a suspension chord. A signal proportional to acceleration drives a voltmeter, which can be observed above the specimen in Fig 6.

The problem of setting an acceptable upper bond of frame response needs further clarification.
It is a cumbersome process to establish theoretically the relation between frame point acceleration and the direction and magnitude of the flow of vibrational energy through the frame for every normal mode of interest.
A series of simple tests was undertaken, to determine an upper limit of a 'strategic' point acceleration ensuring that the amount of response of the coupled-driven or uncoupled plate due to flow of energy other than through a coupling is

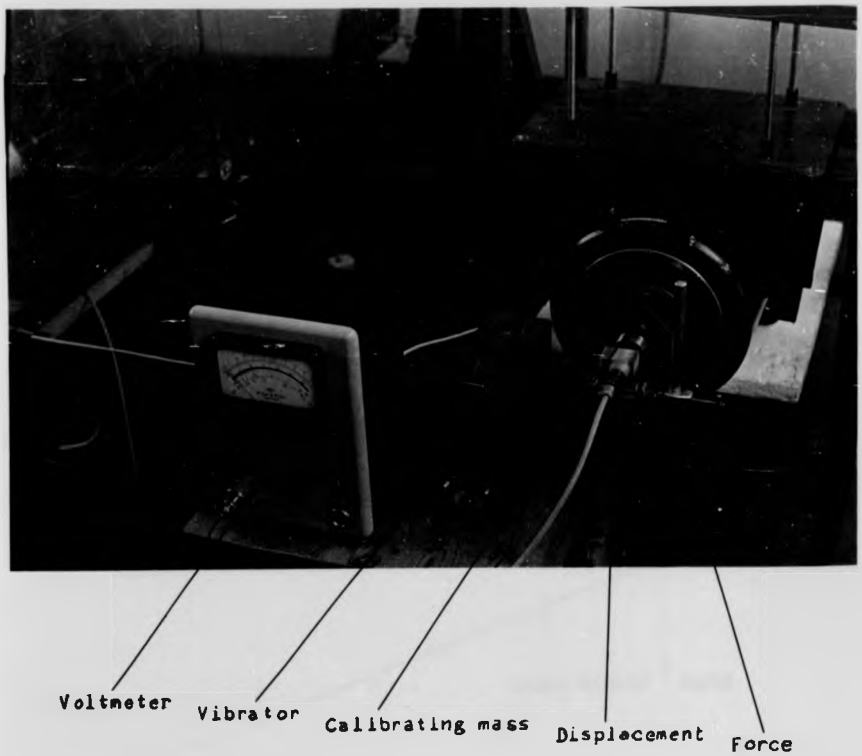

Fig 7. A set up of instrumentation for a dynamic calibration of the force and displacement transducers.

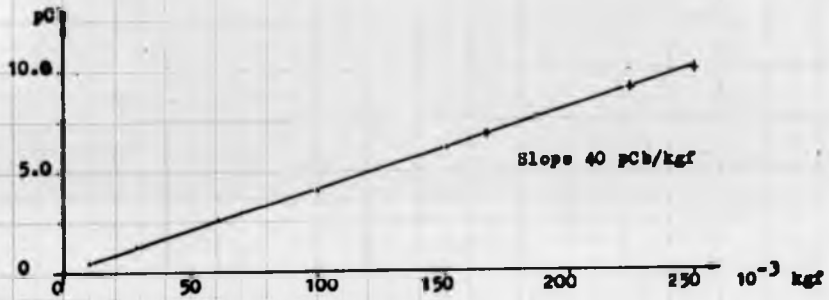

a) Force transducer .

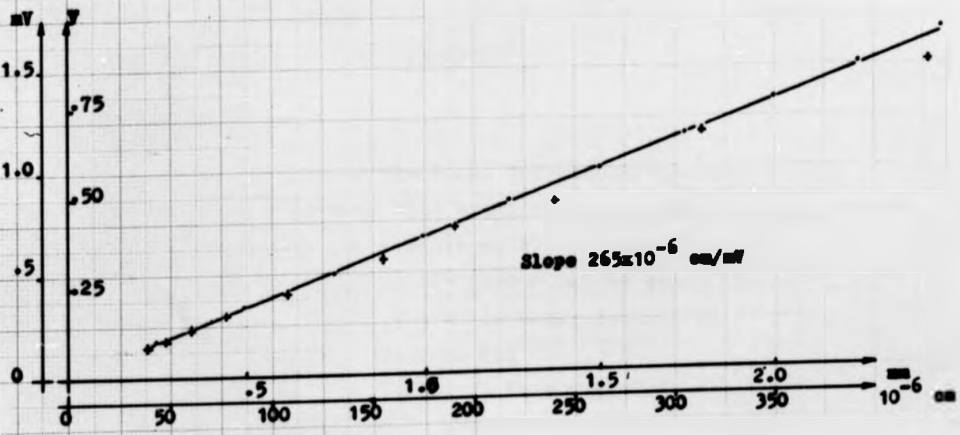

b) Proximity meter .

Dynamic reading + , static .

Fig 8. Calibration curves for force transducer and for displacement transducer ,static (inner coordinate system) and dynamic. (Static readings marked with dots)

less than 5%.

The experimental set up and procedure are similar to those adopted for measurement of coupled plates response, except that the specimen in this test consists of separate plates of the same dimensions as the coupled plates. Response of both plates was detected simultaneously as plate 'a' was excited sinusoidally, sweeping through the frequency band of interest. Each of the 30 normal modes of each plate, elected to serve as models, was examined. Then response ratio was compared against acceleration levels of the point described earlier. The kind of response level of the uncoupled plates to excitation of plate 'a' can be observed in Fig 27b/1.

It was established that an upper bond of that point acceleration of 25 cm/sec^2, keeps flanking energy well below the required level at all frequencies.

III. Calibration.

Static calibration of the force transducer can be performed by loading the transducer with known masses and measuring the d.c. voltage output. For dynamic calibration known masses including the mass of an accelerometer can be fixed in front of the force transducer, the whole being mounted on a vibration generator, as shown in Fig 7.

A calibration curve obtained by this method is offered in Fig 8a from which it is evident that a unique characteristic exists for both static and dynamic operation (at least within the frequency range 300-1200 Hz). The same is true of the capacitive proximity meter system, static calibration of which, against some high-accuracy linear measurement devices presents no problem. Dynamically, it is not possible to calibrate the proximity meter alone in the absence of the

output system. It is therefore necessary to incorporate this during the test and reconvert the results with the aid of the filter transfer function (see below) in order to obtain the effect of the proximity meter itself. The probe of the proximity meter was set across an accelerometer of 55.4 mv/g, mounted on a vibrator, excited to maintain constant acceleration. Readings of accelerometer signal and proximity meter filtered output were taken at various frequencies in the range of interest. The resulting calibration curve is shown in Fig 8b.

To determine the frequency dependence of the response of the filter system a reference signal of 1.0 volt rms was fed to the filtering network. The output voltage was measured at various frequencies after the tunable filter elements had been adjusted. Fig 9 shows the attenuating effect of the networks as a function of frequency over the range of interest and, inset, a representation of the relative Q-factors of the electrical and mechanical systems. This demonstrates the extent to which adjacent modes of vibration of the plate structure can fall within the bandwidth of the electrical filter.

In addition to static and dynamic calibration it is essential to verify that the experimental rig fulfils its purpose in several important respects. These are principally that the specimen is unconstrained by the manner of the support or by the manner of excitation and that flanking transmission of onergy to the specimen does not occur to any significant extent.

Misalignment in the suspension or in the position of the vibrator are the only means by which constraint can be introduced to the specimen, resulting in higher modal

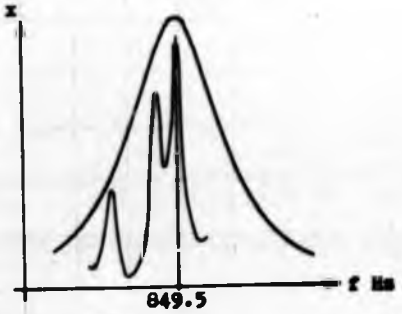

b) Relative Q factor of electrical (outer curve) and mechanical systems at one particular frequency.

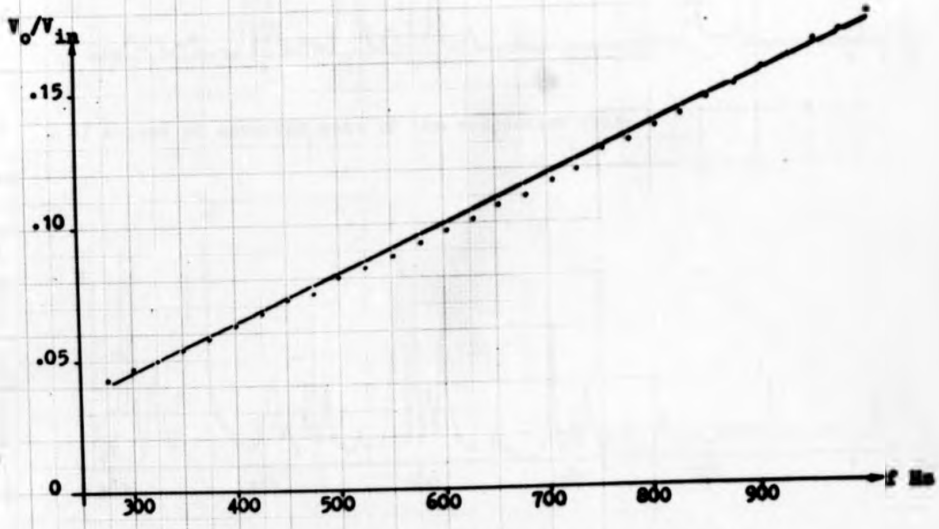

a) Attenuation of filter network as a function of frequency.

Fig 9. Response of electronic filtering network.

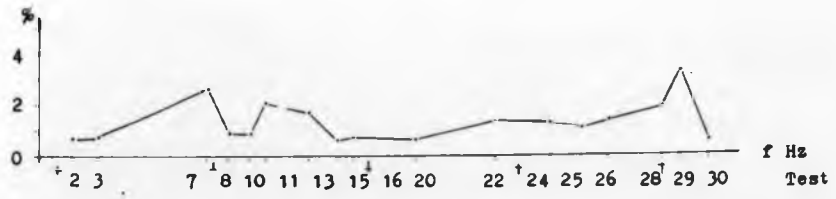

a) A plot of the response of uncoupled plate 'b' .

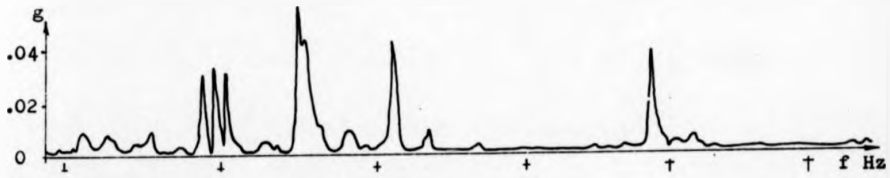

b) A plot of apparent mass of the suspension frame.

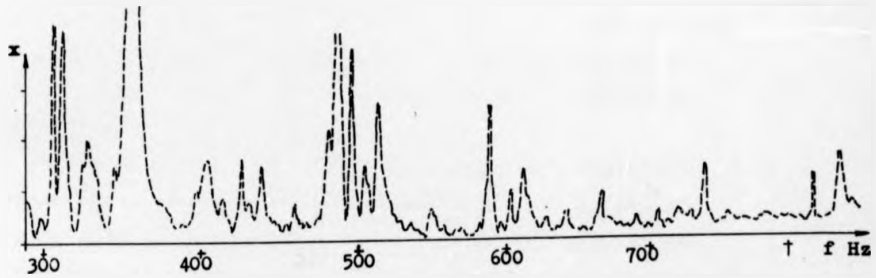

c) A plot of the input point response of the coupled system.

Fig 10. Plots showing the response of components of the experimental rig to specimen excitation in plate 1.

frequencies. For the purpose of assessment two separate identical rectangular plates were used. Repetition of the procedure of mounting the plates into the suspension frame and connecting the vibrator resulted in consistent modal frequencies with repeated trials. It was verified that modal frequency was also independent of time and of room temperature and humidity. Taking records of modal bending waveform of different times and different room conditions showed complete repeatability within a reasonable range of time.

Transmissibility of vibrational energy to the supporting structure was assessed in terms of the drive from the vibration generator, the electric motor powering the scanning rigs and building vibration.

The flanking transmission resulting from the vibration generator was found, not unreasonably, to be dependent upon the power and response levels, and upon mode shapes. The transmission from the excited plate to the frame never exceeded 3.3% and further attenuation occurs between the frame and the second plate. This is confirmed in a plot of frame acceleration response versus frequency of excitation (Fig 10).

Disturbance due to the electric motor and mechanical transmission excited different components of the rig to varying extents ranging from a high response level of the motor base to a very small response of the front bearing of the scanning rig unit. This confirms the value of the use of anti-vibration mounts to join sub-assemblies, and the air-bearings. The suspension frame did not respond to motor excitation. An appreciable vibration level of the building was noticed when heavy workshop machinery was operated or when nearby doors were slammed. In all cases

isolation was found to be so good that to ascribe a figure to the transmissibility, other than due to specimen excitation, would have demanded additional attention to correlate the low level of response with the source of interest.

IV. Preliminary Results.

The experimental procedure is straightforward and need not be described in detail except for several points which have a direct effect on the results.

Whenever the shape of a mode is distorted it is probable that points which would otherwise be nodal points will exhibit motion. The amount of distortion of a mode can therefore be related to the motion of a theoretical node. Such motion is readily detectable with the rig described above and its magnitude can be used as a basis for deciding which modes are not acceptable for the purposes of studying energy transmission. This is evidenced by the vacancies in Fig 22 and table I which show theoretical modal frequencies for a number of nodal patterns and experimental resonant frequencies for these clearly defined modes which are the subject of energy transfer investigation.

The diagram in the middle of Fig 22 shows, in the same format, the percentage difference between the measured frequencies and the calculated frequencies and also the test number which is indicative of the order of occurrence of the coupled modes with increasing excitation frequency as shown in Fig 12.

Two alternative techniques are available for the determination of damping ratio - a free vibration, rate-of-decay method and a steady-state vibration, peak amplitude method.

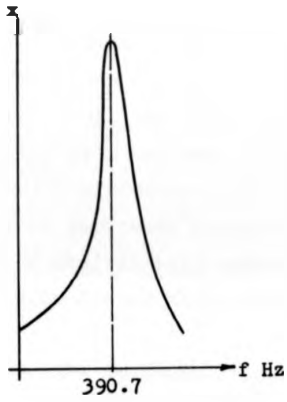

a/1) Peak-amplitude versus frequency plot .

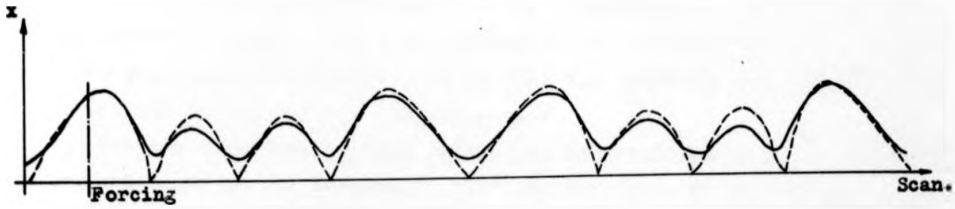

a/2) Bending waveform of mode 5x3 at 390.7 Hz.

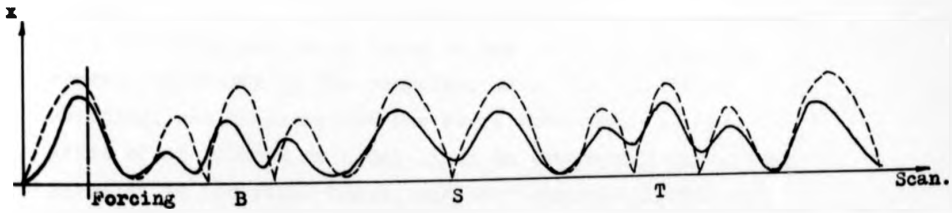

b) Bending waveform of mode 6x5.at 702 Hz.

Full line, recorded waveform.

Fig 11. Records showing the level of agreement between theoretical and experimental bending waveforms.

Use of the decay-rate technique is restricted to cases of large mode separation for otherwise, the motion decaying in a mixture of modes, the value of decay rate will vary considerably over the space of the record.

The actual procedure used for determining damping ratio via the peak amplitude method makes use of the greater accuracy of digital volt meters and frequency counters as compared with linear measurements of hard-copy analogue records.

Firstly, the peak amplitude plot is recorded to check that a single peak is enclosed between two adjacent half power points. Then the voltage of maximum displacement response is measured, and the value of voltage at half power computed. Finally the oscillator is tuned to the frequencies, above and below resonance, which correspond to the half-power voltage. These frequencies then specify the bandwidth and hence the 'Q' factor and damping ratio.

Bending waveforms of test plates can be predicted by a method based on the assumption that the waveforms of vibrating plates and beams are similar. The waveform of a mode is obtained as the product of the characteristic beam functions in two orthogonal directions, each having boundary conditions compatible with the plate boundary conditions. Characteristic beam functions are to be found in ref. 11 from which the bending waveforms of the response, along the circle of scanning, can be predicted for every mode specified in terms of the number of nodal lines in orthogonal directions parallel to the plate edges, and the boundary conditions. The process is simplified by matching the centre of scanning of the transducer to the geometrical centre of the test plate.

The method of Warburton (11) was used to predict modal frequencies corresponding to a specified mode. The expected bending waveform along a circular path was then determined, and the modulus plotted (corresponding to rectification of the transducer signal of plate displacement) giving a theoretical curve with which experimental curves could be compared. The sort of agreement achieved in practice is shown in Fig 11. It can be seen that the principal discrepancies occur in the vicinity of the nodes where noise in the electrical signals, and the finite size of the transducer prevent the level from falling to zero.

V. Discussion.

It has been shown by Shapiro (17) that a plate suspended at the four corners, which with free boundary conditions are points of maximum displacement is distorted only in small restricted regions depending on the size of the plate, and the vibrational mode shape. The choice of the detail of the suspension is mainly a choice between increasing damping in soft mountings on one hand, and increased stiffness of the plate and flanking energy in rigid attachment on the other hand. Both give interference with modal properties. Clearly any design must ensure that the plate can swing as little as possible in order to keep a constant mean gap between the plate and the scanning probe.

Three alternatives were examined. First, the plate was suspended between four nylon chords, one at each corner, fastened to the frame under tension. This leads to tension in the plate, resulting in increased stiffness and hence in resonant frequency. The effect can be computed in a manner similar to that for beams, (see p.374 of ref.14). It was

observed in experiment that for a tension of 50 kg, which was the minimum required to prevent rigid body motion of the plate, the plate being excited in mode 5x5, the resonant frequency increased from 558 Hz to 624 Hz, an increase of 11.8%.

The second possibility was to fix the corners rigidly to steel wires, the wires being in tension across the frame. This showed an unacceptable amount of transmissibility between uncoupled plates via the wires and the frame (about 20%) and an increase in resonant frequency due to constraint of the corners of the plate. The third and acceptable alternative was a modification of the latter, shown in Fig 4d. The corners of the plate were attached to the wires through flexible mountings. This caused only a slight increase in damping and introduced a negligible amount of non-linear effect of amplitude-dependent stiffness and damping.

In dynamic testing where a signal proportional to the force input from the source is important for energy calculation and in a control loop, a consideration is given to the effect of the mass of the parts linking the force transducer and the specimen. The reason being that such a mass is seen by the force transducer causing an error in the reading of force input to the vibrating system of the order of that mass times the acceleration.

It is possible to compute the effect of this additional mass from knowledge of the weight of the part (less the aluminium material removed in drilling a hole) and the accelerations involved.

The error is smaller in the lower modes but becomes significant in the higher frequencies, reaching about 9% of the force transmitted from the force link to the specimen in

one particular mode. In all other modes error does not exceed 4%.

In our experimental precedure we are interested in discrete modal frequencies and it was necessary to calibrate the signal from the force transducer for each of those frequencies. So although an error of 4% is small as compared to other sources of error, this problem was tackled by calibrating the signal for the additional mass as well .

VI. Conclusions.

Bearing in mind that the rig has been specified and designed primarily as a tool to investigate energy balance, several selected modes of vibration can serve as models for energy flow rather than the plate as a whole. These modes have been chosen on a basis of minimum interference and such that modal parameters can be assessed with reasonable accuracy.

Calibration of the measuring system was performed and proved reliable through agreement between static and dynamic testing.

Evidently extraneous interference with the dynamic behaviour of the system is within acceptable limits in most vibratidal modes.Those subjected to higher interference are easily detected by means of a simple analysis and treated accordingly.

It has been shown that response distribution can be assessed experimentally in great detail without interfering with the motion of mode - which is the main advantage of this rig over those relying on contact measurement at discrete points.

The rig and instrumentation have proved to be satisfactory for the purpose.

4. EXPERIMENTAL RESULTS.

In this section which consists of 3 parts, we deal with experimental data.
In the first part, results are introduced together with the conditions and situations affecting the accuracy and reliability. Some of the results are preccessed and presented in a suitable form for analysis.
The second part discusses error in the experimental data in view of the information presented.
In the third part results are analysed. Response distribution is related to coupling parameters through the analogy to the model development in the appendix. Energy distribution is computed and discussed.

In general the section follows the pattern of the thesis focusing on response distribution, regarding energy distribution as a matter for further development. Thus only a limited amount of information on parameters related to energy distribution is available.

In all 30 coupled modes have been tested, of which 21 coupled modes were identified in terms of m x n nodal lines. Of those 7 uncoupled pairs of modes provide data for the computation of energy distribution.

I. Presentation.

An overall description of the dynamics of the coupled plates system is given in Fig 12, through a plot of peak-amplitude versus frequency of excitation.

The condition at which the plot is obtained need to be considered. The response of any point of the plate depends on the location of that point relative to the mode shape, in

addition to modal parameters and boundaries. Thus a maximum response level will be recorded by a transducer facing an antinode, whereas zero amplitude will be recorded at a node, (except for the effect of the finite size of the transducer). It follows that a point of the plate is likely to undergo any response level, ranging from an antinode to a node, depending on the point of measurement and mode being excited.

In the event of the point being located at a node, that mode will display no response resulting in this mode being absent from a plot of peak-amplitude versus frequency. It means that for each mode, the response must be measured at a different point to ensure compatible records.

The only position which offers an approximate plate response for every mode is the point of excitation by constant force amplitude. As the frequency of excitation approaches a resonant, the demand for energy needed to drive the system drops sharply, because it is required to cover damping losses only. Then a greater motion can be maintained by the force, which makes nearly every resonant pronounced as compared to the off-resonant motion.
But even at resonant, input point response depends on the mode shape, though less than otherwise, so a modal response may become obscured when the force is located precisely at a node of a low response mode.

Since response was measured at the input point keeping exciting force at a constant amplitude, the plot of Fig 12 is of input receptance versus frequency of excitation. It provides an assessment of modal density and approximate modal response, which are essential in a preliminary selection of modes to serve for experimental models.

From the plot in Fig 12 it would seem that modes

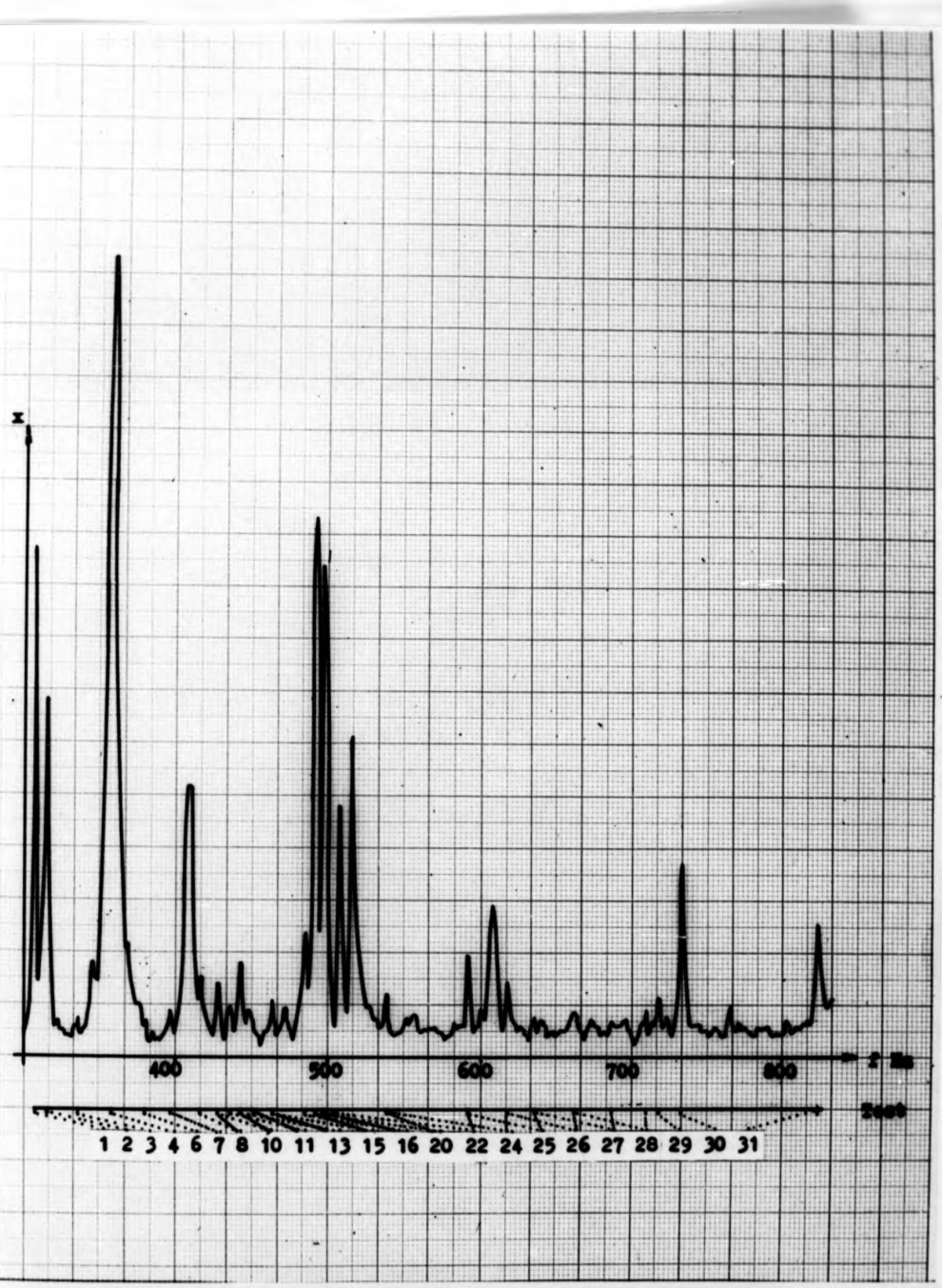

Fig 12. A plot of input receptance (in plate 1) versus frequency of excitation of the coupled plate system.

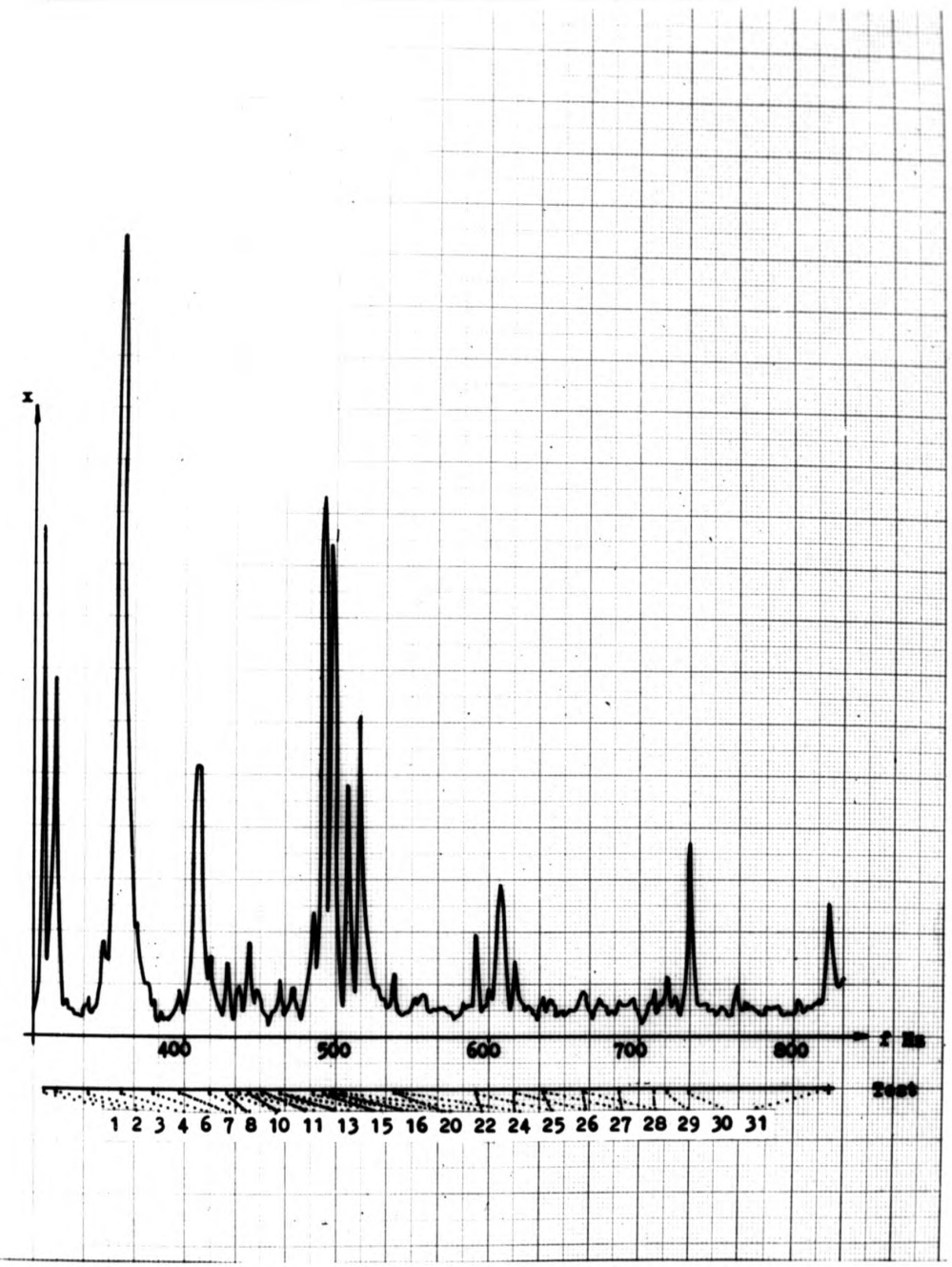

Fig 12. A plot of input receptance (in plate 1) versus frequency of excitation of the coupled plate system.

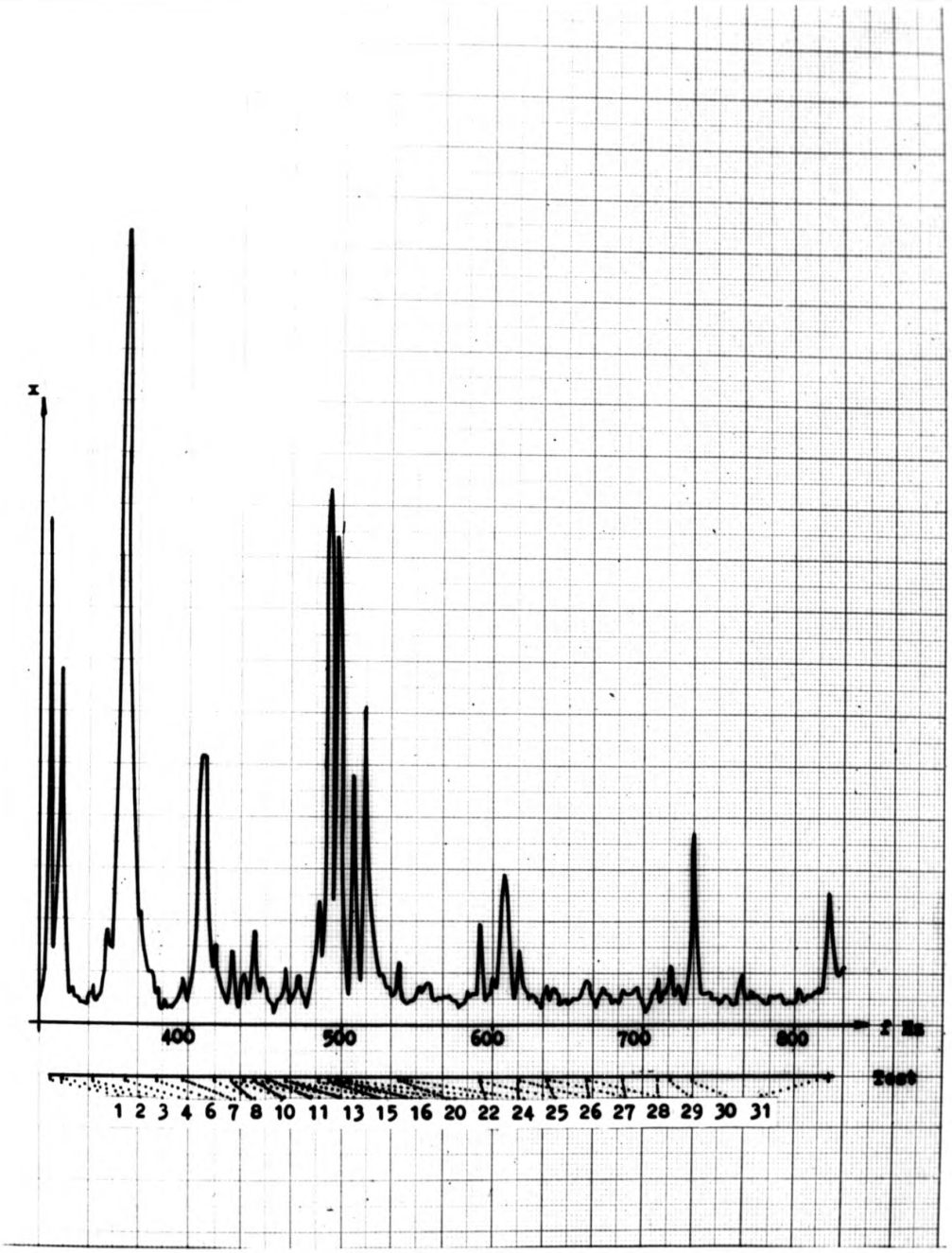

Fig 12. A plot of input receptance (in plate 1) versus frequency of excitation of the coupled plate system.

displaying the highest response are preferred as models. This is true for a preliminary selection only. In the course of the tests it was observed that some modes of the high response presented practical difficulties such as instability of the response, or mode shapes causing a significant amount of flanking energy. This shows that additional factors are involved in the considerations.

So the procedure began with a selection of 30 coupled modes from the plot of Fig 12 being marked by serial numbers, to become test numbers when each coupled mode is tested individually. Those were chosen, at this preliminary stage, on the merits of mode separation, relative modal response, and by the distribution of modal frequencies over the frequency band of interest. The stage that follows, to identify the modes in terms of the nodal pattern, which eventually reduced the number of modes of interest to 17, will follow later in the section.

An effort was made to obtain experimental data, as detailed as possible, on the mode of motion of the coupling region, owing to lack of a concurrent theory on the response of coupled modes of elastic systems in general, and coupling region in particular.

In addition, tests with the different types of coupling were performed with the object of understanding the modal interaction in (nearly) extreme cases, one subjected to elastic interaction between the constituent coupled modes, the other coupled at a point, bearing similarity to the case of a driven plate excited at a point by a disturbing force.

The records of Fig's 27 display plates response, as the subsystem plates were coupled alternately in 2 different ways.

Bending waveforms that are displayed in Fig 27a, were recorded as the plates were coupled in a manner, such that the coupling formed an integral part of the plates. Fig 27b displays bending waveforms of the same coupled subsystems. Here the coupling is a sandwich clamp, made of aluminium to maintain low inertia resistance. This is a bridge 15cm wide as compared to the former being 33cm wide.

The analogy between the 2 cases was based on the frequency of excitation and alternatively on mode shape, although after the test had been carried out additional factors appeared to affect the dynamics of the system.

The first set of tests was performed as both types of the coupled systems were excited successively at nearly the same frequency 486 H_z. A normal mode is present in each of the subsystem plates in Fig 27a/1 and in Fig 27b/1.

The second set of tests was performed, aiming at exciting the same normal mode 5x7 in subsystem 2, in both coupling situations. As expected, the frequencies of excitation are wide apart for each type of coupling in this test. Evidently a normal mode is present in each of the subsystem plates in Fig 27a/2 as in Fig 27a/1. But in Fig 27b/2, where the plates are coupled at a point, a normal mode was excited in subsytem 2 only.

Records of all the stages of the tests related to the coupling at a point, Fig 27b, comprise plots of peak amplitude versus frequency of excitation for the benefit of the analysis to follow in section 6 II.

The trend of coupled modes towards continuity of the nodal pattern in the coupling region, in elastic coupling (Fig 27a), is important in analysing the records of coupling response and its relation to the mode shape.

Coupling response is expressed by amplitude X_c and slope ϕ_c at a point. At that point, the slope is represented by the difference of the amplitudes measured at pre-determined fixed points on either side of the coupling in the direction at right angles to the coupling centre line, as illustrated in Fig 13b. The drawing shows a typical coupling response situation, where the number of nodal lines $n_1=n_2$. (i.e. the nodal lines at right angles to the centre line of the coupling). Although this is a particular case, it applies to 10 of the 17 modes of interest.

The 2 parameters were measured at 15 points equally spaced along the centre line, and distributed over the entire length of the coupling in each coupled mode.

This information was utilised to examine modal response in the coupling region in particular.

In Fig 13a amplitude response along the coupling centre line, in 4 selected modes, being a sample of the data collected is presented. This plot amounts to a bending waveform of the coupling centre line. For the simple cases (where $n_1=n_2$) it is a straightforward matter to work out the nodal pattern of the coupling region, once the vibrational mode has been identified.

A plot of the slope at each of the 15 points of measurement is offered alongside, to complete the picture of the coupling response. Note that slope was taken in X-Z planes, located at each of the 15 points, while the bending wave is described here in the Y-Z plane, where all the 15 points lie.

Since the coupled modes in the plates determine the mode shape at the region of the coupling, it is possible to evaluate the amount of distortion in that region as the expected location of nodes is compared against the plots of

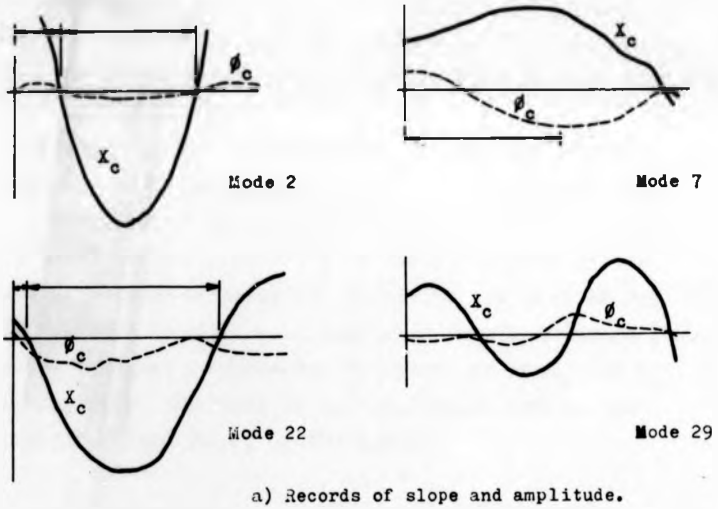

a) Records of slope and amplitude.

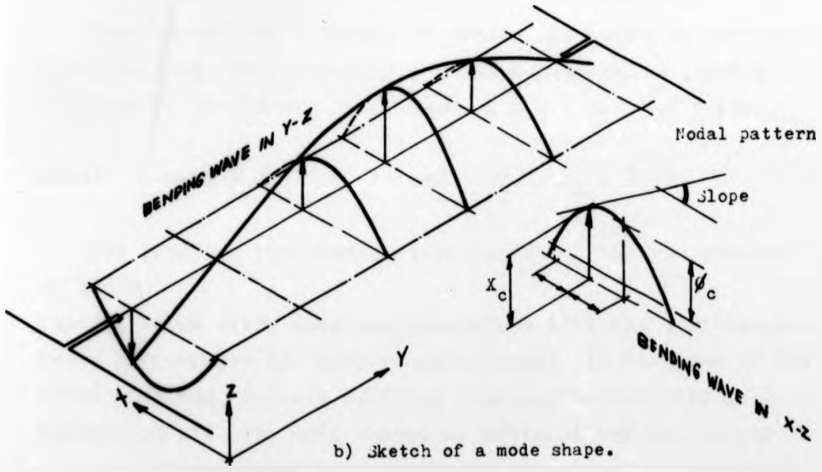

b) Sketch of a mode shape.

Fig 13. Coupled mode response at the coupling region.

coupling amplitude and slope responses.
For example, in the simple case when $n_1 = n_2$ a point of a nodal line must be matched by zero amplitude and slope at that point on the plot of Fig 13a. But if $n_1 \neq n_2$ then a point of a node shows zero amplitude and either a maximum or minimum slope on the plots, as implied from the continuity of the nodal pattern.

The aforesaid is in addition to an expectation for the bending waveform corresponding to the characteristic beam function to appear in the plot of the amplitude if $n_1 = n_2$. Hence nodal points expected from identification of the constituent coupled modes are marked on the plot of Fig 13a.

Next, the information is converted into a suitable form of coupling response parameters. The readings of X_c and ϕ_c initially taken for each of the 30 coupled modes, are averaged for that mode, in the manner,

(4.1) $\bar{X}_c = X_c$ rms and (4.2) $\bar{\phi}_c = \phi_c$ rms

Since it was not possible to excite all modes of interest with the same force amplitude, it is necessary to express response in receptance form. Then eq'n 4.1 and 4.2 become,

(4.3) $\alpha_x = \bar{X}_c/F$ and (4.4) $\alpha_\phi = \bar{\phi}_c/F$

Thus coupling response is represented by the receptances α_x and α_ϕ.
Table I below lists coupling parameters with the corresponding modal frequencies and coupled modes expressed in terms of the nodal patterns, because coupling response is analysed in connection with the mode shape, as mentioned before. It was

convenient some times to denote coupled modes and test conditions with reference to the serial number of the test or the frequency of excitation at which those modes were coupled. Hence the test numbers and frequencies are also listed in the table. The vacancies in the test numbers indicate the quantity of coupled modes chosen from Fig 12 to serve as models in the early stage which had to be discarded in preliminary tests.

Test No.	Excitation	Coupled modes		Coupling	
	f_n	Plate 1	Plate 2	α_x	α_ϕ
	Hz	Nodal pattern mxn		10^{-3}cm/kg	
2	313.7	0x6	0x6	10.186	.975
3	329.6	5x3	4x3	3.623	.487
7	390.8	5x4	4x4	2.357	.474
8	415.0	6x2	0x7	.940	.128
10	430.1	1x7	1x7	5.456	.533
11	436.0	3x6	3x6	1.652	.852
13	457.9	6x3	5x3	1.188	.370
15	480.2	5x5	4x5	4.876	.742
16	486.4	4x6	2x7	4.174	.352
20	534.9	6x4	5x4	1.518	.375
22	587.8	5x6	7x1	18.026	2.070
24	612.5	6x5	5x5	.876	.610
25	637.0	3x8	7x2	1.295	.845
26	665.3	8x0	6x3	.992	.195
28	707.7	4x8	2x8	3.005	.432
29	718.5	5x7	2x9	1.669	.260
30	734.7	7x5	5x6	3.199	.989

Table I. Experimental data of modal response of the coupled plates system.

Experimental data on coupling response introduced here can be classified into data reduced to a suitable form for computation, through averaging and normalising, given in table I, and the remaining data mentioned above which is essential for understanding the dynamical behaviour of the coupling.
The first part, table I is used in part III of the section to compute response ratio, which is the essence of the thesis, while the latter part is used whenever coupling response is discussed and analysed.

Now we turn to present data related to the elements. The technique of recording bending waveforms of vibrational modes is of particular importance, being applied to detect response distribution, error introduced into the experimental data, and identify the modes excited in the elements.
Hence an appreciable amount of records of bending waveforms were compiled, a sample of which is presented, to demonstrate the validity and value of the information they yield, and the ways in which that information is extracted.

Fig's 15,19,20,21, and 29 are related to the analysis of the level of agreement between recorded and theoretically constructed bending waveforms.

A method to construct theoretically the bending waveform, of a given vibrational mode, along the circle of scanning was described in section 2 II. Fig 29 presents a page from a catalogue of the bending waveforms of all the modes included within the frequency band of interest. The catalogue is a basic tool for applying this technique.
In Fig's 19, 20 and 21, 3 distinct cases are shown, in which 2 factors are involved. These are: The effect of exciting a

mode at frequencies in the vicinity of, but other than, the precise natural frequency, and interference of an adjacent mode excited off its' natural frequency. Those effects can be expressed and indeed detected through the location of the frequency of excitation on the plot of peak amplitude versus frequency, that in Fig 12.

Hence, all 3 presentations comprise a recorded and a theoretical bending waveform, and a peak amplitude plot showing the immediate range of frequency, being an extract of the plot in Fig 12.

Thus it becomes possible to analyse the agreement between waveforms with respect to interaction with adjacent modes,

The records of the latter 3 figures were obtained from an uncoupled plate, different from those used as specimen in the study of response and energy distribution. Mode numbers in those records are related to the order of appearance of modes in the progress along frequency scale for that particular rectangular plate, freely suspended.

The kind of agreement between waveforms analysed in Fig's 19, 20 and 21 is qualitative only, which can be used normally except when an assessment of error in experimental data is required. Then it is necessary to evaluate the agreement between recorded and theoretically constructed bending waveforms.

In Fig 15 we exhibit this process being applied in Part II.

The technique of recording bending waveforms for the purpose of a quantitative assessment of waveform agreement is somewhat different from that engaged to detect subsystems' response.

Such a procedure essentially begins with the choice of the level of excitation. The appropriate answer would be to

correlate the predicted and experimental response at a point on the plate in such a manner, that the level of excitation and all the scale factors involved yield a point response, measured on the plotter, to be identical with the predicted response at that point. Then in the event of an absolute agreement between the waveforms their graphs overlap.

In this work we avoided this exact method by a shortcut technique. The scale of the plotter was changed, records of different scales were compared repeatedly to a theoretical waveform until a best possible wave agreement was achieved. The records obtained from this trial and error technique are approximate and lie between the 'correct' and 'over-optimistic' limits. Still it was preferred over the exact method since a great difficulty was encountered, in experiment, to locate the transducer detecting plate response, in a pre-determined point.

A very small shift of location resulted in a significant difference of the point response.

The process presented in Fig 15 above, deals with assessment of error in experimental data being detected. The technique to probe such error, or otherwise to extract the information from recorded and theoretical bending waveforms is associated with the normalising factor.

In section 2 we outlined techniques to obtain the normalising factor N, and ways by which the factor can be utilised to detect and analyse systematic errors.

In order to obtain the normalising factor, a set of pre-determined 11 radii of scanning was planned, so that sampling was distributed over each plate surface. For each radius, when scanning simultaneously over both subsystems

plates, an average amplitude response $\bar{X}_m$ was obtained. for each subsystem. Then the average normalising factor of each subsystem, $N_{1,r}$ and $N_{2,r}$ related to radius of scanning r, can be calculated using eq'n 2.6, namely,

$$(4.5) \qquad N_{1,r} = (\bar{X}_m/\bar{X}_t)_{1,r}$$

and

$$(4.6) \qquad N_{2,r} = (\bar{X}_m/\bar{X}_t)_{2,r}$$

where both results are related to the same r, but each normalising factor obtained for a different plate.

The overall agerage normalising factor of coupled mode m_1 x n_1 and that of m_2 x n_2 can be worked out from sets of 11 results of eq'ns 4.5 and 4.6 where,

$$(4.7) \qquad \bar{N}_1 = N_{1,r} \text{ rms} \qquad (4.8) \qquad \bar{N}_2 = N_{2,r} \text{ rms}$$

as r takes all the 11 values in each of the equations.

In Fig 14 the process of eq'ns 4.7 and 4.8 is demonstrated in a graphical form. For every coupled mode of interest, a plot of $(\bar{N}-\bar{N}_r)$ versus r is presented. Coupled modes are denoted by their resonant frequencies and test numbers.

This form of presentation exhibits fluctuations of values of $\bar{N}_r$ about the mean value of $\bar{N}$, which is an important tool to detect error in the system. By displaying values of $\bar{N}_r$ for each plate separately a more detailed appreciation is possible.

Curves of $\bar{N}_1-\bar{N}_{1,r}$ and $\bar{N}_2-\bar{N}_{2,r}$ of the constituent coupled modes are plotted alongside to be compared to each other.

The set of curves representing plate 1 are referred to as group (a) and those of plate 2 as group (b). Thus each coordinate system related to a coupled mode.situation contains a curve of each group.

The data introduced hitherto, constitutes all the information needed to pursue the object of the work, namely to obtain a parameter indicative of response ratio of the conservatively coupled elements.
The remaining presentation is related to topics, off the main interest of the project and data confirming the validity of our approach regarding the crucial coupled modes concept.

An experimental evidence to prove that coupled elements can be represented by coupled normal modes of vibration, is provided in Fig's 23 and 24.
The nodal pattern was 'mapped' applying an acoustical technique, and then photographed. The technique is demonstrated in Fig 6 and was introduced in section 3.

The proof is given by a display of a nodal pattern of a pair of coupled normal modes, continuous across the coupling, each of which being identified as an individual mode in terms of m x n nodal lines.

A clear proof is that of Fig 23 in particular. The constituent coupled modes are easily recognised and the nodal lines counted. Hence it is also simple to extract information as to the dynamic situation at the region of the coupling.

It should be stessed that such a good nodal pattern exhibiting the coupled mode concept is not an isolated case, although one sample only was recorded as a typical example.

The set of curves representing plate 1 are referred to as group (a) and those of plate 2 as group (b). Thus each coordinate system related to a coupled mode situation contains a curve of each group.

The data introduced hitherto, constitutes all the information needed to pursue the object of the work, namely to obtain a parameter indicative of response ratio of the conservatively coupled elements.
The remaining presentation is related to topics, off the main interest of the project and data confirming the validity of our approach regarding the crucial coupled modes concept.

An experimental evidence to prove that coupled elements can be represented by coupled normal modes of vibration, is provided in Fig's 23 and 24.
The nodal pattern was 'mapped' applying an acoustical technique, and then photographed. The technique is demonstrated in Fig 6 and was introduced in section 3.

The proof is given by a display of a nodal pattern of a pair of coupled normal modes, continuous across the coupling, each of which being identified as an individual mode in terms of m x n nodal lines.

A clear proof is that of Fig 23 in particular. The constituent coupled modes are easily recognised and the nodal lines counted. Hence it is also simple to extract information as to the dynamic situation at the region of the coupling.

It should be stessed that such a good nodal pattern exhibiting the coupled mode concept is not an isolated case, although one sample only was recorded as a typical example.

Aided by means of mode identification, Fig 24 serves for that purpose as well.

The degree of distortion of nodal patterns varies from a well conditioned mode in Fig 23, (i.e. mode having a nodal pattern which approximates the theoretical pattern), to a badly distorted pattern in Fig 6. Bending waveforms recorded in experiment and those constructed theoretically, are shown in Fig 24, lined up beneath the respective coupled modes. So the degree of agreement between theory and experiment in bending waveforms can be compared against the nodal pattern and experimental set up.

The concept of coupled modes appears to have an application in the reversed direction, once it has been verified. The coupled normal modes present in Fig 6 were not identified despite using every available technique. Assuming a coupled mode situation, the coupling region was examined through records of slope and amplitude response which triggered off a process leading to identify the modes. This process is described in Fig 30 and discussed in appendix.

The problem of mode identification is further demonstrated in Fig 28, dealing with a distorted nodal pattern in a manner different from that of Fig 30.

Bending waveform and 'map' of the nodal pattern are recorded. Neither would reveal the identity of the mode in terms of m x n nodal lines. The mode has been identified through comparing the bending waveforms of the uncoupled, to that of the coupled element.

Having verified the concept of coupled modes, mentioned above implies that modal mass and damping of the individual elements remain approximately unchanged due to coupling. This means that those parameters can be determined from the

separate plates, provided that the coupled and uncoupled corresponding modes are similar.

A procedure to obtain modal damping and modal mass required to accommodate eq'ns 1.5 and 1.9, governing energy distribution, was devised in section 2. It involves testing the separate plates to obtain the parameters marked with an asterisk in the R.H.S. and L.H.S. columns of Fig 2.

The appropriate experimental data and calculated magnification factors Q, are presented in table II below. As explained earlier, the subscripts a and b of the uncoupled plates change into subscripts 1 and 2 respectively when the plates become coupled.
Test numbers correspond to the numbering of tests of coupled modes, given here for the convenience of comparing the table to other presentation.

Test	Plate a			Plate b			$\mu = \frac{M_a}{M_b}$	$\frac{C_a}{C_b}$
	Mode mxn	f_n Hz	Q	Mode mxn	f_n Hz	Q		
3	5x3	313.7	62.7	4x3	313.4	38.2	10.46	6.96
7	5x4	382.4	136.6	4x4	384.0	39.6	3.94	1.15
11	3x6	395.9	87.1	3x6	433.5	87.8	.19	.20
13	6x3	426.8	147.2	5x3	455.8	239.9	6.42	11.17
16	4x6	467.9	78.0	2x7	480.0	166.0	.24	.52
26	8x0	645.4	179.0	6x3	632.4	98.8	1.84	.99
30	6x5	701.9	219.3	5x6	729.2	169.6	2.05	1.65

Table II. Experimental data of modal response of the separate plates.

An obvious result of research work using plates specimen vibrating in normal modes, is the accumulation of data on related topics which are not directly relevant to the particular course of work elected.

Such is the information of comparing measured and predicted modal frequencies and the shift of those frequencies owing to coupling, to be discussed in appendix II.

Modal frequencies of each of the elements in the coupled and uncoupled state, are listed in Fig's 22 and 25. For the uncoupled elements, modal frequencies were computed as has been suggested by Warburton. These are compared against the corresponding frequencies obtained in experiments. Results are given in Fig 22 by a chart of the nodal pattern versus modal frequencies, together with the difference between the computed and measured frequencies versus modal frequencies.

The Rayleigh method, from which Warburton derived the method to calculate modal frequencies (11), gives values which are slightly higher than the true values. Hence those calculated frequencies can serve for an upper limit of the frequencies of the corresponding modes obtained from experiments. In addition the difference between the true and calculated frequencies tends to become smaller at higher mode numbers. This trend is also important as an indicating tool.

A similar chart in Fig 25 displays the shift of modal frequencies of the uncoupled elements due to coupling. The technique of identifiying modes through bending waveforms using the scanning rig was fully exploited in the process.

The data of each plate is presented in a separate chart, care taken to indicate modes which are subsequently coupled

together. Thus it becomes possible to observe the direction of modes shift, on the frequency scale, towards the frequency where they are coupled. In the absence of an acceptable theoretical approximation, to calculate modal frequencies of elastically coupled systems, the chart has been comprised solely from experimental data.

This material was used in Fig 26 to show the relationship between the total amount of shift of the modal frequencies owing to coupling (i.e. $\Delta f = f_1 - f_2$), and the difference in the number of nodal lines n_1 and n_2 of the coupled modes $\Delta n = n_1 - n_2$, in absolute values.

The necessary experimental data has been collected as outlined in the section 2. Evaluation and analysis of the data will ensue.

II. Consideration of errors.

Before commencing with the analysis of our findings, the data obtained in the experimental work is examined in order to assess its reliability and accuracy. Such a discussion is essentially inspired by the reports of the 'watch-dog' measures incorporating the normalising factors $\bar{N}_1$ and $\bar{N}_2$, the drift factor S_d, and the factor indicating the presence of flanking energy S_{fr}.

In Fig 14 values of the normalising factors $N_{1,r}$ and $N_{2,r}$ (i.e. of radius of scanning r) are shown to fluctuate about the values of the mean normalising factors $\bar{N}_1$ and $\bar{N}_2$, respectively, some of which fluctuate violently.
In order to grasp the meaning of that phenomanon, we review our techniques to determine the modal response $\bar{X}$ with which N is associated. The process is described by eq'n 2.7 which is

applicable when 2 conditions are met.
First, that the recorded bending waveform, whose mean amplitude is $\bar{X}_m$, and the corresponding theoretically constructed bending waveform, whose mean amplitude is $\bar{X}_t$, are of a similar shape. Second, that both $\bar{X}_m$ and the mean amplitude of the whole element $\bar{X}_p$ are associated with the same normal mode of vibration.
It follows that the values of the normalising factors $N_{1,r}$ and $N_{2,r}$ defined by eq'ns 4.5 and 4.6 and hence $\bar{N}_1$ and $\bar{N}_2$ defined by eq'n 4.7 and 4.8 should remain unchanged, whichever the radii of scanning.

Any deviation from the two conditions mentioned above introduces error into the process resulting in fluctuations of the curve of $(\bar{N} - N_r)$ as observed in Fig 14. Hence the deviation from a mean is proportional to the amount of distortion in the plates response, qualitatively only, because the amplitudes of the curve are relative to the mean. In a quantitative implication of Fig 14 the position of the mean $\bar{N}$ above the zero should be considered as well. Normally this position depends on scale factors of the instrumentation and the level of excitation, a sort of a dimensional factor, but it is proportional to the amount of distortion of the mode shape as detected by the transducer measuring plate response. To illustrate this case, supposing that the whole mode is distorted in a manner resulting in higher values of $\bar{X}_m$ of an element.
Consequently the values of N_r become higher and ultimately $\bar{N}$ is higher, (see eq'ns 4.5 and 4.7 for example).
Should the modal response be predominantly well conditioned, the value of $\bar{N}$ would shift slightly only. The first case may exhibit small fluctuations above a mean being shifted

upward. Then one may erroneously assume that no error is indicated. This is the case of plate 2 in test No. 30 as presented in Fig 15.

The kind of agreement which can be observed between the waveforms is inconsistent with the corresponding curve of Fig 14 which exhibits very small fluctuation about the mean, if any. Hence the mean is shifted here. In contrast, plate 1 of the same test shows a much better agreement between the waveforms while the graph of Fig 14 suggests poorer agreement as compared to plate 2, which demonstrates the second case, of a well conditioned mode.

Those two examples do not invalidate the concept of a normalising factor N, but rather indicate its limitations and demand a search for further means of dealing with errors.

Hence it becomes necessary to resolve the various factors which comprise the plots of $(\bar{N} - N_r)$ into their component-factors in order to study separately each factor affecting determination of plate response.

An additional criteria is needed, to provide a quantitative assessment of the amount of error in the normalising technique. The first step in the procedure is to relate recorded and theoretically constructed bending waveforms. We obtain the factor N_r by dividing through the mean amplitudes of the waves of that r as described by eq'n 2.6. Hence N_r is product of a calibration factor and a factor which is a measure of the amount of agreement between the waveforms. The first, remains unchanged in each graph of Fig 14, while the latter fluctuates as the agreement between the waveforms, and hence the agreement between mode shape varies.

Thus the fluctuations of the graphs exhibit variations of

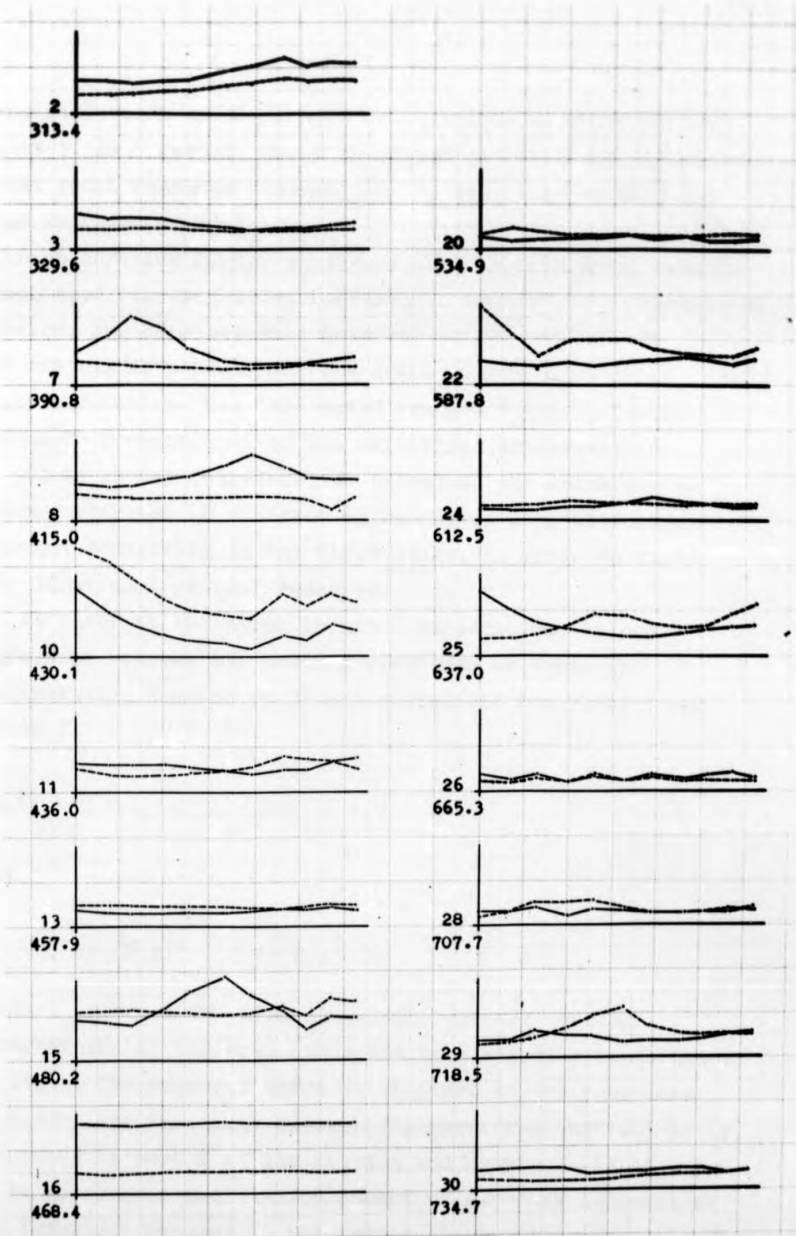

Fig 14. Plots of the normalising factors N versus radii of scanning r, for coupled plate 1 (Full line) and coupled plate 2. Coupled modes are indicated by test number and modal frequency in Hz.

the distortion of the respective vibrational modes in the plates. As a result, error is introduced into the assumption that modal response distribution is described by eq'n 2.2 and represented by $\bar{X}_p$.

The calibration factor mentioned here as that which remains unchanged for each mode, referred to earlier as a dimensional factor, can be determined from the actual calibration of the signal network and the scale factors of the instrumentation. Yet this would resolve $\bar{N}$ into a factor which is proportional to the variations in distortion.

It is chosen therefore, to establish the error due to mode distortion in a direct approach, dealing with each element separately in the first stage, in order to study the individual plates' response.

We refer to the error in modal response due to poor agreement between the bending waveforms as error in reliability, denoted by S_r and calculated for plate 1 and plate 2,

$$(4.9) \qquad S_{1,r} = (A_{1,m}/A_{1,t}) - 1$$

and

$$(4.10) \qquad S_{2,r} = (A_{2,r}/A_{2,t}) - 1$$

where A_m denotes the area under the recorded bending waveform and A_t the area under the theoretically constructed waveform. The recorded curve is obtained in the procedure to assess the agreement between the waveforms quantitatively, described in part I of the section and shown in Fig 15.

We appreciate the limited amount of accuracy inherent in the technique because of the method of choosing the scale of

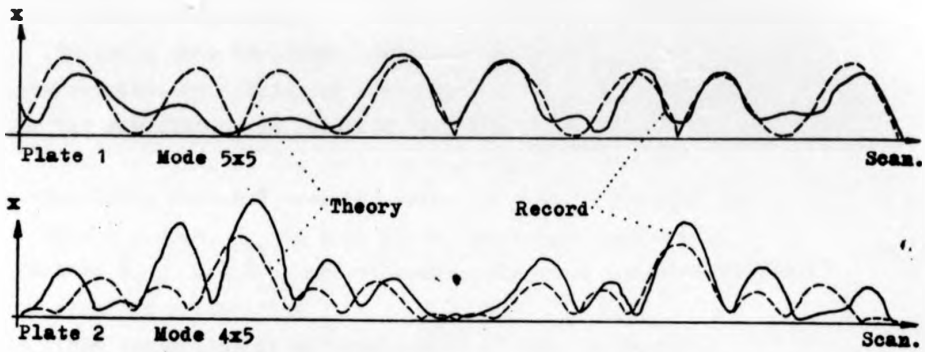

a) Test 15 480.2 Hz

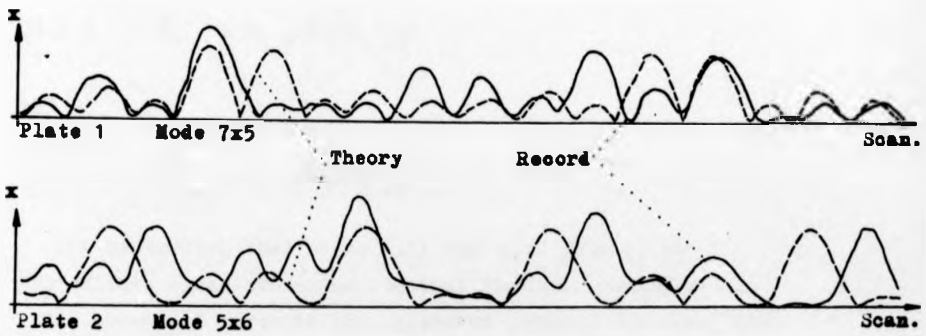

b) Test 30 734.7Hz

Fig 15. Bending waveforms of the coupled plates showing agreement between theoretical and recorded waveforms for quantitative assessment.

the records. Still, the approximation is acceptable since the technique is applied to cases where the mode shape can be identified beyond doubt.

In using this technique, recorded and predicted waveforms are obtained for radius of scanning r = 28cm. The validity of the computation is extended over the whole area of each element by applying the ratio of the value of the mean normalising factor $\bar{N}$ over the value of that factor for the radius r = 28cm, N_{28} in each plate. We assume that the new factors $\bar{S}_{1,r}$ and $\bar{S}_{2,r}$ are approximately space-average factors of error in reliability.

This assumption is an implication of the previous statement that fluctuations of the graphs of $(\bar{N}-N_r)$ are proportional to the variations in the distortion of a mode shape. Thus the factors are given by,

$$\bar{S}_{1,r} = S_{1,r}(\bar{N}_1/N_{1,28}) \tag{4.11}$$

and

$$\bar{S}_{2,r} = S_{2,r}(\bar{N}_2/N_{2,28}) \tag{4.12}$$

The assumption that eq'ns 4.11 and 4.12 provide an approximate space-averaging requires further consideration.

An amount of error in the agreement between the waveforms, results in a different amplitude response distribution, over an element, from that expected through prediction of the vibrational mode shape. This implies straightaway that the effect of a computed factor $\bar{S}_r$ on energy distribution in that element is proportional to the radius of scanning. The larger the radius - the larger the area to which the

specified error applies, and consequently, the error in energy distribution. That is to say that by using eq'ns 4.11 and 4.12 to extend the error factors $S_{1,r}$ and $S_{2,r}$ over the whole plate elements, a similar weight is assigned to every radius. Then if the mode shape is equally distorted over the plate area, the error introduced into energy calculations owing to using those equations will be proportional to the ratios of the ring shaped areas whose mean radii are the radii of scanning.
For the purpose of an overall assessment of the error associated with assuming bending waveform agreement, this procedure gives a satisfactory approximation.

The component error factors $\bar{S}_{1,r}$ and $\bar{S}_{2,r}$ can now be used to study plate vibration in general, or to trace the causes for distortion of the vibrational modes through plots of $\bar{S}_r$ of each plate versus frequency of excitation.
A still further detailed study can be pursued by plotting $\bar{S}_r$ of each plate versus radii of scanning, thus resolving the information contained in Fig 14 into 2 components, one describing distortion distribution. But this investigation is beyond the scope of the section.
Since the discussion centers on the main interest of the project, average response ratio, rather than the isolated response components is important. It follows that we take ratio of error factors of the coupled plates in the same fashion as response ratio is calculated, namely,

$$S_r = \bar{S}_{1,r} / \bar{S}_{2,r} \qquad (4.13)$$

In this way the reliability information is reduced to the amount it would reach if the individual factors were applied

to the individual space-average responses $\bar{\bar{X}}_1$ and $\bar{\bar{X}}_2$ and then ratio computed. So finally we can plot the overall effect of error in reliability in a single graph.

This is presented in Fig 17 in a plot of S_r in db versus modal frequency of the coupled modes and test numbers. The maximum error of -3.19 db occurs in test 7, although from the curves of Fig 14 it would seem that the values of test 10 fluctuate as violently, while the latter shows an error of -.08 db.
This can be understood when the curves of plate 1 and plate 2 in Fig 14 are compared. Both curves nearly coincide, in test 10, which means that the difference in the location of the mean value $\bar{\bar{N}}$ is accommodated by the scale factor.
In contrast, test 7 comprises a comparatively flat curve of plate 2 with a very fluctuating one in plate 1, resulting in the high amount of error.

By reducing the data through eq'n 4.13 we give up an amount of information. This is no disadvantage in view of our ultimate goal.

The negative or positive values of the curve of S_r in Fig 17 indicate that the error associated with waveform agreement is greater in plate 2 or plate 1 respectively. Thus it may be concluded that in 2 out of 10, coupled modes displaying a significant error, plate 1 is predominant. The other 8 are dominated by errors which stem from the driven plate 2. The fact that the remaining seven coupled modes display little error, merely means that the area under their respective measured bending waveforms A_m and predicted waveforms A_t are nearly equal.
The areas are proportional to amplitude response and since the rms value computed as a space-average, the areas would be

proportional to the square of response ratio as well, and hence to energy distribution.

From the aforesaid we learn that applying the method of normalising the theoretical space-average, time-maximum whole plate response $\bar{X}_p$ through the factor N (eq'n 2.6) yields the actual average plate response $\bar{X}$. Using the error factor S_r of eq'n 4.13 provides a measure of the error in the assessment of the average plate response.

Next we discuss the error due to flanking energy which is indicative of the validity, in each test, of eq'n 1.7 based on the assumption that energy flows from one plate to another via the coupling only.

In selecting coupled modes to serve for experimental models we required that the response of suspension frame to specimen excitation should not exceed a specified level, as described in section 2.

The presence of flanking energy in the frame in which the specimen is suspended, when the drive motor is shut down, can be part of the energy generated by the disturbing force only. That amount of energy may flow from the primary plate through the frame to the driven plate avoiding the coupling. Similarly the energy may flow from the driven plate to the primary plate, thus setting up a feed-back loop. In either case we lose control of the quantities of energy flowing via the coupling due to transmission to the frame. An extensive study would be necessary, as well as additional facilities, to determine the direction and magnitude of flow of flanking energy, and its losses in the path of transmission.

So we shall establish the general trend in frame response in relation to vibrational modes of interest, through an

evaluation of the transmissibility factor S_{fr} between the input point of the specimen and a point on the suspension frame where the suspension chords are attached to that frame.

The only parameter of the frame response, open to measurement is acceleration of discrete points. In order to determine the force transmitted to the frame it would be necessary to find the dynamic mass, to determine the mode of vibration and the distribution response of the frame for each frequency of interest.

Since we are not interested in accounting for the flanking energy but rather to keep it within the acceptable limits we apply a slightly modified version of transmissibility where the ratio of amplitude response is computed instead of forces. Then the upper bond of acceptable acceleration is 25 cm/sec^2 at all frequencies. This arrangement is more practical. The procedure involved keeping a watch on frame acceleration signal not to exceed 1.5 mv.

The reason for this upper bond is given in section 3, because it involved some simple testing reported there. The error factor becomes,

$$S_{fr} = \ddot{X}_{fr}/(2\pi f_n)^2 X_{in} \qquad (4.14)$$

where $\ddot{X}_{fr}$ is the frame point acceleration response in cm/sec^2 and X_{in} the specimen input point response.

The plot of S_{fr} versus modal frequency is presented in Fig 10 in a separate coordinate system. We observe that the transmissibility is kept well below the limit for most of the modes, except tests 11 and 29 where the errors are 2.1% and 3.3% respectively.

Comparing the curve of frame acceleration response to that of Fig 12 shows that the frame response is related to mode shape and in particular to the magnification of the normal modes present in the specimen. But by taking ratio in eq'n 4.14 this fact becomes obscure in the plot of S_{fr}.

The error due to flanking energy was regarded negligible thus confirming the validity of eq'n 1.7 and the associated assumption. The plot of S_{fr} is presented in Fig 10 for the purpose of studying plate vibration and the efficiency of the experimental rig to be discussed in appendices.

Next, we proceed to examine the repeatability of the systems' dynamic behaviour.

Experimental data has been recorded over a period of 3 months, which gives rise to a possible error through drift in calibration of the instrumentation, or variations in the systems' response due to changes of temperature, humidity and aging of materials. The technique adopted to detect such error, introduced in chapter 2 yields the error due to drift S_d, being defined as the change in the response ratio of a coupled mode, as modal frequency and force amplitude remain unchanged. The error is considered positive when the response ratio is increased.

When such a check was undertaken, it was associated with the conditions of unchanged modal frequency and forcing level which can always be met. By realignment of the plates, or the vibration generator, the modal frequency can be repeated. The remaining condition is merely a matter of adjustment.

Testing repeatability was performed in both coupled plates simultaneously, for each of the 17 coupled modes of interest. Our main concern of drift is associated with 2 particular dates when the bulk of records of response of the elements

were obtained. Coupling records were obtained in the earlier date and hence are excluded from the consideration.

Drift between the early date and the later date, denoted (E) and (L) respectively, calculated for each plate, is given by,

$$(4.15) \qquad S_{1,d} = \frac{\bar{X}_1 \ (E)}{\bar{X}_1 \ (L)} \qquad \text{and} \qquad (4.16) \qquad S_{2,d} = \frac{\bar{X}_2 \ (E)}{\bar{X}_2 \ (L)}$$

As before, this information is presented in a form to comply with response ratio presentation. By taking ratio of drift error we obtain the overall error introduced into the records S_d,

$$(4.17) \qquad S_d = S_{1,d}/S_{2,d} - 1$$

Values of S_d versus modal frequency are displayed in Fig 17. They were summed up algebraically with those of S_r to give an overall account of error.

A different response level of an element may result from a drift in the calibration of the signal network, a change in the dynamic response, or a combination of both in any proportion.

Since no appreciable amount of drift of the calibration of the instrumentation was observed it is safe to assume that the error indicated by S_d is associated with minor changes in system dynamics, i.e. the dynamic mass, damping , and stiffness of the elements and the coupling.

Those parameters are susceptible to changes in the response distribution where small changes may have a cumulative effect on the response ratio directly, and indirectly by altering the parameters.

That it is possible for the response, of one subsystem or both subsystems, to drift while the natural frequency remains unchanged, becomes apparent from looking into the dynamic behaviour of the theoretical model in eq'n 6.10 put into different form. To maintain the generality of the analysis ω is considered an arbitrary frequency, kept constant. Then,

$$(4.18) \qquad \omega^2 = \frac{k_2+k_n-k_\phi}{M_2} + \frac{k_x+k_\phi}{M_2}\frac{X_1}{X_2}$$

We realise that a change of X_1, X_2 or X_1/X_2 can be compensated by a corresponding change in any number of the other 4 parameters, or 6 if damping is included, leaving ω^2 intact. In actual fact a change of the response is essentially associated with a change of mode shape, hence the rest of the modal parameters change.

Once the response ratio is found to have changed, no practical technique is available to reinstate it without altering modal frequency. So it was regarded an error to be added to that of waveform agreement in Fig 17.

From Fig 17 it is clear that S_d has little effect over the general amount of error in the experimental data, except in the first 3 modes. The curve is dominated by the kind of agreement between the recorded and theoretically constructed bending waveforms, i.e. the amount of mode distortion.

So far, discussion of error and reliability has centered on subsystems' response parameters.

An examination of the coupling response will now follow. This is greatly aided by the records, a sample of which is displayed in Fig's 13 and 30.

Nearly all 30 records are meaningful in the sense that a good correlation appears to exist between amplitude and slope response, and between amplitude and mode shapes which have been identified.

Qualitatively, 2 out of the 17 modes serving for models indicate a discrepancy in the absence of a node expected through mode shape. Otherwise the amount of distortion is small.

Test 2 exhibits a well conditioned mode shape. Since modes 0x6 are present on both sides of the bridge, the slope is very small along the coupling centre line, approaching zero when the amplitude becomes zero, i.e. as one of the six nodal lines intersects with the coupling centre line. (For the relation of test numbers to mode shapes, see table I in part I of the section).

In contrast to test 2, test 7 is an example of a distorted waveform as well as nodal pattern indicated in Fig 13 and indeed in Fig 17, having the highest error of S_r and that of S_d. The evidence of Fig 14, describing the normalising factor N, suggests that this must be attributed to plate 1. This is a case of $n_1=n_2$ which is presented in Fig 13b. The expected point where a nodal line intersects with the coupling centre line is marked. At that point the amplitude and slope must be zero. Evidently the point was shifted to the right hand side of the plot, thus indicating distortion.

The modes of tests 22 and 29, where $n_1 \neq n_2$ still obey the 'rules' regarding the slope and amplitude in the coupling region, except for a slight difference from the simple cases, in the sense that points of zero slope do not match with points of zero amplitude, although nodes are at the correct location as predicted. This phenomenon is expected since the

difference between the number of nodal lines at right angles with the common boundary, results in nodal lines joining the constituent nodal patterns at an angle with the y axis, hence with the coupling centre line.

This can be observed schematicaly in Fig 27 a/1, and in a record of the nodal pattern of Fig 28.

In test 22 the mode present in subsystem 1, which is directly excited, appears to be predominant in the coupling region. This is implied from the location of the nodes conforming to the nodal pattern of the mode excited in the plate.

The response of subsystem 2 is higher than that of subsystem 1 in mode 29. Consequently nodes are located in some mean position between those predicted for $n_1=7$ and $n_2=9$.

The overall majority of the coupled modes response in the coupling region fall into the category of modes 2 and 22, as described here.

The reason to analyse coupling region response is to facilitate a concurrent assessment of the reliability of an expression of coupling parameters, governing response ratio, alongside with appreciating that of the measured response ratio.

Rather than working out a quantitative presentation of the errors associated with coupling response, groups of modes will be discussed on their merits.

III. Analysis.

In this part we discuss response and energy distribution. Findings related to plate vibration and the apparatus are discussed in the appendices.

a) Response distribution.

The primary object of this research project was to establish the relationship between response ratio of the coupled plates and a set of parameters, open to measurement, representing the coupling and whole system response. This is guided by an analogy of the simple 2-degree-of-freedom model developed in appendix I as a crude approximation of the experimental model.

The aim is to facilitate assessment of the response of a coupled plate by measurement, other than the individual plates, using practical techniques which can be adopted for industrial purposes. e.g. Such techniques which do not require to modify a given system or to provide inertial rest of a subsystem, i.e. a situation of zero acceleration.

Examination of the validity and accuracy of such relationship being determined and expressed mathematically, is based upon a conceptual analysis and on comparing values of response ratio, obtained by computation using that expression, to those measured directly in experiments.

In the theoretical model, response ratio of the 2 masses is related to the coupling conditions in eq'n 6.14 in terms of transverse and rotary receptances.

It is required to find a combination of parameters, defined in the elastic system, to provide an analogy of eq'n 6.14 which will accommodate the parameters obtained from the experimental data.

The task of seeking analogy of the left hand side of the equation, representing the ratio of the response of the 2 subsystems, is significently different from that of interpreting the right hand side of the equation - the coupling conditions, in terms of parameters of an elastic system, involving a conceptual difficulty.

It is convenient to define the motion of the elastic subsystems in terms of rigid body motion whose amplitudes become the space-average response amplitudes $\bar{X}_1$ and $\bar{X}_2$ of the normal modes given by eq'ns 2.2 and 2.7 when applied to each coupled plate.

Further we wish to establish an analogy between the coupling receptances of the model, i.e. the right hand side of eq'n 6.14 and the measured coupling receptances, presented in table I.

Although the parameters in both cases are given as coupling rotary and transverse receptances, it is clear that there is no obvious analogy here.

In the theoretical model it was assumed that the coupling lever was hinged to each massive body at the point, characterised by the coordinate of displacement, so as to transmit the excitation from the primary to the driven body. Such a link is capable of transmitting transverse motion only. So, that both, transverse and rotary, modes of the coupling are excited by transverse motion of the primary mass, and transformed back into transverse motion when driving the coupled body.

Thus the transverse motion of the exciting force is resolved in the coupling into transverse and rotary components to provide the analogy of such motion in the coupling of the coupled plates system. The excitation is transmitted from

the primary to the driven body by the coupling lever whose motion may consist of varying relative magnitudes of transverse and rotary components.
Extreme cases occur when either the amplitude or slope of the lever become zero. From eq'n 6.14 we see that when the amplitude receptance $\alpha_x = 0$ then $X_1/X_2 = -1$ and the two masses move in anti-phase, the linking lever rotates only
As the slope receptance $\alpha_\phi = 0$ then $X_1/X_2 = +1$, the two masses move in phase and the coupling lever moves in translation only.

The experimental model comprises 2 subsystems, of distributed mass and elasticity, coupled together by an integral bridge. This kind of coupling stretches over a finite length thus connecting points of different slopes and amplitudes.
Consequently elastic interaction occurs between the constituent elements, depending on the mode of motion present in each element, affecting mode shapes in both coupled plates.
There is no provision for this kind of interaction in the theoretical model.

An extreme case of mode of motion of the coupling in the elastic system similar to those of the model described above is normally not likely to appear.

The case when the motion is transmitted by rotary motion only, along the entire length of coupling, requires that a nodal line coincides with the coupling centre line. It has been mentioned earlier that the edges of free plates are of maximum displacement for each bending wave at right angles to the coupling centre line. Hence such a case requires an extraneous constraint, that is to change the

condition of the coupled edge into a hinged boundary.

The second case of zero rotary motion along the coupling centre line may occur if the nodal lines, parallel to the coupled edge in both plates are located in such a distance from the coupled edge, as to be matched by an amplitude response ratio, making the coupling centre line an antinode. This also requires that the nodal lines $n_1 = n_2$ which is nearly the case of mode 2 in Fig 13a.

But contrary to the theoretical model, this does not imply equal response of both subsystems.

Further in comparing the model with a coupled plate system it is important to note that in a primary rigid body, input point, space-average, and coupling motions are described by the same coordinate, while in an elastic element not only these are different parameters, but also the motion is transmitted from the point of forcing to the area of the element and the coupling in different ways in normal modes, from off-mode motion. The nearest equivalent to the rigid body motion is that of normal modes, being particular cases for elastic systems.

An important feature of this comparison, which has a practical implication on the problem of noise transmission is related to the dynamic vibration absorber effect. In the theoretical model, the natural frequency of the driven mass remains significant in the sense that at this frequency only, energy is not shared between the coupled masses, but drained to the driven mass, as shown by setting $\omega^2 = K_2/M_2$ in eq'n 6.10 in section 6 I.
Such a state is not possible in the kind of coupling where elastic interaction occurs between the coupled elements. Moreover, the coupled mode is one entity although

a different nodal pattern can be identified in each element.

At this stage, the conceptual drawbacks which appear to restrict the extent of the analogy between the theoretical and experimental models may be summarized.

(i) The motion of an elastic system can be assumed equivalent of a rigid body motion in the state of a normal mode only. Yet in contrast to the model, motion of the element, the coupling, and the point of forcing, are described each by a different coordinate.

(ii) In elastic coupling, both rotary and transverse motions transmit excitation and elastic interaction being distributed over a finite length of the common boundary. In the model, coupling at a point by a hinge, enables the system to have an additional significant frequency, although a 2-degree-of-freedom system.

So, being interested in normal modes of vibration, the analogy can still be used to guide our choice of the course of action in analysing findings.

It becomes essential, therefore, to look into the kind of relationship in the RHS of eq'ns 6.10 and 6.14 in an attempt to offer a mathematical expression of similar characteristics, consisting of parameters of the elastic system.

The first alternative involves finding parameters of the experimental model which can be the equivalent of parameters of theoretical model.

From eq'ns 2.4, 2.5 and 6.2 it becomes apparent that the subsystems' parameters of the theoretical model defined in the uncoupled and coupled-blocked situations. (i.e. such that one subsystem is allowed to vibrate, while the other

is held fixed). Determination of analogous parameters of the elastic subsystems is not feasible. Moreover, it is impractical to resort to decoupling a given coupled system in order to obtain dynamic parameters. That consideration rules out the possibility to apply eq'n 6.10 directly to the elastic system.

Nevertheless, comparing eq'ns 6.10 and 6.14 reveals that response ratio is expressed in terms of the systems' parameters in the numerator, and coupling strength in the denominator.

The aforesaid implies that response ratio is inversly proportional to the coupling strength, and that the RHS of eq'n 6.14 can be a combination of the coupling response parameters.

This trend is an essential part of the characteristics of eq'n 6.14 and must be satisfied by the analogous expression. In order to simplify the process we regard the RHS of eq'n 6.14 as the independent variable, and the LHS as the dependent variable. Then the equation yields a plot of a straight line at 45 degrees to the axes, being of the form $y=x$. This means that we expect a plot of measured response ratio versus response ratio, calculated by an expression, analogous of the RHS of eq'n 6.14, to conform to the straight line of $y=x$.

Response ratio of the coupled plates is obtained by taking ratio of the space-average, time-maximum response $\bar{\bar{X}}_1$ and $\bar{\bar{X}}_2$ of plate 1 and 2 respectively. Applying eq'n 2.7 to each plate we obtain,

(4.19) $\bar{\bar{X}}_1 = \bar{\bar{X}}_{1,p}(\bar{\bar{X}}_m/X_t)_1$ and (4.20) $\bar{\bar{X}}_2 = \bar{\bar{X}}_{2,p}(\bar{\bar{X}}_m/\bar{\bar{X}}_t)_2$

and taking ratio, denoted by m (for measured) we have,

$$(4.21) \qquad (\bar{X}_1/\bar{X}_2)_m = \frac{\bar{X}_{1,p}}{\bar{X}_{2,p}} \frac{\bar{X}_{1,m}}{\bar{X}_{2,m}} \frac{\bar{X}_{2,t}}{\bar{X}_{1,t}}$$

Subject to the evaluation of the error in the data of the parameters of eq'n 4.21 it might be advisable to correct the values obtained from the equation according to the plot of S_{r+d} in Fig 17.
But it is more informative to compare measured and calculated response ratios with reference to that plot because of the limited amount of accuracy inherent in the technique to determine S_r which is predominant in Fig 17.

Next we turn to obtain a response ratio to be calculated through an analogy of the RHS of eq'n 6.14 in terms of elastic parameters.

As yet no mathematical formulation, in elastic systems is available, correlating the response of subsystems to coupling response parameters. We resort therefore to an empirical method in search of such an expression.

Despite the analysis it would be only obvious that the first expression that we examine for an analogy of the RHS of eq'n 6.14 is that term itself where α_x and α_ϕ have been drawn from table I. The expression takes the form,

$$(4.22) \qquad (X_1/X_2)_c = \frac{\alpha_x - \alpha_\phi}{\alpha_x + \alpha_\phi}$$

where $(X_1/X_2)_c$ represents the response ratio and the subscript c denotes 'calculated' values.

Now testing procedure is set whereby any function, analogous of the RHS of eq'n 6.14 is displayed in a plot of

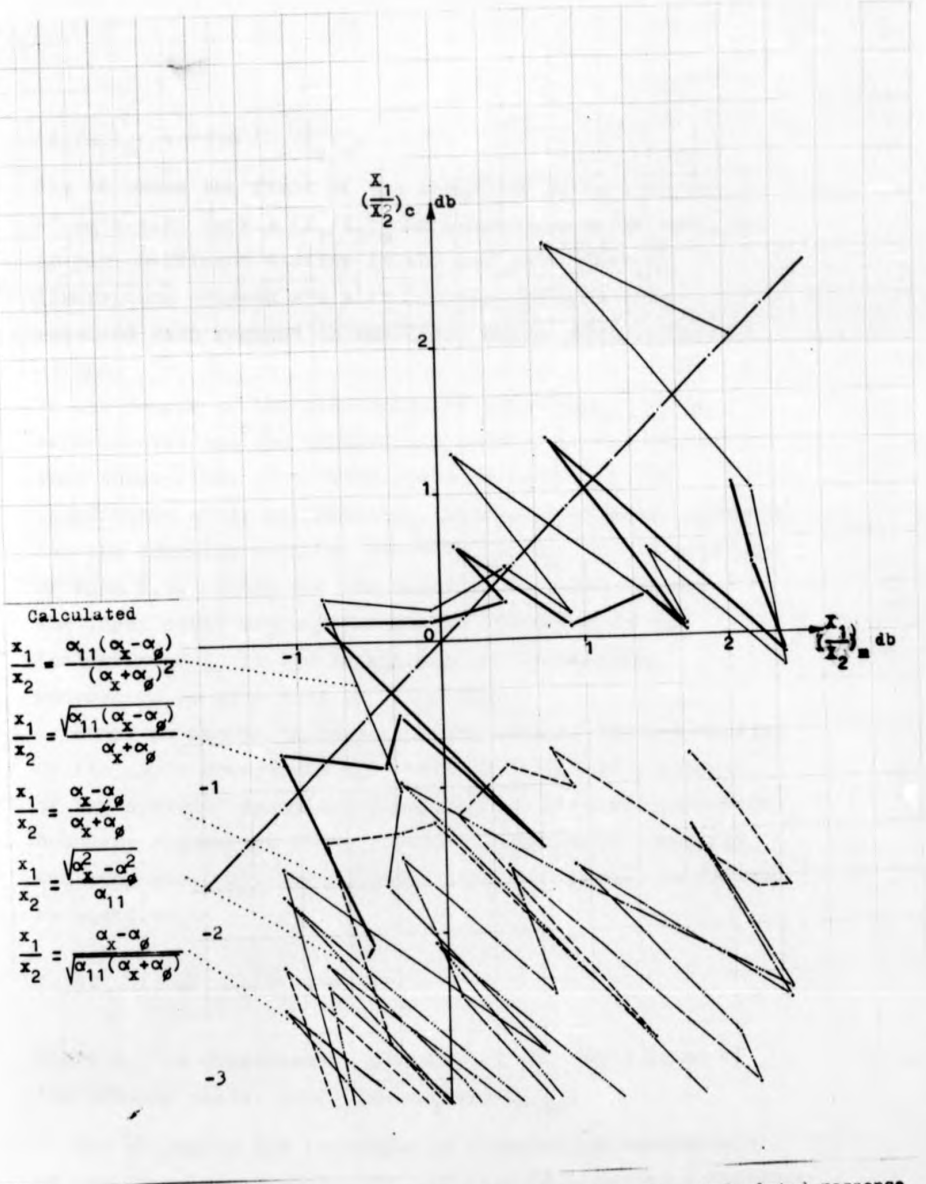

Fig 16. Plot of measured versus calculated response ratio, Calculated response ratio was obtained from 5 different expressions of α_{11} , α_x and α_ϕ .

$(X_1/X_2)_m$ versus $(X_1/X_2)_c$.

Fig 16 shows the field of the procedure where the plot of eq'n 4.22 versus $(X_1/X_2)_m$ is compared against the plot of y=x, mentioned earlier in the analysis. Thus the discrepancy between the plot and the straight line, measured with respect to the line, varies from -.4db to -3.3db.

In the course of the discussion of the analogy of the experimental and the theoretical models, it was stressed that three kinds of motions are represented in the coordinates of displacement X_1, namly, input point, element, and the coupling motions. The term $(\alpha_x - \alpha_\phi)$ in the numerator of eq'n 6.14 allows for the systems' response through the input point response as may be indicated by the inclusion of X_1 in the definition of the coupling receptance by eq'n 6.13 of the model.

Hence we choose to represent the elastic coupled system by its input receptance α_{11} which is in itself a measure of the systems' dynamics, depending on material properties, boundary conditions (that includes conservative coupling) and body geometry. The measured input receptance is defined by equation,

$$(4.23) \qquad \alpha_{11} = X_{11} / F$$

where X_{11} is displacement response at the input point of the primary plate, sometimes denoted $X_{1,in}$.

Now we employ the technique of formulating expressions of the three receptances, α_{11}, α_x and α_ϕ, having a response such that a plot of $(X_i/X_2)_m$ versus $(X_i/X_2)_c$ yields a plot close to y=x.

An infinite number of combinations is available, and with the aid of a digital computer it would probably be possible to find a combination which yields a plot of y=x from the experimental data, or at least showing a negligible amount of divergence.

We adopt the attitude, therefore, that an expression must satisfy in some manner the analogy of the coupling strength, and as a whole remain as simple a combination, not exceeding second order (or half order), even at a cost of giving up an amount of accuracy. The acceptable amount of error can not be determined before hand, and will be decided in the course of the procedure.

With those guide lines borne in mind, 48 different expressions were combined and examined.

Rather than try randomly chosen expressions, a procedure was outlined whereby such an expression is obtained. This starts with the expression of the RHS of eq'n 6.14 itself being modified using one or more of the operation : add or subtract a term, compute an inverse, and finally convert the expression thus obtained into a form of an average of elastic parameters of one kind or another so that the overall combination remains, as much as possible, a clear analogy of the original term of eq'n 6.14 except in a few cases.

This procedure repeated for each of the 48 expressions on the basis of the guide lines, while examining the effect of the recent manipulation on agreement with the plot of y=x.

In order to offer a closer view of that procedure some of the expressions are presented in table III below. They are marked by the test serial number and the maximum

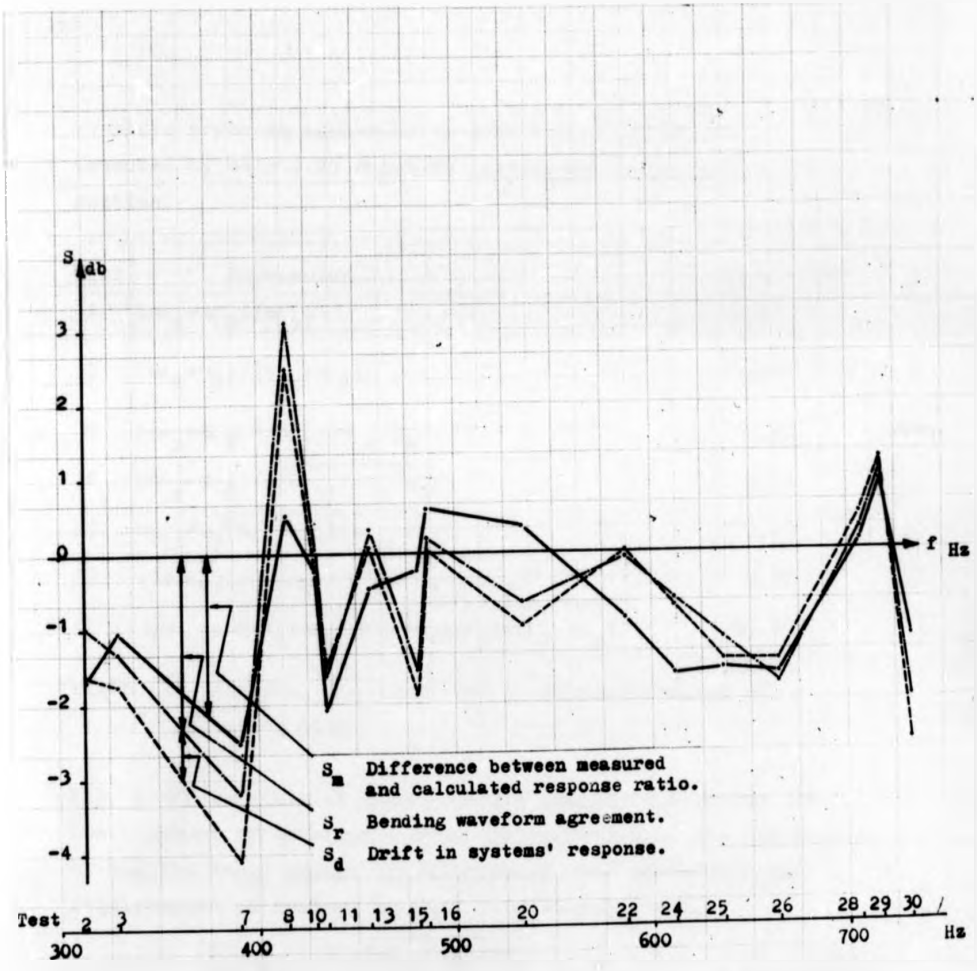

Fig 17. Plot of the difference between measured and calculated response ratio of the coupled plates, compared to errors in experimental data.

absolute error in agreement is indicated. The error was computed by eq'n 4.25 which is introduced later in the section.

Test	Expression	Error (db)
1	$(\alpha_x-\alpha_\phi)/\alpha_{11}$	10.00
3	$(\alpha_x+\alpha_\phi)/(\alpha_x-\alpha_\phi)$	8.01
6	$(\alpha_x+\alpha_\phi)^2/\alpha_{11}(\alpha_x-\alpha_\phi)$	4.86
15	$(\alpha_x-\alpha_\phi)/\sqrt{\alpha_{11}(\alpha_x+\alpha_\phi)}$	8.54
25	$\alpha_{11}/\sqrt{(\alpha_x+\alpha_\phi)(\alpha_x-\alpha_\phi)}$	7.43
38	$\sqrt{2\alpha_{11}(\alpha_x-\alpha_\phi)/\alpha_{11}^2+(\alpha_x+\alpha_\phi)^2}$	3.77
42	$\sqrt{\alpha_{11}^2+(\alpha_x+\alpha_\phi)^2/2(\alpha_x+\alpha_\phi)(\alpha_x-\alpha_\phi)}$	16.29

Table III. Asample of expressions to provide analogy of eq'n 6.14

Fig 16 offers plots of 5 alternative expressions having the lower amount of divergence from our expectation. The expression having the least amount of discrepancy, yet satisfying the requirements of analogy to eq'n 6.14 is presented,

$$(4.24) \qquad (X_1/X_2)_c = \frac{\sqrt{\alpha_{11}(\alpha_x-\alpha_\phi)}}{\alpha_x+\alpha_\phi}$$

In this expression the denominator presents an analogy of the coupling conditions. If the terms $(\alpha_x-\alpha_\phi)$ can be regarded a single quantity, then the numerator is the geometric mean of the quantities α_{11} and $(\alpha_x-\alpha_\phi)$. A characteristics of a geometric mean is that if the two

quantities vary in such a way that their sum remains constant, then their product increases as their difference diminishes, until the quantities become equal, when their product has its greatest value.

Should a situation occur that $\alpha_{11}+(\alpha_x-\alpha_\phi)=$ Constant, then a possibility may arise when $\alpha_{11}=(\alpha_x-\alpha_\phi)$ and consequently the numerator of eq'n 4.24 becomes,

$$\sqrt{(\alpha_x-\alpha_\phi)(\alpha_x-\alpha_\phi)} = \alpha_x-\alpha_\phi$$

and eq'n 4.24 is transformed into eq'n 4.22 so that . this is the particular and only case when the response ratio of the elastic system is governed by the same equation as the simple model.

Note that the bottom equation in Fig 16 may lead to the same result if $\alpha_{11}+(\alpha_x+\alpha_\phi)$ = Constant.

Although it is not possible to analyse if either sum may become constant without a theoretical development, we compare the feasibility of the two sums being constant.

In the case of the numerator of eq'n 4.24 this requires α_ϕ to grow faster than α_x with an increase of α_{11}, while in the second case having the sum constant requires that either α_ϕ or α_x diminishes. The latter condition can not be met in coupled plates because if α_ϕ is not zero it will increase with α_x.

The general trend of the plot of eq'n 4.24 and the top equation in Fig 16 (which is the square of eq'n 4.24) versus $(\bar{X}_1/\bar{X}_2)_m$ follow the curve y=x, although fluctuating about it. The amplitudes of fluctuations of eq'n 4.24 are smaller displaying error between .17db and 2.52db, hence that equation

is preferred. The plots of the remaining 46 expressions tested, were mostly confined to one side of the line y=x, or the other side.

In order to correlate the deviation from our expectation in Fig 16 with the error in the experimental data presented in Fig 17 we refer to the amplitude of fluctuations of a plot about the straight line y=x as the difference between the measured and calculated response ratio denoted by S_m and calculated,

$$(4.25) \qquad S_m = (\bar{X}_1/\bar{X}_2)_m(\bar{X}_1/\bar{X}_2)_c - 1$$

values obtained from this equation yield a plot of S_m versus modal frequency in Fig 17.

Apparently the difference S_m can be attributed mainly to the error in the measured response ratio. This is suggested by the kind of agreement between the curves of S_m and S_{r+d}.

Bearing in mind this close resemblance of the curves despite the method employed to determine the agreement between the recorded and predicted bending waveforms, and that the region of the coupling displayed distorted mode shapes in 2 modes only, (as in mode 7 of Fig 13a) it would be correct to say that the factors S_r and S_d dominate the amount of error in S_m, whereas the other factors mentioned above and the agreement between the experimental and the theoretical models played a limited role only.

The analysis of this part of the section corroborates the preference given to eq'n 4.24 as an empiric equation to compute the space-average, time-maximum response ratio of a pair of coupled plates, being an approximation.

This latter point is implied from the technique applied

to measure the response ratio which depends on a well conditioned mode shape, and the effects of rotary inertia mainly.

It ought to be pointed out that, like rotary inertia, the relative importance of coupling rotary as compared to transverse motion increases with mode order, as the number of nodal lines m, (parallel to the coupled edges) become greater. This may require that slope receptance α_{ϕ} be expressed in eq'n 4.24 in a manner, compatible with the change of the relative effect.

b). Energy distribution.

Calculations of energy are essentially subject to the consideration of reliability, error and accuracy discussed in the previous parts of the section, because they are based on the measured response ratio of the coupled and uncoupled elements.

The method suggested in part a) of the section applied to calculations of response ratio of coupled plates only, since it is related to coupling response parameters.

Thus energy parameters are computed using table II and the measured response data.

It was chosen to calculate and plot 6 parameters versus modal frequency for each of the 7 modes whose experimental data is available, to give an insight into energy relations, assess interrelation between parameters and compare trends to previous investigations referred to in section 1.

This information is presented in Fig 18 in two groups. Group (a) shows parameters related to energy sharing in ratio form. A plot of (measured) squared response ratio is

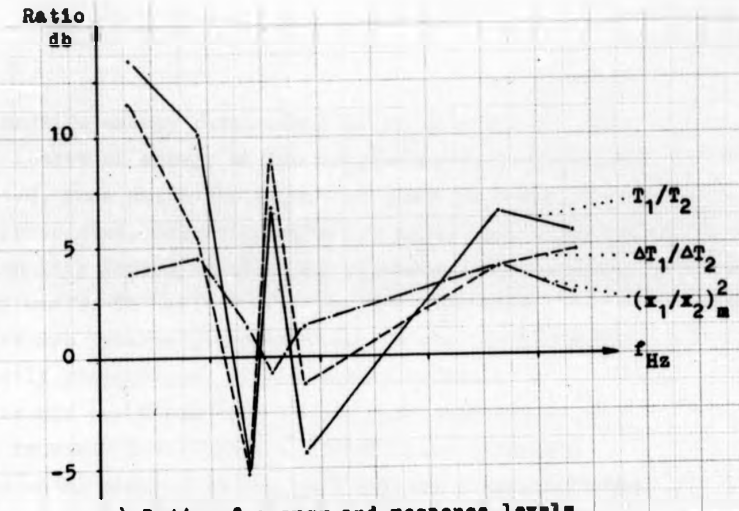

a) Ratio of energy and response levels.

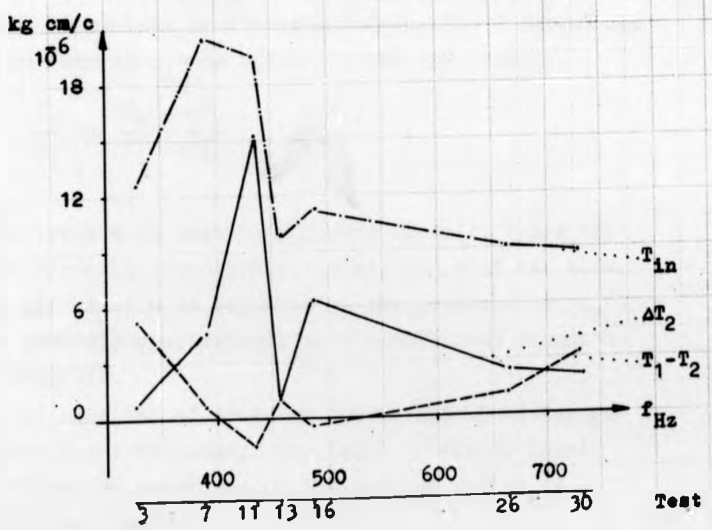

b) Level of energy per cycle of oscillation.

Fig 18. Energy distribution in coupled plates system.

given alongside energy ratio computed by eq'n 1.5 and the ratio of losses of energy in the coupled plates, calculated by eq'n 1.8, from which the effect of modal mass and damping can be appreciated. Observing eq'n 1.5 shows that μ is the proportionality factor correlating response ratio squared, to energy ratio. The effect of μ is such that those parameters are inversely proportional in the first 4 modes and directly proportional in the last 3 modes.

To this end our claim that it was more appropriate to focus on response ratio until a satisfactory technique to obtain modal parameters has been devised - was confirmed by the important effect of the variations of the modal mass.

A similar consideration seems to stem from comparing the plots of energy ratio T_1/T_2 and loss ratio $\Delta T_1/\Delta T_2$.

The proportionality coefficient between the 2 curves can be obtained from comparing eq'ns 1.5 and 1.8 namely,

$$(4.26) \qquad \frac{T_1}{T_2} = \mu \frac{C_2}{C_1} \cdot \frac{\Delta T_1}{\Delta T_2}$$

Although μ appears in this coefficient as well, these two curves are directly proportional in all modes of the plot. Hence the effect of μ is adjusted by the presence of C_2/C_1 which are inversly proportional in a complicated manner as eq'n 2.5 suggests.

Group (b) consists of plots of the levels of energy per cycle versus modal frequency. The level of energy input from the vibration generator to the coupled system is obtained by the equation,

$$(4.27) \qquad T_{in} = FX_{in}(2\pi f)$$

which was given in section 2, where X_{in} is the input point displacement response and f the frequency of the exciting force F. The amount of energy flow, through the coupling from the primary to the driven plate, per cycle is obtained using eq'n 1.9 where the generalised coordinate q is replaced by the space-average, time-maximum coordinate $\bar{X}$.

Finally we calculate the time-maximum difference in the level of the kinetic energies, per cycle $(T_1-T_2)/f_n$, stored in the coupled plates system. It is sufficient to determine the kinetic energy stored in one element, say plate 2, to obtain the energy difference using the energy ratio as follows,

$$(4.28) \quad T_2\left(\frac{T_1}{T_2} - 1\right) = T_1 - T_2$$

where T_1/T_2 is given by eq'n 1.5 and T_2 can be computed using eq'n 1.1 where the generalised coordinate of velocity $\dot{q}$ is replaced by $2\pi f\bar{X}$,

$$(4.29) \quad T_2 = {}^1/_2\, M_2(2 f_n\bar{X})^2$$

The mass of the element $M_2 = M_b$ is obtained by regarding the normal mode of a separate plate a single-degree-of-freedom system, as suggested in section 2, and authorised by the coupled mode concept. Then,

$$(4.30) \quad M_b = \frac{C_b}{4\pi f_{n,b}} \left(4Q_b^2 - 1\right)^{1/2}$$

where C_b is given by eq'n 2.3 being applied to the separate element b, and eq'n 4.30 likewise.

The values of the energy difference per cycle thus obtained and plotted in Fig 18 complete group (b). Comparing the graphs of the flow and energy difference reveals the peculiar phenomenon that the flow ΔT_2 is consistently inversely proportional to (T_1-T_2). In fact the highest rate of flow occurs in mode 11 where the energy difference has a negative value, that is the receiving element stores more energy than the transmitting one. Energy does not tend towards equipartitioning, as can be concluded from the fact that ΔT_2 still has a finite value as T_1-T_2 intersects with x axis.

Energy alwaysflows from the primary plate to the driven plate independent of the energy difference and the level of sharing of energy, since ΔT_2 is always positive.

The fact that ΔT_2 is inversely proportional to T_1/T_2 is quite obvious and can be shown mathematically as eq'n 1.5 is substituted into eq'n 1.9 and we obtain,

$$(4.31) \qquad \Delta T_2 = \frac{T_{in}}{1+\frac{1}{k}\frac{C_1}{C_2}\frac{T_1}{T_2}}$$

The physical interpretation is that as the ratio of energies stored in the coupled plates is increased, the amount of energy needed to maintain the motions changes accordingly. Thus if T_1/T_2 is greater ΔT_2 becomes smaller as compared to ΔT_1 which is clearly visible in mode 3 and 13 in particular.

It has been mentioned in several parts of the thesis that studying energy distribution was considered a matter for further development. The main reason for that, was lack of

means and techniques to obtain modal parameters to a good accuracy in experimental work and in practice.

Determination of modal mass and damping by the technique engaged in the project is closely linked with measuring the distribution of energy dissipation in an element. Accuracy of such results depends largely on the similarity between the vibrational modes present in the coupled and separate plates, where the error is proportional to the square of the error in the amplitude response distribution. Consequently this error handicaps a detailed analysis of energy distribution.

An additional factor of limitation was in that the ratio of energy dissipated in the two elements depends on damping coefficient of the modes, hence being fixed quantities per a pair of coupled modes.

In a more comprehensive study of energy distribution related to coupling conditions it would be essential to introduce some technique of varying the dissipation of the driven element. Then the effect of varying amount of energy flow through a coupling of fixed physical size can be examined.

This topic is further discussed in the ensuing section.

5.CONCLUSIONS.

In this section we sum up the main findings of the thesis and evaluate their validity, applications, and potentialities. This is done by introducing conclusions related to the object together with an assessment of their applicability.

A brief survey follows, of potential applications of the findings of the project to practical structures and to additional roles in laboratory research. Problems arising from limitations inherent in the technique related to the accuracy and validity of the results, and restrictions which stem from the particular conditions of the experimental work having a bearing on the applicability of the findings are pointed out.
Additional research effort is suggested alongside, to answer those problems, thus improving the generality of the method of estimating response distribution suggested in the thesis. Some additional development of the apparatus being directly related to this survey are mentioned.

The section closes with concluding remarks and summary of the suggested additional research. Although conclusions related to the potentialities of the research rig are important, they were excluded from this section and are given in the appendix.

I. Response distribution.

In this thesis, it has been shown experimentally that the space-average, time-maximum ratio of the response of elements conservatively coupled, is proportional to an empiric expression of the space-average, time-maximum rotary and transverse receptances of the coupling, and time-maximum

receptance of the point where the disturbing force is applied.

The first two receptances represent modal coupling conditions, and the latter receptance represents the systems modal response. Those receptances in the expression of the response ratio (eq'n 4.24), are open to measurement, and indeed can be measured employing only comparatively simple means and techniques.

Hence a method is suggested whereby a nondimensional modal response ratio, called henceforth the 'ratio factor', is obtained from applying the expression to the 3 modal receptances for a given coupled system vibrating in a normal mode. The ratio factor thus obtained is a measure of the response ratio in such a manner that if the mass distribution of the coupled elements is known, the square of ratio factor becomes a measure of energy sharing between the coupled elements.

The method of using the ratio factor to establish modal response distribution is a practical tool to tackle the basic problem of a pair of coupled elements, as Ungar puts it "If one plate is exposed to a disturbing force so that it vibrates a given amount, how much will the coupled plate vibrate".

In particular this method can provide straightaway a useful tool to examine the effectiveness of creating impedance mismatching, by changing the dimensions or geometry of an element, to minimize noise transmission.

Having established a method of dealing with response distribution of a simple model of coupled plates as a first step, one can think of the ensuing step being the potential applications of the 'ratio factor' method to complex structures, which we prefer to categorise by two different typical

combinations of practical coupled structural elements, somewhat simplified. The first example is described in terms of a chain of coupled elements of the superstructure of a submarine say, linking the engine room and the hull, where sound emitted from the craft is of a particular concern for operation purpose. From the point of view of noise transmission, this case may be regarded a series connection of structural members.

The procedure of estimating the response of hull panels to engine excitation is essentially broken down into determinations of the response sharing between pairs of constituent elements of the structure, by measuring the coupling and input point receptance. In such a process, the subassembly of the structure on either side of a structural joint, selected for a coupling, is considered a subsystem.

The second example of a potential application of the method, based on the 'ratio factor' to complex structures can be considered a parallel combination of structural elements from the consideration of energy transmission, where the element of interest is connected to several other structural members along different edges. A typical example is that of a car body. The roof panel receives its excitation due to road and engine vibration from the undercarriage through the pillars on which it is supported. If the role of the pillars as vibration transmitters can be established, it would greatly assist to reduce noise in the car. This can be done by a simultaneous determination of the sharing of response between the car understructure and the pillars, thereby the relative amount of excitation of the pillars is obtained. The process is repeated for the coupling between the top part of the pillars and roof panel, the pillars

being sources of excitation. Twofold information is thus obtained. Firstly, whether the transmission of vibration is suppressed or magnified through the effect of resonant motion of a pillar. Secondly, if and which of the pillars has a predominant role in exciting the roof panel.

The ratio of the response of constituent structural members is obtained from applying eq'n 4.24 to the coupling and input receptaces which can be measured simultaneously at any number of structural joints of the system, being regarded coupling, without interfering with its dynamical behaviour, which is fundamental to treating cases of multiple coupling.

Hence those examples demonstrate the wide range of potential applications of the method, of estimating response ratio, to practical structures.

An important tool for investigating energy transmission in structures is the coupled mode formulation of structural vibration problems.

It was verified and demonstrated in the thesis, through experimental evidence, that it is possible to divide a structure, vibrating in a normal mode, into isolated sub - structures and then to couple together modes of these substructures to obtain a formulation of the dynamical behaviour of the coupled system.

It was further shown how this formulation can be utilized to assess the distribution of modal parameters as mass, damping, and stiffness, in coupled plate system.
Thus applying the method suggested to estimate response ratio by measuring the coupling and input receptances to accommodate eq'n 4.24, and the coupled mode formulation, to a system of

coupled elements . can yield the energy distribution parameters.

II. Validity and extension of findings.

In the preceding part of the section we introduced our finding that space-average, time maximum ratio of the response of coupled elements is obtained from an expression of the space-average, time-maximum rotary and transverse receptances, and the time-maximum input point receptance, which are open to measurement, followed by a brief survey of the potentialities of the method to estimate response distribution, based on the 'ratio factor'.

But application of the method to practical problems involves a number of assumptions and conditions that require further investigation. These stem from the particular conditions of the testing set-up and procedures which were essential to provide a simplified research model, obviously applicable to a limited scope of practical problems, until further developed.

One problem area concerns the assumption that rotary inertia has a negligible effect on energy distribution over an element vibrating in a low order mode. Consequently there is no provision in the expression of eq'n 4.24 to allow for this effect.
Such an assumption holds as long as the relative importance of rotary motion is small in order of magnitude as compared to transverse motion, which is normally the case in low order mode. The task to determine the relative importance of those kinds of motion in modes, other than the range of modes in the experiments, is difficult and often not possible.

Hence a significant error in the results of estimating

response ratio will be associated with testing a system where the relative importance of the effect is unknown, where it is known to be pronounced due to exciting high order mode, and where the coupled elements each have widely different characteristics with respect to the relative importance of rotary inertia.

The effect of the relative importance of rotary as compared to transverse motion in the coupling region, on the ratio factor is likely to increase with increase mode order . Eq'n 4.24 being an empiric expression is essentially related to the sample of data obtained in the experiments. Hence findings hold for the kind of response of the system experienced in the frequency band of interest, i.e. the range of mode order which were present in the tested elements.

One may assume that as the spacing between the nodal lines m, parallel to the coupled edge, become smaller in higher order mode, the relative magnitude of the slope in the coupling is increased as compared to the amplitude. In the kind of structures used for the specimen in the project, a similar effect will occur in the coupled elements. The error introduced into the estimate of response ratio owing to higher order mode is expected to be proportional to the difference in the rate of change of the relative importance of rotary motion in the coupling, as the relative importance of rotary motion in the elements.

No conclusion can be made, at this stage, as to the magnitude of such error and whether it will tend to over or underestimate the response ratio obtained from eq'n 4.24 as presented.

In order to extend the results to higher frequencies as well, it becomes necessary to incorporate rotary motion in the

consideration of response ratio of the coupled elements and to study its relationship to coupling and excitation parameters in higher order mode where the effect of rotary motion is more in evidence.

This course of action poses two main difficulties. It would seem that a preliminary stage of such work will be essentially engaged in developing techniques to assess actual rotary motion distribution over an element, and a method by which both rotary and transverse motion responses could be expressed by a single parameter in a manner compatible with their relative importance . The latter step is mandatory in order to establish the relative effect of rotary coupling motion in higher order mode, unless it can be verified that the effect of rotary inertia remains insignificant in the range of frequency and common structural components, in normal engineering practice.

A second problem area concerns the conditions of the coupling as implied from the kind of experimental model, and regarding the assumption of a conservative coupling. In realistic structural joints, a truely conservative coupling is possible only if the two subsystems are connected integrally. For other means of connecting together structural members, a relative motion of the elements at the joint is bound to occur, resulting in losses of energy. But if those losses can be regarded as small, as compared to the losses associated with the motion of the elements, the assumption of a conservative coupling is justified.

We have shown that the expression (eq'n 4.24) of rotary and transverse coupling receptances and input receptance determines a 'ratio factor' which is a measure of average

response distribution in a system elastically coupled, i.e. where elastic interaction occurs between the constituent modes. Thus the applicability of the expression is restricted to similar types of coupling.

Further research effort is suggested in order to extend the method over a wider range of types of conservative coupling, encountered in structural joints. This may comprise two main aspects. The kind referred to as point coupling (of which a typical example is spot welding), and coupling of two elements, each vibrating in a different characteristic waveform.

In the first case the motion of the coupling region may consist of normal mode components superimposed on off-mode motion, as the case in Fig 27b. Then the coupling acts to transmit excitation, allowing only a limited amount of elastic interaction between the coupled elements, of types and magnitude depending on the number and positions of the points of coupling with respect to mode shapes, and the kind of motion coupled, which may be rotary, transverse, or some combination of both.

This study is an important link in the investigation to minimize noise transmission in structures by impedance mismatching techniques and applying the dynamic vibration absorber effect. In this context, an investigation focusing on the relationship between the size, number, and positions of points coupling needed to maintain an equivalent dynamical behaviour to that of a given elastically coupled system, may prove particularly rewarding. It may be possible to design a structural joint acting as a mechanical filter through replacing a seam welding by a number of spots welding, keeping the static strength, arranged in such a manner as

to supress the flow of vibrational energy of pre-determined modes of interest through the coupling.

The latter aspect, dealing with coupling elements vibrating in different waveforms may prove more complicated, involving reconsideration of defining point response of an element and modes of motion in general, and similarly the kind of coupling response parameters may be questioned.
For such a situation, it is proposed to examine the possibility that different kinds of modes are present in each of the elements, superimposed on each other in that element.
Then it is possible that constituent modes of the same kind may be coupled, forming a system vibratirg simultaneously in two different pairs of coupled modes.

An additional problem area concerns ways and means of excitation. In our experimental model, a single sinusoidal disturbing force was applied at a point, thus exciting normal modes in turn. This condition poses no problem in laboratory model testing where the mechanics of vibration is investigated through normal modes.

Complex structures are likely to be excited by more than one source, giving rise to simultaneous excitation of several normal modes.

Restricting our interest to point excitation, it would seem that two cases, related to the location of the forcing points are significant. When several disturbing forces are present, they may be acting in one side of the coupling, or located on both elements.
Four kinds of variables are associated with each disturbing force, namely, position of input point, frequency of excitation, force amplitude, and the phase angle between the force

amplitudes of the generators which in the general case varies with time, depending on the relative frequencies of excitation, and may result in beating effect between the modes.

Relationship between those parameters of excitation are important in the study of modes interaction with particular reference to reducing noise transmission in structures by counter vibration, reported by Mizutani (1).

The degree of accuracy to which the average response ratio is obtained from the expression of the measured coupling and input receptances, was determined by comparing the ratio factor to the average response ratio, measured directly from the coupled elements using a non-contacting apparatus. This technique had to rely upon the presence of well conditioned mode shapes in the vibrating coupled elements for an assessment of the response distribution through the normalising factor. This scheme can operate perfectly where mode distortion is negligible. In the event , modes were distorted to various degrees, which required auxiliary techniques to be developed to appreciate the error involved, being subject to the limited amount of sampling, and the reduction of the detailed information, thus obtained, to manageable parameters.

Consequently the degree of reliability in the process is linked to the amount of distortion of mode shapes as represented by the bending waveforms and the curves of Fig 14. The higher the distortion the lower the reliability becomes. So the accuracy of the values obtained from eq'n 4.24 is related to the agreement between the curves of S_m and S_{r+d} in Fig 17, evaluated between the limits of .5db and 2db.

In addition this technique required that predominantly normal modes be present in both coupled elements, which is not essentially the case in practical structures .

The problem of appreciating the accuracy of results obtained from eq'n 4.24 and the dependence of the technique on the shape of the mode present in the elements, can be eliminated by a modification of the experimental apparatus.

It is feasible to improve the process by increasing the population of sampling, of the amplitude response of the elements, to such an extent that the values obtained from direct measurement, may be regarded as true space-average independent of mode shape and identification.

This development of the research rig is described in appendix IV in some more detail.

III. Concluding remarks.

The research work reported in the thesis was initiated to establish a method whereby response ratio could be determined experimentally from measurable parameters in such a manner that, given a pair of coupled structural elements and a source of excitation, it could be possible to determine the response distribution in the system.

It was shown that this object has been achieved in that, the average response of a class of coupled elements can be obtained from an expression of the coupling and input receptances.

Additional research work has been proposed, to extend the method, based on the ratio factor, in frequency range, and to other structures to improve its generality for practical applications.

That can be summarized in the following categories :

a) To investigate the effect of the relative importance of rotary as compared to transverse motion, in the coupled elements and the coupling, in higher order modes.

b) To study additional types of conservative coupling, which can approximate structural joints. This course of action was provided with a powerful tool by verifying the coupled mode formulation for simple systems, in the thesis. It would be helpful if joints were classified in terms of motion interaction or quantity of energy, which can be determined in experiment. Such classification can be more related to system dynamics.

c) When normal mode excitation is specified, a wide range of variance of the parameters of excitation exists. The relationship between those parameters has a bearing on the response and energy distribution in the vibrating system. This relationship is an essential aspect of the general case of normal mode vibration, which should be investigated, in practical complex structures.

d) Further development of the experimental apparatus is proposed, both to improve research facilities to aid the work suggested above, and as an industrial tool for estimating dynamic stress and recording vibrational mode shape in panel type components.

This project is by no means first attempt undertaken to investigate the dynamical behaviour of coupled elements.

The innovation of this thesis rests with the approach and techniques by which the problem of estimating response distribution in coupled elements is tackled. To stress this point,findings are compared with present day techniques,

to show the reasons which warrant this research.

Methods engaged hitherto to estimate the dynamic response of coupled vibrating elements can be classified with reference to the ways in which coupling conditions are specified. These are either by vibrational parameters such as mass, damping and stiffness, or through an energy quantity, the coupling loss factor.

The method of the thesis is compared to that of Lyon and Eichler to determine response ratio in coupled plates (5). These authors derived response ratio from the equation of energy sharing, i.e. the ratio of kinetic energies stored in the coupled elements, where energy ratio is expressed by the loss factors of the individual elements and the coupling loss factors.

To determine the loss factors it was necessary to test the separate plates and then to test them coupled, assuming the same modes of vibration in the corresponding elements in both situations. Then both coupled plates were assumed to have identical masses in order to compute response ratio from energy ratios.

The alternative method specifying coupling conditions in terms of vibrational parameters requires the determination of coupling stiffness . This can be determined only by comparing the stiffness of an element in the uncoupled state to that of the coupled but blocked state, assuming again similar mode shapes in the element. Hence in the particular example, the method suggested in the thesis seems to be advantageous over those compared, because it neither requires to interfere with an existing structure, nor to create a situation of zero acceleration in order to suggest an approximation of response sharing .

So far we have compared the procedures. As for the accuracy of the results, it is felt that no common basis exists to compare the degree of accuracy and reliability of the results obtained through the various methods, because the non-contacting measuring device employed in this work is bound to give better assessment of response distribution than by measuring acceleration response at descrete points, used in previous investigations, despite the criticism of accuracy in the preceding part.

This research, results in providing useful means to tackle the problem of noise transmission in structures. Experimental apparatus to facilitate measurement of motion distribution, verification of the coupled mode formulation to promote better understanding and assessment of normal modes, and the expression (eq'n 4.24) of measurable parameters to estimate response distribution in coupled elements.

It is suggested that the impotance of obtaining the empiric expression is not in the limited scope of examples which can be treated, but rather in showing that this different approach to estimate response distribution in coupled structural members is worthy of further research effort to explore its potentialities.

6. APPENDIX.

I. Theoretical model.
II. Plate vibration.
III. Types of coupling.
IV. Experimental rig usefulness.
V. List of references.
VI. List of symbols.
VII. List of illustrations.

I. Theoretical model.

A simple 2-degree-of-freedom model is taken to facilitate a theoretical treatment of the relationship between energy distribution and coupling parameters in particular, and the dynamics of a coupled vibrating system in general.

The validity of the analogy between the model and the elastic system is of a limited scope and offers only an approximation as will be discussed in section 4.

The model consists of 2 mass-spring-dashpot subsystems, stiffness coupled, in two coordinates to represent both transverse and rotary motion coupling.

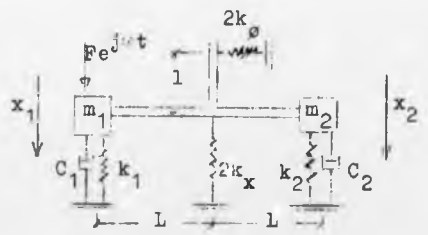

L = l

In this model it is assumed that the bodies m_1 and m_2 are infinitely rigid, connected by a massless rigid lever. That no friction is associated with the motion and all springs are linear within the range of motion.
For small oscillations, the equations of motion are,

$$m_1\ddot{x}_1+C_1\dot{x}_1+k_1x_1+2k_x\frac{x_1+x_2}{2}+2k_\phi\frac{-x_1+x_2}{2}=Fe^{j\omega t}$$

(6.1)

$$m_2\ddot{x}_2+C_2\dot{x}_2+k_2x_2+2k_x\frac{x_2+x_1}{2}+2k_\phi\frac{-x_2+x_1}{2}=0$$

The solution in the complex plane is $x=-jx\omega$ and $x=-x\omega^2$ Then setting:

$$(6.2) \qquad K_1 = k_1+k_x-k_\phi \qquad K_2 = k_2+k_x-k_\phi \qquad K_3 = k_x+k_\phi$$

we obtain the amplitude response of each of the masses:

$$(6.3) \qquad x_1 = F\frac{\sqrt{(K_2-m_2\omega^2)^2-\omega^2C_2^2}}{D} \qquad \text{and} \qquad x_2 = -F\,\frac{K_3}{D}$$

where

$$(6.4) \qquad D^2 = \left[(K_1-m_1\omega^2)(K_2-m_2\omega^2)-K_3^2\right]^2 + \\ +\omega^2\left[C_1^2(K_2-m_2\omega^2)^2+C_2^2(K_1-m_1\omega^2)^2+ C_1C_2(C_1C_2\omega^2+2K_3^2)\right]$$

The first term on the RHS of eq'n 6.4 is the frequency equation of the undamped coupled system, and the second term represents the effect of damping. The natural frequencies corresponding to the 2 normal modes are obtained when eq'ns 6.3 increase indefinitely, i.e. as eq'n 6.4 becomes zero.

In order to simplify further the analysis of the model, and because we chose a lightly damped experimental specimen, we put $C_1 = C_2 = 0$. Eq'ns 6.3 become,

$$(6.5) \qquad x_1 = F\,\frac{K_2-m_2\omega^2}{D} \qquad \text{and} \qquad x_2 = -F\,\frac{K_3}{D}$$

and eq'n 6.4 reduces to,

$$(6.6) \qquad D = (K_1-m_1\omega^2)(K_2-m_2\omega^2)-K_3^2$$

Now eq'n 6.6 yields the natural frequencies when $D = 0$,

$$(6.7)\qquad \omega^2_{a.b.} = \frac{1}{2\mu m_2}\left[\mu K_2 + K_1 \pm \sqrt{(\mu K_2 - K_1)^2 + 4\mu K_3^2}\right]$$

where μ is given by $\mu = m_1/m_2$.

The -ve and +ve signs correspond to the natural frequencies of the normal modes 'a' and 'b'.

Now we wish to determine the parameters that represent the strength of coupling, in eq'ns 6.5. The response of a simple 2-degree-of-freedom lumped system, stiffness coupled in single coordenate is,

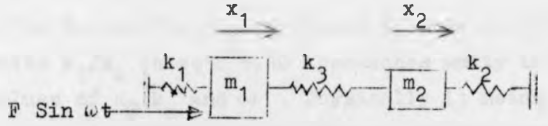

$$(6.8)\qquad a_1 = F\,\frac{K_2 - m_2}{D'}^2 \qquad\qquad a_2 = F\,\frac{K_3}{D'}$$

where

$$(6.9)\qquad D' = (K_1 - m_1\omega^2)(K_2 - m_2\omega^2) - K_3^2$$

The similarity between eq'n 6.5 and 6.8 is apparent. From the similarity between eq'n 6.6 and 6.9 we conclude that K_3 in our model is analogous to k_3 in the simple system and hence is a measure of coupling strength, as becomes evident from examining eq'ns 6.5.

As K_3 decreases and approaches zero,

$$x_2 = 0 \qquad \text{and} \qquad x_1 = F\,\frac{1}{K_1 - m_1\omega^2}$$

That is, the system becomes decoupled and reduced to a single-degree-of-freedom. This occurs when $K_3 = k_x + k_\phi = 0$. The limiting value $K_3 \to \infty$ occurs when k_x, k_ϕ or both increase indefinitely. This situation is best examined in terms of the mode shape. From eq'n 6.5 we get

$$(6.10)\quad \frac{x_1}{x_2} = -\frac{K_2 - m_2\omega^2}{K_3} = -\frac{k_2 + k_x - k_\phi - m_2\omega^2}{k_x + k_\phi} = -1 - \frac{k_2 - 2k_\phi - m_2\omega^2}{k_x + k_\phi}$$

As the value of $k_x + k_y$ and hence K_3 increases to infinity the ratio x_1/x_2 in eq'n 6.10 approaches unity independent of the values of k_ϕ, k_x and ω . Physically it means that the 2 masses move together as a solid unit and the system is reduced again to a single-degree-of-freedom, having a different mass and stiffness.

Eq'n 6.10 expresses response ratio in lumped systems. It has a significant point at the frequency $\omega^2 = K_2/m_2$ which can be referred to as a "blocked natural frequency" of the system, allowing only m_2 to vibrate, making $x_1/x_2 = 0$. At this point we observe the dynamic vibration absorber effect where all the available energy is drained to maintain the resonant motion of mass m_2. The implication, as observed in eq'n 1.5 is that we have at that frequency $T_1/T_2 = 0$.

In our consideration of the elastic coupled system, we are primarily interested in the state of resonance.

For the dynamic vibration absorber effect to occur in that state, one of the natural frequencies of the coupled system must be equal to K_2/m_2. We examine such a situation in the simple model. Using eq'n 6.7 we put,

$$\frac{K_2}{m_2} = \frac{1}{2\mu m_2}\left[\mu K_2 + K_1 \pm \sqrt{(\mu K_2 - K_1)^2 + 4\mu K_3^2}\right]$$

then we have,

(6.11) $4\mu K_3^2 = 0$

This condition is satisfied when $m_1 \ll m_2$ and the system can be regarded as a single-degree-of-freedom, or when $K_3 = 0$ and the system becomes decoupled.

Next, we proceed to establish the relationship between the response ratio of the coupled masses and the coupling conditions. Transverse motion x_c and rotary motion ϕ_c of the coupling are,

(6.12) $x_c = \frac{x_1+x_2}{2}$ and $\phi_c = \frac{x_2-x_1}{2}$

and the receptances,

(6.13) $\alpha_x = x_c/F = \frac{x_1+x_2}{2F}$ and $\alpha_\phi = \phi_c/F = \frac{x_2-x_1}{2F}$

Now we substitute eq'ns 6.5 into 6.13 to obtain,

$k_\phi = -\alpha_x \cdot D^+ 1/2 \ (k_2 - m_2\omega^2)$

$k_x = -\alpha_\phi \cdot D^- 1/2 \ (k_2 - m_2\omega^2)$

and finally we end up with ,

(6.14) $x_1/x_2 = + \frac{\alpha_x - \alpha_\phi}{\alpha_x + \alpha_\phi}$

II. Plate vibration.

In this part we analyse and discuss in some detail findings related to plate vibration, extracted from the experimental data.

The reader may find the treatment of the topic incomplete unless it is borne in mind that it is intended to demonstrate that additional information can be obtained using techniques devised in the project and to present the material compiled in the course of the work in a useful form.

Because of the importance to the thesis, and as it has been comparatively little explored, coupled modes are given particular attention in the later part.

a) Uncoupled plate.

Bending waveforms recorded along the circle of scanning were used in earlier parts of the thesis to detect response distribution and error in experimental results. At this stage it will be shown by analysing several waveforms, that a good deal of information on modal response can be extracted as well from those records.

The best possible agreement between recorded and the corresponding theoretical bending waveforms is displayed in Fig 11a. The rounding of the sharp corners of the recorded as compared to the theoretical waveform is the effect of the inertia resistance of the pen mechanism of the plotter appearing in all records.

In section 3 the possibility of interference of extraneous mode components, with the motion of the excited normal mode was mentioned. It was further suggested that the technique of Kennedy and Pancu (12) can be applied to resolve the excited

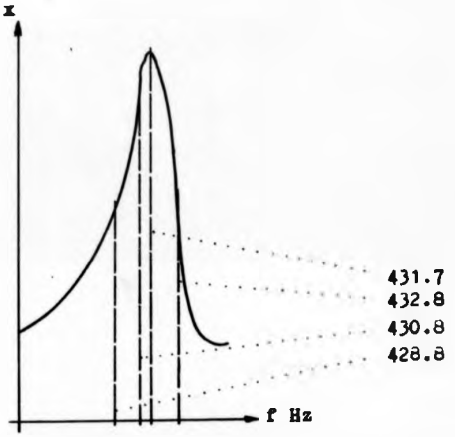

a) A plot of peak-amplitude versus frequency of excitation.

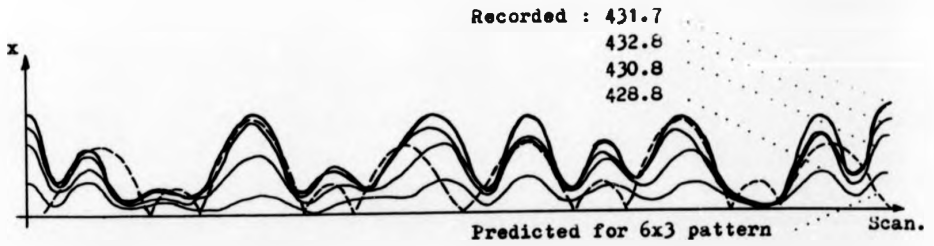

b) Bending waveforms corresponding to the above frequencies.

Fig 19. Bending waveform for mode 6x3 nodal array at the frequencies in the vicinity of peak-amplitude response.

mode components from the components of the modes excited off their modal frequency.

An analysis of the bending waveform and the relevant part of a plot of peak-amplitude versus frequency such as in Fig 12 may reveal the identity of the interfering mode, the reason for interferance and suggest the distorted region of the plate.

This process is shown in Fig's 20 and 21. The illustrations give an indication of interference of more and of less intense modes on adjacent modes where the antiresonance between the modes is at a level above the half power point of the weaker mode.

Comparing the predicted and recorded waveforms of mode 38 in Fig 20, it is evident that at the side of the plate (marked S), the response 'dips' to a much greater extent than expected. This is a clear indication of the presence of some component of an adjacent mode. Observing the plot of peak amplitude indicates that mode 39 at 450.6Hz must have been excited off its resonant frequency, thus interfering with mode 38. The nature of the interference is due to attempting to impose a node in the middle of the waveform (point S) because mode 38 has 6x0 nodal lines, while mode 39 has 6x1. The other nodes of mode 39 could be expected to have a similar effect on mode 38. But since they are in the vicinity of nodes of that mode, and since mode 39 has lower response than mode 38, the magnitude of the interference is small but noticable.

Mode 29 presented in Fig 21 is subject to every possible cause of distortion. The predicted waveform is compared with the recorded waveforms for that mode and for the adjacent mode 30. As can be observed from the plot of peak

amplitude,mode 30 has a higher response than mode 29. The forcing is located at a node of mode 29 which is an antinode of mode 30. Consequently favourable conditions are created to excite mode 30 off its resonant frequency, which results in components of mode 30 being superimposed on the modal response of mode 29.
This effect in the case of a beam was observed by Bishop and Pendered (13).
This region is generally distorted particularly as compared with the other side of the plate (marked T for top) which is relatively uninfluenced by the adjacent mode, and agree with the predicted waveform.

It is interesting to observe how, in several respects, the recorded waveform for mode 29 is a mid-position between the predicted waveform for the mode and the recorded waveform for the stronger adjacent mode.
In fact because of the strength of mode 30 the recorded waveform can be expected to approximate to the theoretical waveform of that mode, in which case the figure admirably demonstrates the influence of the stronger mode on the bending waveform of the weaker mode.
It can be seen that this mode is so highly distorted that averaging the response will not bring theory and experimental records any closer. In addition one antiresonance of mode 29 is above half power point so that a value for damping ratio cannot be determined.

As stated before, such modes were disregarded for the purpose of investigating response and energy distrbution.

An additional item of information related rather generally to vibration of plates is given in the chart of Fig 22. Comparing predicted natural frequencies and measured resonant

amplitude,mode 30 has a higher response than mode 29. The forcing is located at a node of mode 29 which is an antinode of mode 30. Consequently favourable conditions are created to excite mode 30 off its resonant frequency, which results in components of mode 30 being superimposed on the modal response of mode 29.
This effect in the case of a beam was observed by Bishop and Pendered (13).
This region is generally distorted particularly as compared with the other side of the plate (marked T for top) which is relatively uninfluenced by the adjacent mode, and agree with the predicted waveform.

It is interesting to observe how, in several respects, the recorded waveform for mode 29 is a mid-position between the predicted waveform for the mode and the recorded waveform for the stronger adjacent mode.
In fact because of the strength of mode 30 the recorded waveform can be expected to approximate to the theoretical waveform of that mode, in which case the figure admirably demonstrates the influence of the stronger mode on the bending waveform of the weaker mode.
It can be seen that this mode is so highly distorted that averaging the response will not bring theory and experimental records any closer. In addition one antiresonance of mode 29 is above half power point so that a value for damping ratio cannot be determined.

As stated before, such modes were disregarded for the purpose of investigating response and energy distrbution.

An additional item of information related rather generally to vibration of plates is given in the chart of Fig 22. Comparing predicted natural frequencies and measured resonant

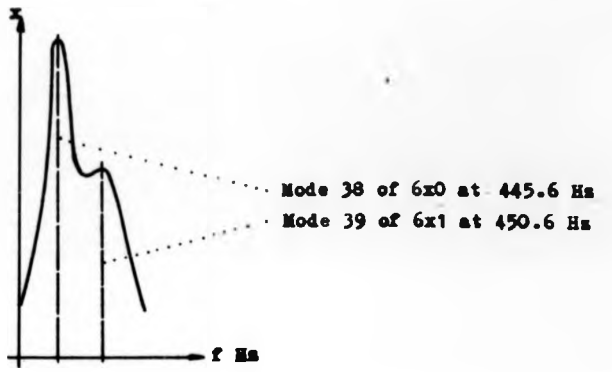

a) A plot of peak-amplitude versus frequency of excitation.

b) Recorded and theoretical bending waveforms of mode 38.

Full line, recorded waveform.

Fig 20. Plot of peak-amplitude and bending waveform showing influence of an adjacent weaker mode on modal response.

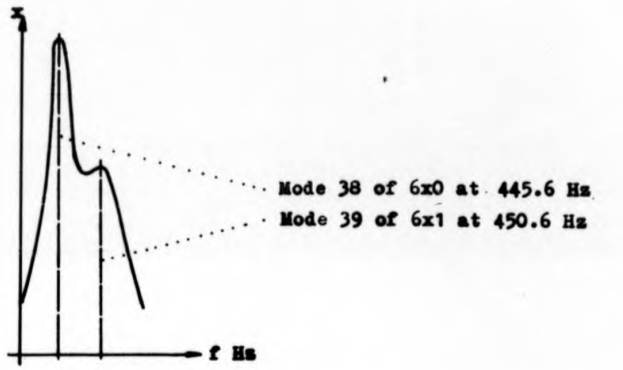

a) A plot of peak-amplitude versus frequency of excitation.

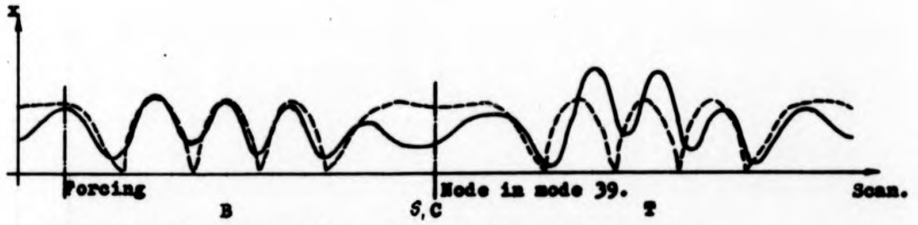

b) Recorded and theoretical bending waveforms of mode 38.

Full line, recorded waveform.

Fig 20. Plot of peak-amplitude and bending waveform showing influence of an adjacent weaker mode on modal response.

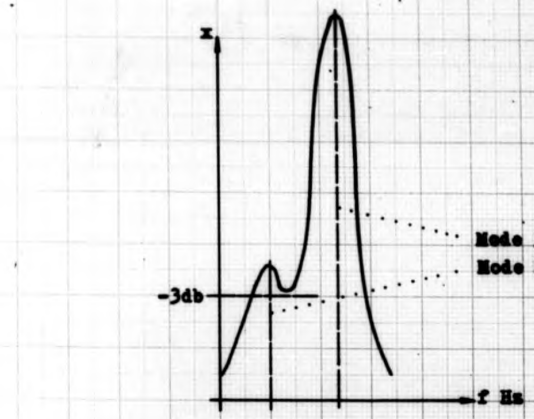

a) Plot of peak-amplitude versus frequency of excitation showing the level at which damping ratio is measured.

b) Measured and theoretical bending waveforms of modes 3x5 and 5x2.

Predicted waveform, thin dotted line.

Fig 21. Plot of peak-amplitude and bending waveform showing influence of an adjacent stronger mode on modal response.

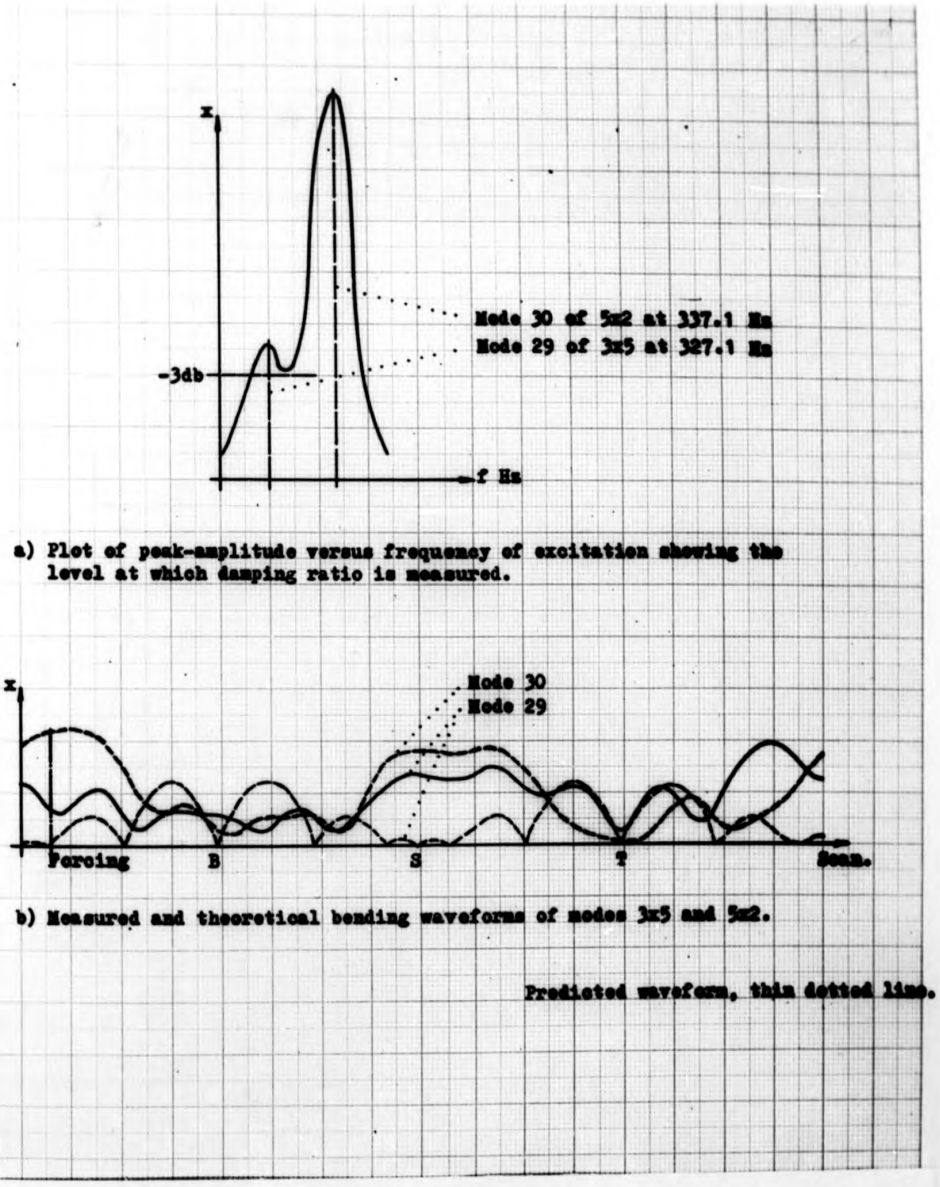

a) Plot of peak-amplitude versus frequency of excitation showing the level at which damping ratio is measured.

b) Measured and theoretical bending waveforms of modes 3x5 and 5x2.

Predicted waveform, thin dotted line.

Fig 21. Plot of peak-amplitude and bending waveform showing influence of an adjacent stronger mode on modal response.

frequencies can be of interest for the purpose of this work.

Natural frequencies were computed, assuming a mode shape, and using the method suggested by Warburton (11). The corresponding modal frequencies were obtained from the resonant state of a separate plate where a similar mode was displayed. Values of both frequencies were plotted versus shape in terms of the nodal pattern. The numbers in the field represent the number of nodal lines m counted in the x direction.

Since frequencies predicted by this method are slightly higher than the true ones, the full lines representing the measured values in the chart are expected to appear always to the left hand side of the corresponding dotted lines representing the computed values. In experimental work it means that the calculated values can serve as upper limit to examine measured frequencies.

Spacing between corresponding lines is proportional to the difference between the computed and measured frequencies. The trend is towards a decrease in that difference with increasing mode order, because the computed values become closer to the true ones. Hence the spacing between the lines is expected to be of the form of a wedge pointing in the direction of higher modes. Indeed this is observed in the chart for m_a = 3,4,5 and 6, and for m_b = 4 and 7.

Divergence from the two trends indicates that one or more measured frequencies are displaced up or down frequency scale. But it is not possible to specify the exact values on the basis of this chart alone, unless a measured value is found greater than a computed one.

Some further consideration can be aided by the plot, in the centre of Fig 22, showing percentage difference

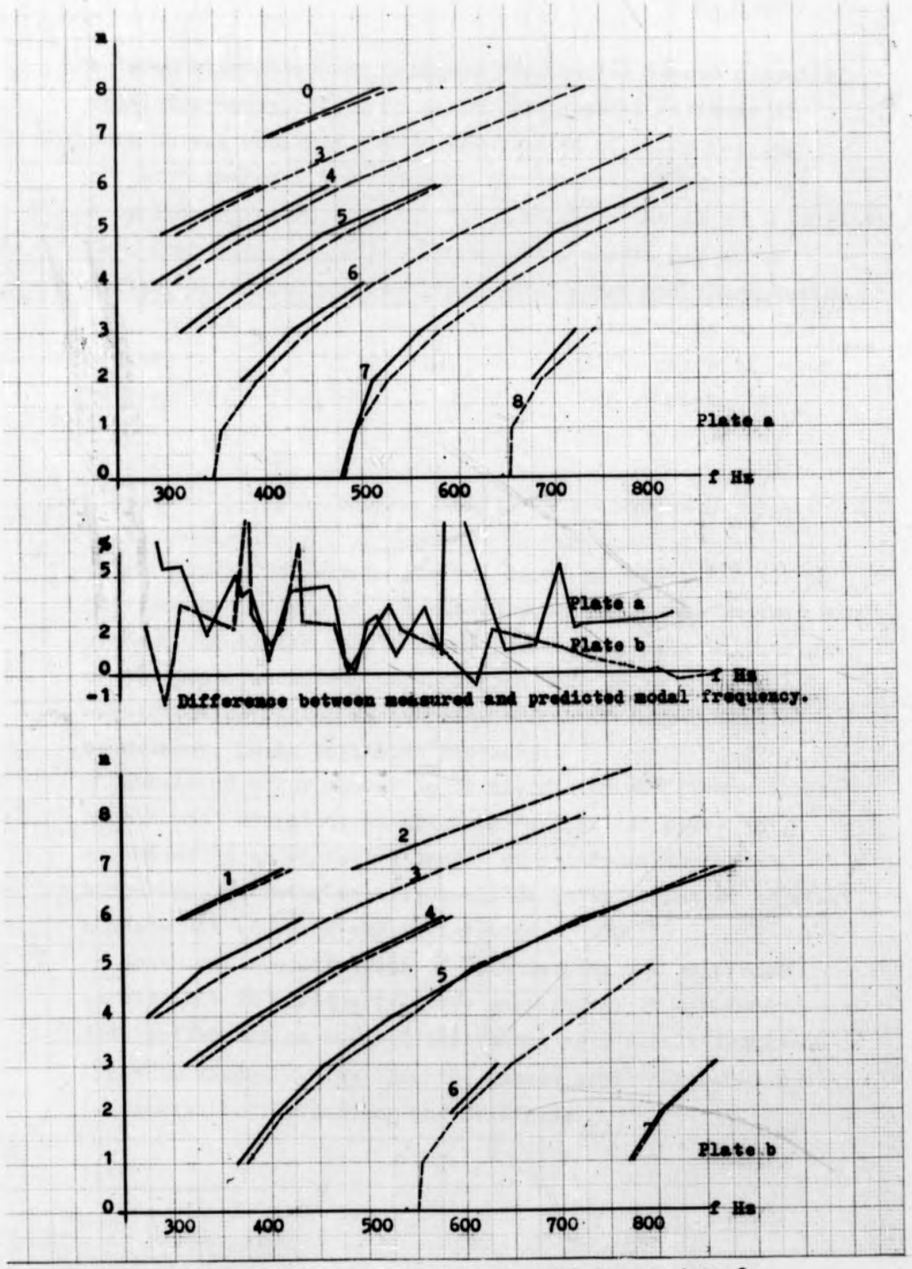

Fig 22. Predicted and measured (Full line) modal frequencies of uncoupled plates in a plot of modal frequency versus nodal pattern expressed in m and n nodal lines.

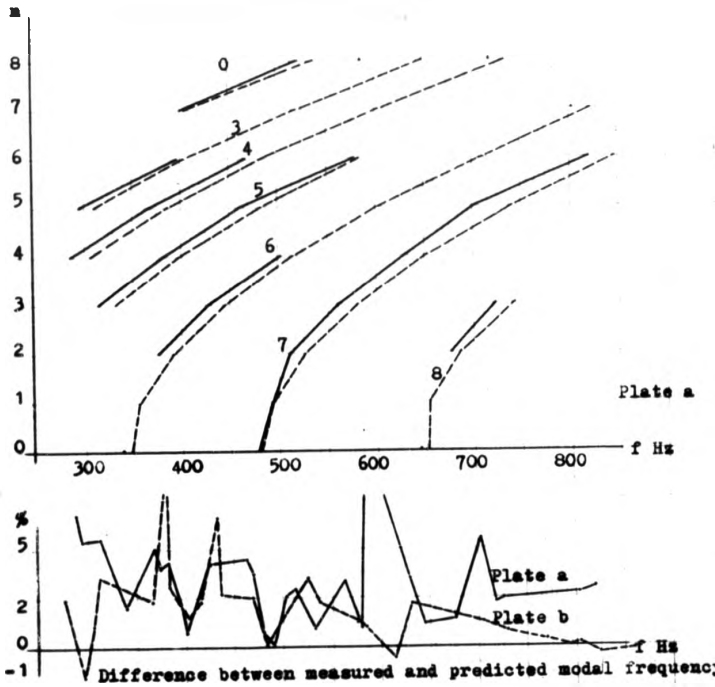

Difference between measured and predicted modal frequency.

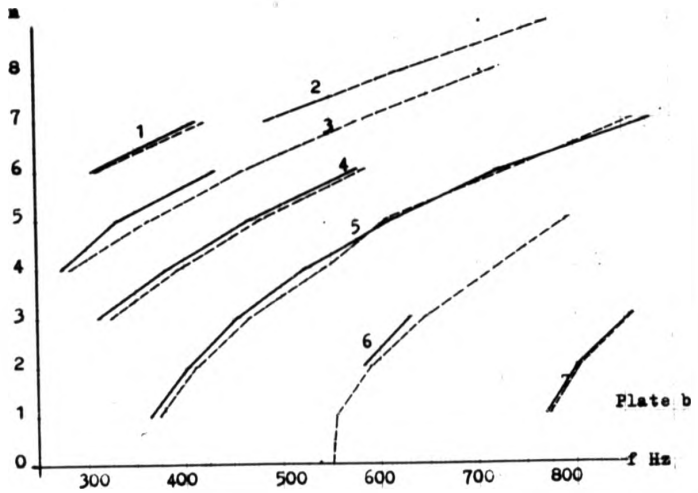

Fig 22. Predicted and measured (Full line) modal frequencies of uncoupled plates in a plot of modal frequency versus nodal pattern expressed in m and n modal lines.

between calculated and measured frequencies versus measured modal frequency, for each plate. The general attitude of both curves conforms to the expectation of error falling off with increase in frequency. An estimate of an average drop from 4% to 2% in plate 'a' and from about 4% to 0 in plate 'b'. Comparing trends in corresponding charts may offer further information about a suggested error and consequently toa possible cause of the error. As an example, an error appears in $m_a = 8$ in the top chart. From the curve of error we realise that the modal frequency of 8x2 of plate 'a' conforms to the trend of the curve, whereas that of 8x3 is above the mean of the curve, suggesting that the modal frequency of the latter mode is below the expected value.

Although this method does not provide precise results, it can assist in looking for the cause of error. Further in the example, a drop of a measured modal frequency in the present set-up can result from excessive damping in the suspension attachment, depending on mode shape and magnification factor because the effect of suspension is non-linear, being amplitude dependent.

Should an error appear to be associated with frequencies higher than expected, as modes 5x5 and 5x7 in plate 'a', it indicates an excessive amount of stiffness in the suspension, vibrator misalignment, or interference of adjacent modes - all of which can be detected.

Note that a combination of both damping and stiffness is possible in various relative magnitudes. If a normal mode motion can be assumed equivalent of a single-degree-of-freedom damped system then the damped modal frequency f_n is related to the damping and stiffness.

(6.15) $$f_n = (4KM - C^2)^{1/2}/4\pi M$$

and changes in one parameter can be adjusted by change of another parameter leaving f_n unchanged. This implies that an error in modal frequency indicated by Fig 22 suggests some distortion or fault but not vice versa.

An additional aspect of information which can be obtained with the aid of computed modal frequencies is mode identification. Since modal frequencies of separate elements can be computed to a good approximation, one can list the modes in terms of mxn nodal lines with respect to the progression of modal frequency. Then it is possible to predict the order of appearance of modes with increasing frequency of excitation. Thus if a mode occurs in frequency scale between two known modes, its identification is implied.

The drawback of this technique is that if the element is constrained or has residual stresses, the order of modes changes, which is easily detectable.

Evidently, should an error in the results be detected, it is essential to apply several techniques in conjunction in order to analyse and trace a possible source of the error. As has been demonstrated in this part of the section, correlating information extracted from the bending waveform, peak-amplitude plot, and the chart of modal frequencies, aids to conclude whether an error is attributed to interference of adjacent mode, suspension attachment, misalignment of the generator, or to a combined effect of several factors. The agreement in Fig 22 can be improved in so far as external factors such as misalignment are involved. The effect of modes vibrating together is beyond control if the exciting force must be located at a fixed position or

modes have too close frequencies.

A 'too close frequency' is understood as that frequency, away from the modal frequency of interest, at which components of an adjacent mode are still noticable in the bending waveform, independent of the location of the disturbing force, other than a node of all the modes involved.

Hence it can be established by a series of experiments whether the interference of an adjacent mode is owing to modal density or an external factor.

b) Coupled plates.

A plate element subjected to transverse sinusoidal excitation at a resonant frequency, vibrates in a normal mode, of a shape depending on material properties, body geometry, boundary conditions, and frequency of excitation. For a rectangular plate the mode shape can be represented by nodal patterns consisting of nodal lines approximately parallel to the edges, independent of the actual size and boundary conditions of the plate. (See table 1 of ref.11).

If a part is cut off the plate, or boundary conditions altered, the characteristics of the shape of the normal modes remain unchanged, in the sense that the nodal pattern still consists of nodal lines parallel to the edges, so long as the body geometry has not been changed, unlike other modal parameters. Should a slot be cut across part of the plate, along a line dividing the plate into two rectangular parts, e.g. as in Fig 3, the changes that follow can be considered in terms of boundary conditions, so that a free boundary appears along the cut part. Hence each part is expected to preserve the characteristics of the nodal pattern. But depending on the new boundaries

modes have too close frequencies.

A 'too close frequency' is understood as that frequency, away from the modal frequency of interest, at which components of an adjacent mode are still noticable in the bending waveform, independent of the location of the disturbing force, other than a node of all the modes involved.

Hence it can be established by a series of experiments wh.ther the interference of an adjacent mode is owing to modal density or an external factor.

b) Coupled plates.

A plate element subjected to transverse sinusoidal excitation at a resonant frequency, vibrates in a normal mode, of a shape depending on material properties, body geometry, boundary conditions, and frequency of excitation. For a rectangular plate the mode shape can be represented by nodal patterns consisting of nodal lines approximately parallel to the edges, independent of the actual size and boundary conditions of the plate. (See table 1 of ref.11).

If a part is cut off the plate, or boundary conditions altered, the characteristics of the shape of the normal modes remain unchanged, in the sense that the nodal pattern still consists of nodal lines parallel to the edges, so long as the body geometry has not been changed, unlike other modal parameters. Should a slot be cut across part of the plate, along a line dividing the plate into two rectangular parts, e.g. as in Fig 3, the changes that follow can be considered in terms of boundary conditions, so that a free boundary appears along the cut part. Hence each part is expected to preserve the characteristics of the nodal pattern. But depending on the new boundaries

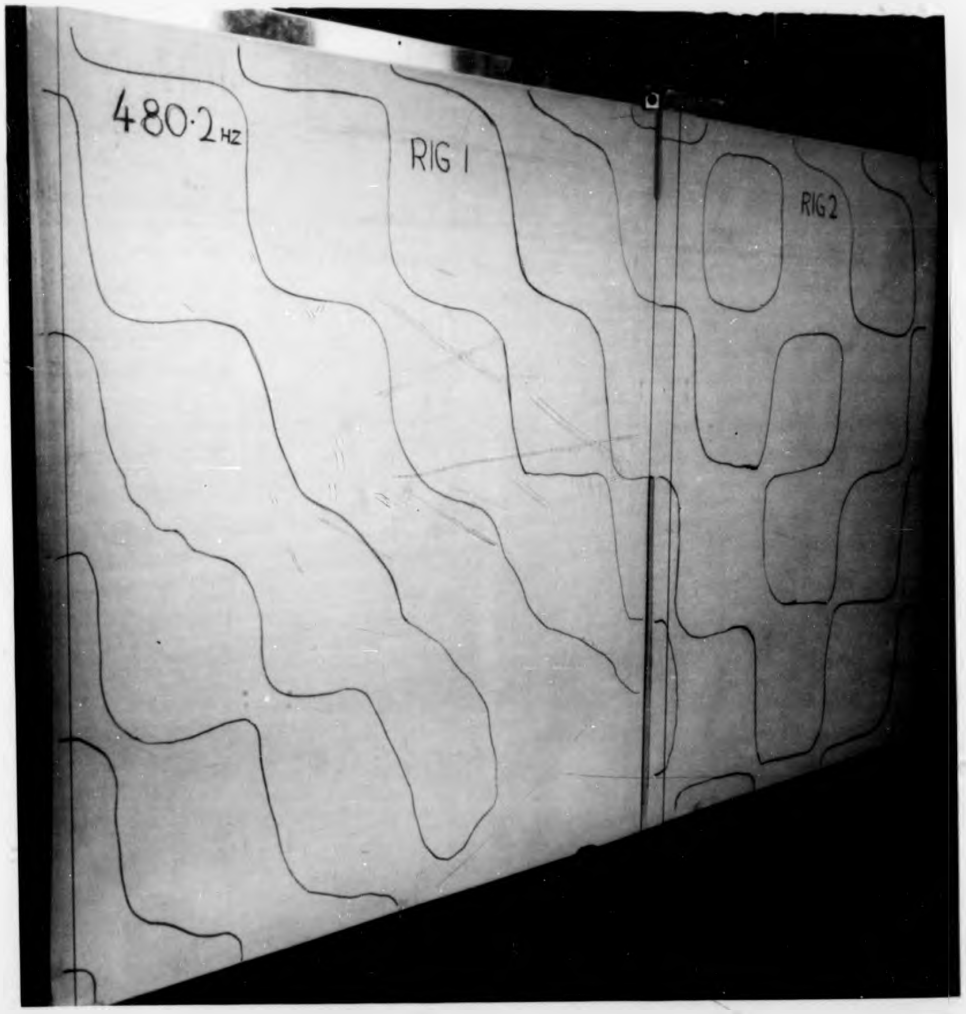

Fig 23. Recorded nodal pattern of mode 5x5 (Rig 1) coupled with mode 4x5 (Rig 2).

Fig 23. Recorded nodal pattern of mode 5x5 (Rig 1) coupled with mode 4x5 (Rig 2)

and length to width ratio of each part, different modal parameters appear.

If the plate was partly cut only, allowing elastic interaction between the constituent parts, the mode of motion of the system still forms one entity, that of a normal mode, although the mode of each part can be labelled with reference to some recognised mode shape as represented by the nodal pattern. Then the continuity of the overall nodal pattern of the system which existed before cutting, remains.

This consideration is firmly supported by the evidence displayed in Fig 23. It is perfectly clear that single normal mode is present in the plate system, (see also Fig's 6 and 24), where nodal lines in the coupling region are consistent with the systems' general pattern. The fact that parts of the system can be denoted with reference to recognised nodal patterns may be thought of as a resultant which can be resolved into its components. Consequently one can assume that it must be possible to couple together the 2 parts in the specified conditions, expecting the component normal modes in each part.
It is legitimate, therefore, to base a study of the dynamical behaviour of a coupled system on assuming coupled modes representation, similar to the modes of separate plates, at the appropriate frequencies.

From the aforesaid it is implied that various pairs of modes may appear to be coupled in a coupled plate system, always consisting of nodal lines parallel to the edges. If the coupled plates are not identical, the coupled modes will be different. Then the transition from the nodal pattern of one mode to the nodal pattern of the coupled

mode takes place in the coupling region where constituent modes are linked together, their motion at the common boundary being superimposed. This kind of mode coupling is shown in Fig 24, and schematically in Fig 27a.

In earlier discussion of Fig's 20 and 21 regarding distortion of mode shapes owing to interference of ad adjacent modes, their proximity was in frequency scale. Here the proximity is in the sense of having a common boundary. One mode is directly excited transmitting excitation to the other one, sometimes resulting in distortion of the coupling region.

It is possible that the distortion of mode shape in one subsystem affects the other subsystem owing to the partnership imposed by the coupling, but not always, and conversely it is possible that both mode shapes are distorted while coupling region alone remains intact. An example of each case is presented.

A kind of distortion of mode shapes in coupled and uncoupled rectangular plates, experienced in the course of this work and reported by the author (17), is associated with the diagonals of the rectangles, referred to henceforth as the 'Diagonal effect'.
It is visible in rig 1 of Fig 23 that the pattern is slightly 'pulled' along the diagonal between the right hand bottom corner and the left hand top corner, being hardly noticable in rig 2. This is a dynamic effect caused by a static error. The rod protruding from the plate near the right hand bottom corner marks the point of forcing. This is also evident by the absence of the nodal pattern in that region. Having the vibrator misaligned in the direction perpendicular to the plane of the plate loaded the element

with a small bending moment by the 2 corners of the other diagonal resisting shift from equilibrium.
The tendency of the generator to cause a similar effect in rig 2 through the elastic interaction between the modes effected by coupling, was met by the resistance of the left hand bottom corner of rig 2, causing a faint diagonal effect in that vicinity.

A triple diagonal effect can be seen in Fig 24, resulting from the combined effect of the generator misalignment and the location of the strings supporting the dead weight of the plate, which are shown in Fig's 3 and 6 at the middle of the top edge of each subsystem. In each plate a diagonal effect appears between the far bottom corner and the point of support, being more pronounced in rig 1.
A third diagonal, can be observed, from the far bottom corner of rig 2, right across the coupling to the point of support of rig 1. The effect of this kind of distortion on the bending waveform of rig 1 is shown in Fig 24 through a superposition of the theoretical and experimentally recorded waveforms.
The main discrepancy occurs in the top and bottom regions, marked T and B respectively.

Realising this, the strings supporting the dead weight were moved to the far corner as per Fig 4d. Then a similar comparison of bending waveforms was repeated, shown in Fig 15, revealing a marked improvement in agreement between the waveforms, in those regions in particular, thus corroborating with our analysis of the case.

An example of the case where only the coupling region remained comparatively undistorted is that of test 4 where the nodal pattern is presented in Fig 6. Neither the nodal

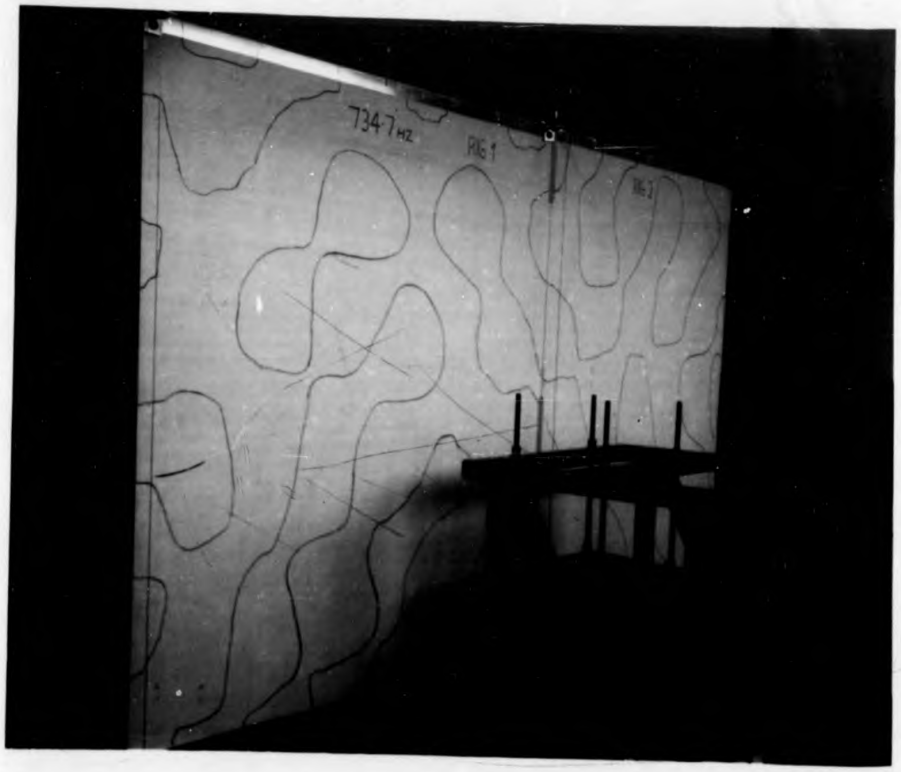

a/ Nodal pattern. Plate 1 Plate 2

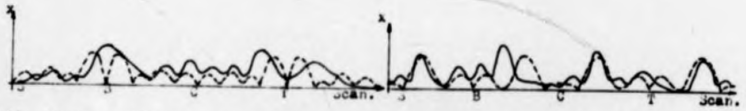

b) Bending waveforms. Mode 7x5 Mode 5x6

Fig 24. Records of the nodal pattern and corresponding bending waveforms of coupled vibrational modes, in test 30. (decorus in full line).

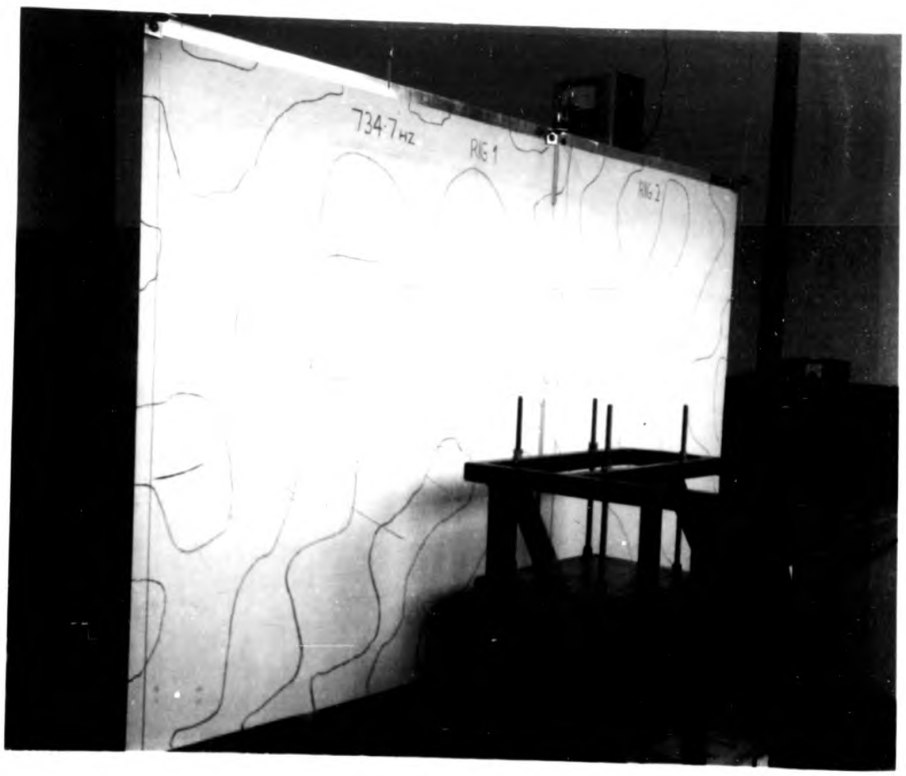

a) Modal pattern. Plate 1

Plate 2

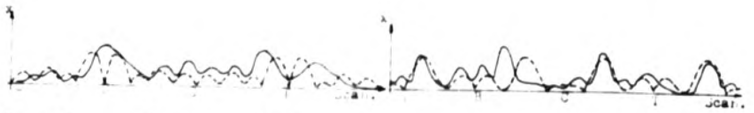

b) Bending waveforms. (Mode 7x)

Mode 9x)

Fig. 24. Records of the modal pattern and corresponding bending waveforms of coupled vibrational modes, in test 30. (Records in full line).

pattern nor the bending waveforms of the subsystem plates reveal the identity of the coupled modes.

The clue is found in the records of coupling response, the graphs of amplitudes and corresponding slopes along the coupling centre line, presented in Fig 30. In that plot we observe that the curve of amplitude displays a neat waveformand that points of zero amplitude are located where nodal lines, representing a nodal pattern having n=6 nodal lines, in the direction at right angles to the coupled edge, are expected.
In addition, points of zero slope match with points of zero amplitude, which implies that both constituent modes may have the same number of nodal lines $n_1=n_2$, because the section of the nodal lines crossing the coupling region is the same as that on the lines n, as in Fig 23.

Now one has to turn back to the catalogue of bending waveforms (Fig 29), and look for the best agreement with the records. The results of this exercise are given in Fig 30 in the waveforms. It can be seen straightaway that an amount of agreement exists, between the waveforms in plate 2 in particular. The figure shows that the least amount of discrepancy occurs in the coupling region (marked C),thus confirming our previous conclusion.

The cause for such a badly distorted mode is probably related to the exceptionally high modal response as can be verified from Fig 12. A combined effect of suspension, dead weight supports and a nonlinear damping and stiffness owing to excessive response, resulted in high flanking energy.

To complete our discussion of coupled modes in coupled plates systems, we deal with modal frequencies.

pattern nor the bending waveforms of the subsystem plates reveal the identity of the coupled modes.

The clue is found in the records of coupling response, the graphs of amplitudes and corresponding slopes along the coupling centre line, presented in Fig 30. In that plot we observe that the curve of amplitude displays a neat waveform and that points of zero amplitude are located where nodal lines, representing a nodal pattern having n=6 nodal lines, in the direction at right angles to the coupled edge, are expected.
In addition, points of zero slope match with points of zero amplitude, which implies that both constituent modes may have the same number of nodal lines $n_1=n_2$, because the section of the nodal lines crossing the coupling region is the same as that on the lines n, as in Fig 23.

Now one has to turn back to the catalogue of bending waveforms (Fig 29), and look for the best agreement with the records. The results of this exercise are given in Fig 30 in the waveforms. It can be seen straightaway that an amount of agreement exists, between the waveforms in plate 2 in particular. The figure shows that the least amount of discrepancy occurs in the coupling region (marked C),thus confirming our previous conclusion.

The cause for such a badly distorted mode is probably related to the exceptionally high modal response as can be verified from Fig 12. A combined effect of suspension, dead weight supports and a nonlinear damping and stiffness owing to excessive response, resulted in high flanking energy.

To complete our discussion of coupled modes in coupled plates systems, we deal with modal frequencies.

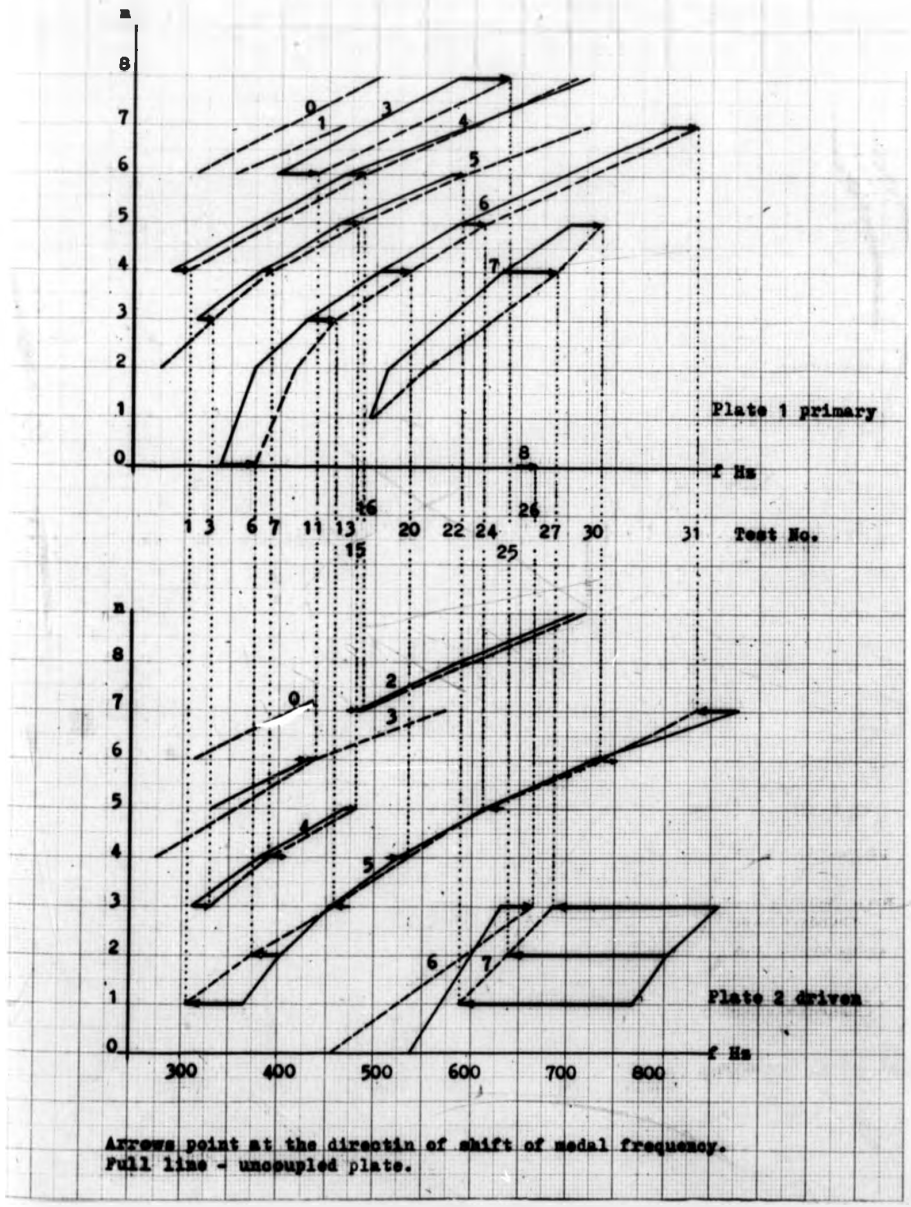

Fig 25. The shift of measured modal frequency due to the presence of a coupling, in a plot of modal frequency versus modal pattern expressed in m and n modal lines.

A coupled plate system excited at a resonance frequency vibrates in a normal mode consisting of component normal modes present in the subsystem. For subsystems different from each other, the constituent modes are different and they are excited at different frequencies if the subsystems are not coupled.
Hence coupling together two elements can be represented by 3 modal frequencies, two modal frequencies of the uncoupled modes and the modal frequency of the system when the modes are subsequently coupled.

The difference between the frequencies at which a given normal mode is excited for 2 situations of specified conditions are referred to as shift of modal frequency. In the present discussion, focusing on the change from separate to coupled conditions, shift owing to coupling is considered.

Information on mode shift, compiled in the course of this work is presented in Fig 25 in the form similar to that of Fig 22. Hence arrows are proportional to the magnitude of the shift, pointing in the direction of shift towards coupling. As has been explained in section 4, this chart consists of measured results only. Each dotted line, representing uncoupled mode, is supposed to face a corresponding full line, representing the coupled mode state. Vacancies indicate that the coupled mode was not identified, either because it is excited at a frequency outside the band of interest, or it could not be identified. Many more uncoupled modes were identified than coupled ones, because coupled modes are more liable to distortion. As mentioned above, identification of uncoupled modes was greatly aided by predicting modal frequency thus setting an order of

appearance of modes in frequency scale. Constituent modes which become coupled are marked in the figure by a vertical dotted line linking them together at their coupled modal frequncy, and relating to the serial number of testing coupled modes.

So an overall appreciation of the shift is obtained. Evidently the shift of modes in plate 1 being directly excited, is of a similar magnitude for most recorded modes, always in the direction of increasing frequency by coupling. In contrast, modes of the driven plate 2, excited through the coupling, shift in a seemingly unpredictable manner, decreasing or increasing frequency in magnitudes of considerable variability. This phenomenon does not appear to depend on the relative magnification of the modes, or the range of frequency at which they are excited.

It seems to be related to the difference between the number of nodal lines n of the coupled modes. In Fig 26 the sum total of mode shift of both coupled modes is plotted versus modal frequency of the coupled modes for each number $\Delta n = n_1 - n_2$ in absolute values. Since the shift depends on the relative transverse and rotary impedance distribution of the edge of each plate which is subsequently coupled, it can not be represented by Δn only. But from Fig 26 this factor seems to have a predominant effect on the shift, because the general trend in the figure is of higher shift for higher difference between the number of nodal lines Δn, a shift being always present.

In the event that a more comprehensive study of this topic is undertaken, it would seem appropiate to incorporate quantitative representation of the relative distortion of modes shapes in the coupled and uncoupled states because

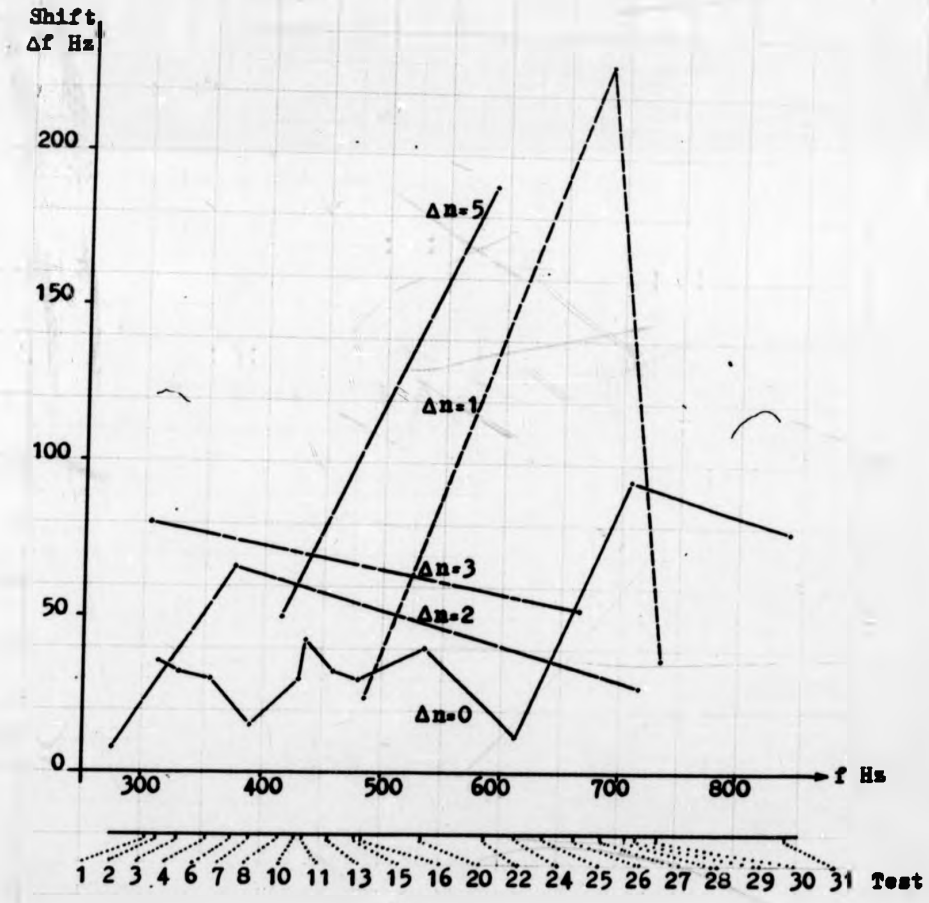

Fig 26. Plots of the total shift of modal frequency Δf due to coupling versus modal frequency f , as compared to the difference Δn in the number of nodal lines at right angles to the coupled edge .

this may cause up or down mode shift by itself, and the shift due to mode distortion should be isolated from shift due to coupling.

In this part, coupled modes in coupled plate systems were discussed along two main lines. Firstly to analyse and show the dynamical interaction between coupled modes, with regards to mode shapes and frequencies, and some of the factors on which they depend. Secondly to demonstrate some of the techniques employed to extract the information.

Other techniques associated with additional experimental data are presented in ensuing parts of the section. It ought to be stressed, however, that this is by no means an investigation of plate vibration as such, being considered a fringe interest of the project.

III. Types of coupling.

Research work of coupled elements remains incomplete unless some consideration is given to types of coupling other than that used in the specimen, to compare dynamical behaviour of systems coupled in different manners.

In general it is possible to define coupling conditions in terms of modal parameters, energy, structural description, and elasticity. It is difficult and sometimes meaningless to attempt to relate two kinds of definitions, structural description and modal parameters, say.

Investigations of energy distribution in coupled oscillators defined coupling conditions by vibrational parameters, mass, damping and stiffness (see ref.5-9 for example).

Probably because of the analogy, although limited in scope, between systems of 2 coupled elements vibrating in normal modes, and the well established two-degree-of-freedom lumped system, Lyon and Scharton still define coupling conditions in the same manner (ref.6 and 7). This is made possible by a convenient but rather unrealistic combination of a beam and a helical spring thus avoiding the need of seeking a method to define coupling in a practical situation,giving up the effect of applying their theroretical development to a real life situation.

The terms 'loose' and 'strong' coupling are widely used in the references mentioned above, but no physical interpretation is made, nor analogy with practical systems, is offered.

The paper which seems to adopt altogether a more practical approach to the topic is that of Ungar and Scharton (8).

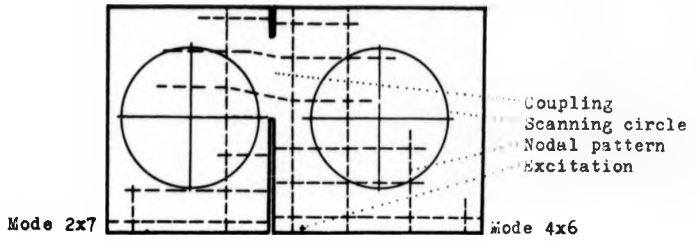

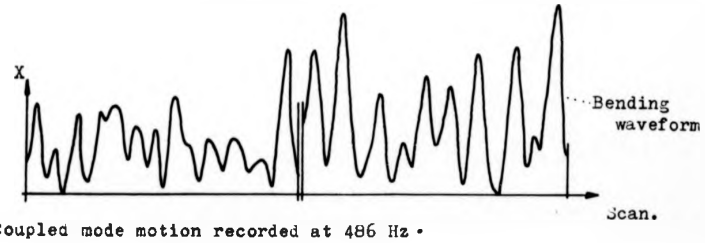

a/1) Coupled mode motion recorded at 486 Hz.

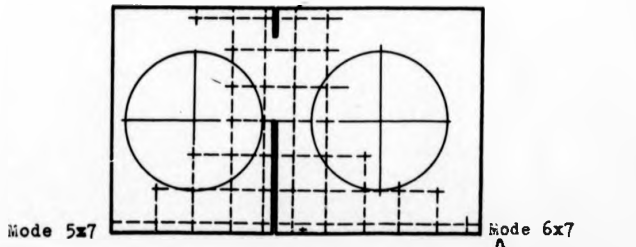

a/2) Coupled mode motion recorded at 832 Hz.

Fig 27a. The response of a plates system ,elasticly coupled.

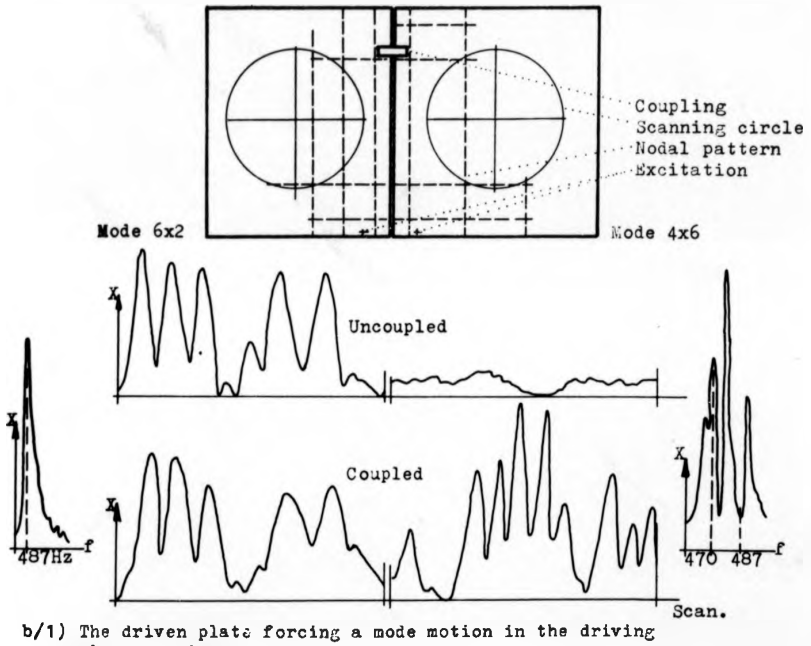

b/1) The driven plate forcing a mode motion in the driving plate at 487 Hz.

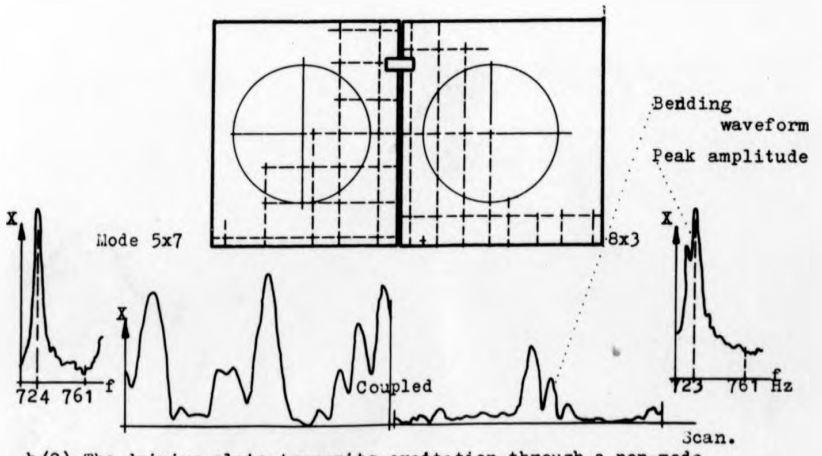

b/2) The driving plate transmits excitation through a non-mode motion at 761 Hz.

Fig 27b. The response of a plates system ,point coupled.

In their analysis, loose coupling is referred to as "coupling that has relatively little effect on the average response of the mode to a force acting directly on it". So, a loose coupling can be inferred from comparing response of an element in the coupled and separate states, which does not require to decouple a given coupled system if the response of the separate system is known from theory.

A similar approach is suggested in the thesis. On a wider sense, types of coupling can range from the kind analogous to transverse excitation at a point, henceforth 'point coupling', to the type of coupling used in the specimen being distributed over a finite length of the common boundary where elastic interaction occurs, referred to as 'elastic coupling' in this work.
The practical analogy in structures can be found to range from spot welding to seam welding and the like, restricting our discussion to comparatively conservative coupling.
(In practice energy is lost in all kinds of joints).

While evaluation of such joints in terms of mass, damping and stiffness coupling would be extremely complicated and not necessarily meaningful, it is straighforward to define or label them in terms of modal response, energy transmission, or mode interaction in model testing.

A set of tests with elastic and point coupling performed in order to compare the system dynamics, is reported in Fig's 27a and 27b respectively. Elastic interaction and transmission of excitation are apparent in both cases, of different magnitudes and taking different forms, because the point coupling still had a width of 5cm, for practical reasons, allowing an amount of distributed effect.

In the first experiment, 3 alternative specimen, comprising

the same subsystems, were excited at nearly the same frequency. The test of elastic coupling reported in 27a/1 exhibited . nodal pattern and bending waveforms of a pair of coupled modes, having modal frequency of 486 Hz, excited at a point of comparatively low impedence.

Next, each of the subsystems was tested at nearly the same frequency, 487 Hz, and at the same point. From the plot of peak-amplitude of the elements in Fig 27b/1 it is obvious that a mode would be excited in plate 2, shown on the left hand side, whereas no normal mode is present in plate 1 as shown by the bending waveforms, because the frequency of excitation is located at a deep antiresonance of plate 1.

As the plates are point coupled, a normal mode is excited in plate 1 as well, despite having the frequency of excitation unchanged. This can be understood as follows.
Mode 6x2 is excited in plate 2 by the off-mode motion of plate 1, which suffices to excite the mode because of its high magnification. Then the coupling motion is increased as required by the resonant condition of mode 6x2 thus exciting the mode of a shape offering the least impedance, in the near region of plate 1, yet which is the closest in modal frequency. The other factor sharing the choice of a mode is the relation between the location of the exciting force and the shape of modes in the vicinity of 487 Hz on frequency scale. Hence mode 4x6 which was excited in plate 1, the primary element, provides a compromise between input point motion and compliance with coupling motion. As can be seen in Fig 27b/1, this mode was excited at a frequency, 17 Hz above its modal frequency, owing to the effect of a sort of motion feed-back. The fact that mode 4x6 was excited in

plate 2 for both elastic and point coupling is merely a coincidence.

The second experiment was performed in order to compare systems' response as the same mode 5x7 was present for both types of coupling. Fig 27a/2 shows that this condition is met at a frequency of excitation of 832 Hz, for elastic coupling, and that a normal mode is present in the primary element as well.
Mode shift from the uncoupled state is 65 Hz.

For a point coupling, mode 5x7 was excited again through off-mode motion in the primary plate at 761 Hz being a shift of -6 Hz only. The peak amplitude plot of plate 1 shows no normal mode in the immediate vicinity of that frequency (Fig 27b/2).

Observing the bending waveform of plate 1, we find that the centre part of the record exhibits a representation of a normal mode whereas the rest of the record, right and left of the centre indicates off-mode motion. The disturbing force is located in an ideal position to excite mode 8x3. The gradient of the plot of peak-amplitude suggests that off-resonant components of that mode can be set into motion. This tendency of the force is encountered by a strong reaction of the coupled mode because the coupling transmits excitation to a point on plate 2 where a node occurs, thus facing a maximum impedance which acts on plate 1 as a damper.
This case is the opposite of the motion feed-back in the first experiment.
Response of mode 8x3, being excited 38 Hz above its modal frequency, is low. A combined effect of the 3 factors, location of force in frequency and space, and the high impedance of the coupled element results in the aforementioned waveform.

Comparison of the experimental data offered in Fig's 27 demonstrates the significant difference in the dynamical behaviour of two systems consisting of the same subsystems coupled by alternative types of structural joints. From response distribution view-point, elastically coupled system is one entity, which means that a normal mode must be present in each subsystem, while in point coupling the subsystems are separate entities, each having its characteristics, changed slightly only in the presence of a coupling.

The latter system is a closer analogy to our two-degree-of-freedom model. Hence under specified conditions, such a system can act in a similar manner to a dynamic vibration absorber, which is an important practical implication.

For energy consideration it is possible to set the energy balance equation on the lines of eq'n 1.3 using eq'ns 1.2 and 4.27, where ΔT_1 becomes the unknown quantity, being applied to both coupling situations. Then the type of coupling can be evaluated in terms of the ratio of modal energy dissipation in each of the coupled elements, or in terms of the ratio of energy input from the source to energy dissipated in a mode of the driven element.

Although a complete scheme which can be applied generally to every coupling situation has not been worked out here, it is shown that in either method suggested above, the drawbacks associated with seeking interpretation of modal parameters in practical elastic systems can be eliminated using energy or motion criteria.

IV. Experimental rig usefulness.

The main role for which the rig was primarily designed, namely to detect response distribution in plate systems, and to represent the identity of normal modes by their bending waveforms was demonstrated throughout the thesis, section 3 in particular.
The incentive for a further discussion stems from our need to sum up the variety of applications, and the desire to suggest in brief a further development of the rig as a tool for industrial applications.

A simple application of the rig, not introduced before is its use to determine resonant frequencies. In section 2 it was argued that since vibrational modes present in the elements contain components of extraneous modes it is necessary to speak in terms of a resonant (rather than natural) state and frequency, being defined as that at which maximum response per unit disturbing force occurs. Fig 19 demonstrates how it is possible to use the correspondence between experimental and predicted bending waveforms to corroborate the value of modal frequency determined from a peak-amplitude plot. Although the degree of agreement between the theoretical and experimental waveforms is not as good as previously it is nevertheless clear that the waveform shape at 431.7 Hz shows better correspondence than those at the other, higher or lower frequencies.

The great advantage of using the non-contacting transducer to detect response, and hence energy, distribution can be demonstrated by a simple example. Supposing that the response is detected using an accelerometer, essentially

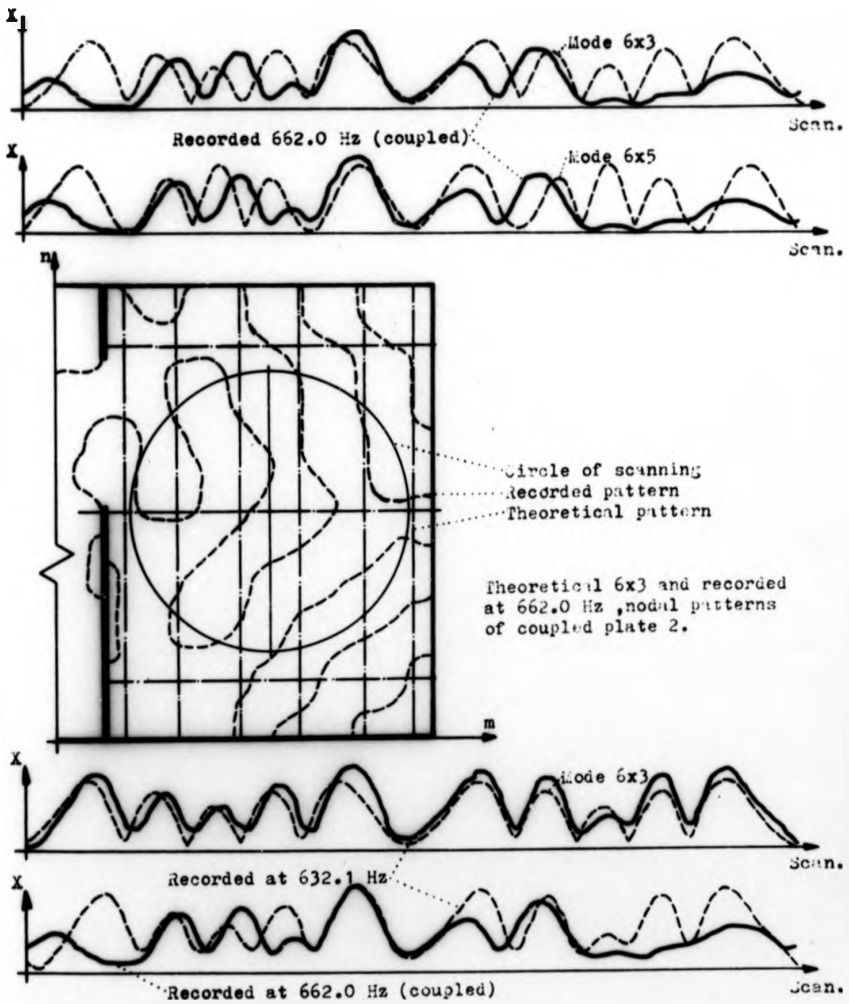

Fig 28. Identification of the vibrational mode of the coupled plates by comparing records of bending waveforms of the coupled and separate plates.

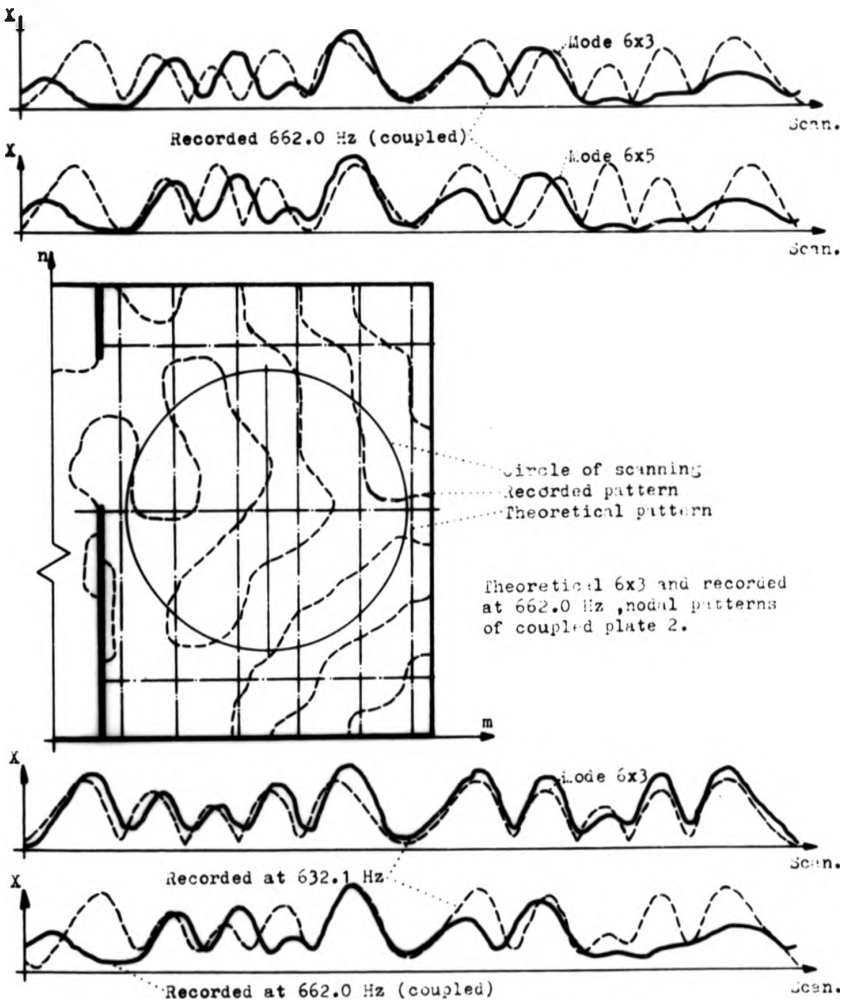

Fig 28. **Identification of the vibrational mode of the coupled plates by comparing records of bending waveforms of the coupled and separate plates.**

a contact sensing device. If it is located at a node, it is less likely to interfere with the motion of the mode but would detect rigid body motion only. Should it be moved away then it will load the plate as a concentrated mass at the rate of its mass times the acceleration. The loading effect depends on the accelerometer mass as compared to the mass distribution of the element. Taking typical values from our records, mode 3 say, an accelerometer of 10 grams weight located at a point accelerating at 3g exerts a force of .003 kg as compared to a disturbing force of .016 kg. Assuming that the exciting force will be increased to drive the loaded system, still 16% of the force will be located at that point, introducing a significant error into the estimate of energy distribution.
In fact such a resistance is most likely to force a node as was shown in (17), thus distorting the mode shape.

The application of bending waveforms for mode identification has been discussed in the thesis in great detail. The technique of recording bending waveforms along a scanning circle may be utilized for an additional application.

It is normally accepted that a resonant frequency excitation is associated with normal mode vibration. This may not be true in the case of systems coupled at one or a few points in a manner which does not allow elastic interaction. Then it is possible that resonant conditions being indicated, are related to the presence of a normal mode in one element only, while the coupled element vibrates in off-mode motion. Such a possibility requires to establish a criteria or a procedure whereby it can be distinguished between off-mode motion and low response mode.

Since mode shapes are sometimes distorted, comparing

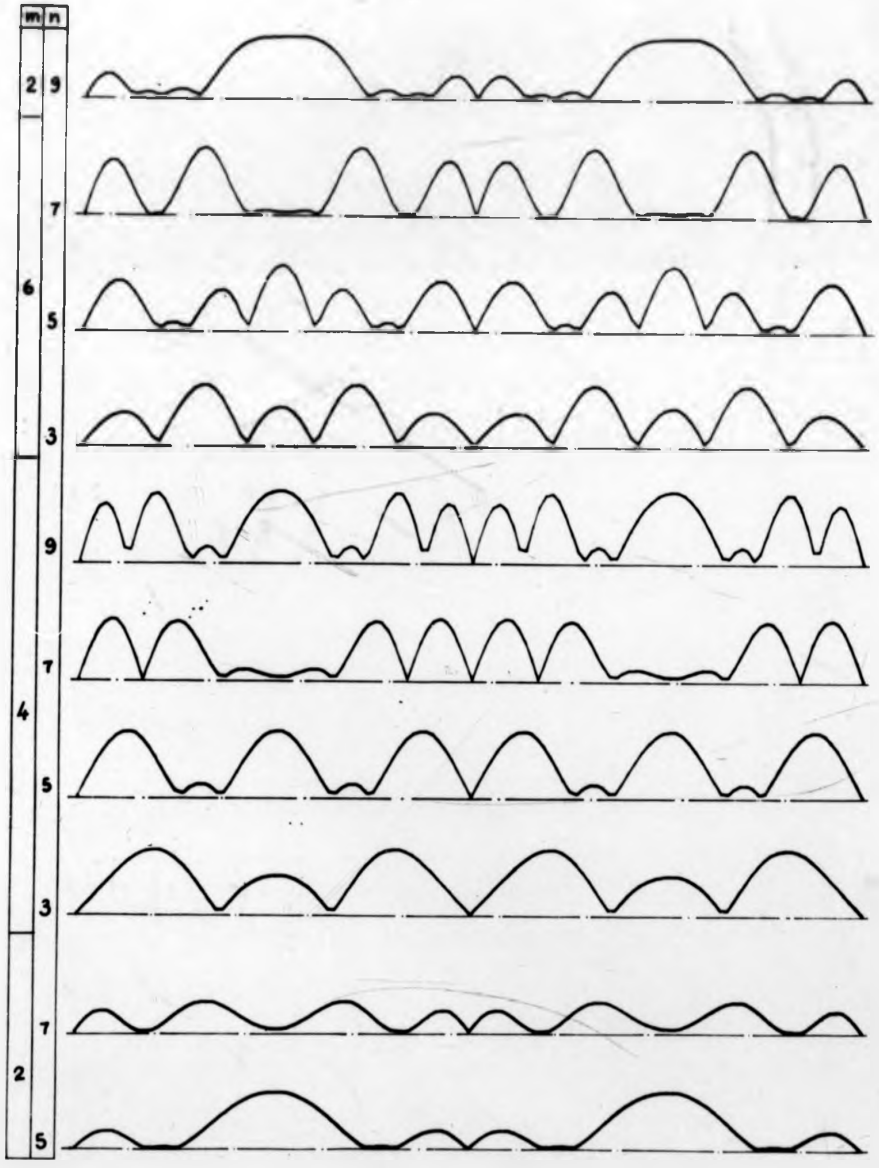

Fig 29. A page from the catalogue of theoretically constructed rectified bending waveforms along a circle o. scanning r=2c cm in plate a. The wave orm is relate to the appropriate mode through the nodal pattern expressed in terms o m and n nodal lines.

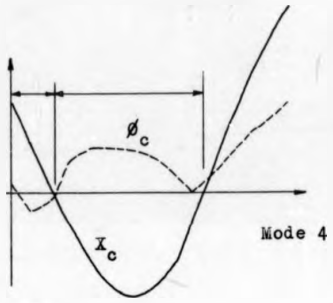

a) Records of slope ϕ_c and amplitude X_c response at the coupling.

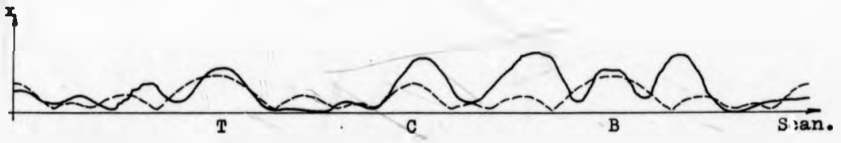

b) Recorded (Full line) and theoretical bending waveforms of plate 1.

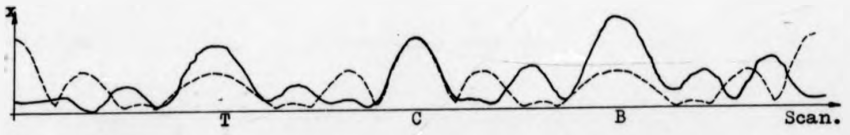

c) Recorded (Full line) and theoretical bending waveform of plate 2.

Fig 30. Data on the coupled modes of test 4 ,excited at 353.7 Hz , where the theoretical waveforms are of modes 2x6 nodal lines.

recorded and theoretical bending waveforms is unsafe. It has been experienced, in the course of the work, that bending waveforms recorded from an element vibrating in any normal mode were absolutely repeatable, whereas those recorded successively at an off-resonant frequency were not similar. So pronounced is the effect that the RHS record of Fig 27b/2 which displays a bending waveform whose centre part only, represents a normal mode, the remaining parts, left and right, were not repeatable.

Now a procedure is suggested whereby immediate successive records of bending waveforms are compared. If the records do not precisely overlap, off-mode motion has been detected.

An interesting problem of identifying a distorted mode shape is reported in Fig 28, where the techniques normally engaged would not reveal the identification of the mode. In searching for the identity through comparing the recorded to the theoretically constructed waveform of the catalogue (Fig 29), both modes represented by the nodal patterns of 6x3 and 6x5 seemed equally likely to be the modes of pure motion. A 'map' of the actual nodal pattern offered no preference of either of the 2 alternatives. The dilemma is shown by the two sets of waveforms at the top of Fig 28.

One may assume quite safely that the likelihood of a presence of a coupling to cause mode distortion is proportional to the stiffness of the coupling and in elastic coupling this may be propotional to the coupling length. Consequently an uncoupled element is expected to display the least distorted mode, as indeed experienced in the project. Relying on that assumption the waveform recorded at 662.0 Hz was compared to the records of the separate

element, showing agreement with that recorded at 632.1 Hz, which is in a better condition. Finally the record of 632.1 Hz was identified by aid of the catalogue as representing a mode of 6x3 nodal pattern.

This case demonstrates a clear advantage of using the experimental rig to identify normal modes of vibration, in particular where identification of the nodal pattern is unnecessary or not possible. This may be the case in an attempt to investigate modes in different conditions, or using specimen where the nodal pattern can not be expressed in terms of simple geometric shapes such as straight lines and circles.

The high versatility of the experimental rig can be further developed to map the nodal pattern and dynamic strain of flat elements. In section 3 we developed a mechanism correlating the angle of the rotating arm carrying the non-contacting transducer to the motion of the carriage of the x-y plotter (Fig 4b). So, a distance along the x axis of the plotter becomes proportional to a position of the transducer on a pre-determined radius of scanning.

If the y axis of the plotter is correlated to the scanning arm in such a manner that y is proportional to the radius of scanning, then a position of the pen on the paper corresponds to a position of the transducer over an element. Then a device may be designed which triggers the pen to mark a dot whenever the transducer passes through a nodal line. This device tracks the phase changes which occur on crossing a nodal line, or alternatively points of minimum amplitude can serve as second best.
As radii of scanning are changed the area of an element is covered as may be desirable, the technique yields an automatic

map of the nodal pattern.

Using the existing design of the rig, with the transducer holder modified to slide along the scanning arm, so that the x axis of the plotter is proportional to the position of the transducer along the arm, being fixed in a pre-determined angle, it is possible to record the bending waveform, (i.e. the deflection) along any straight line over an element as may be required.

The kind of modification just mentioned is of a particular interest from another aspect as well.

In order to eliminate the dependence of assessment of response distribution in an element on the condition of mode shape it would be helpful if the scanning rig was made to increase considerably the amount of sampling of the response distribution.
This is possible through fitting a mechanism which moves the transducer along the scanning arm relative to its rotation so that the radius of scanning will vary automatically with rotation, resulting in a spiral motion of the transducer.
In this way average response distribution can be obtained independent of mode identification and hence extended for irregular body geometry where the nodal pattern can not be described in terms of recognized configuration.

A third improvement of the rig is concerned with detecting the response of curved plates and shells.
The condition attached to using the measuring system of our apparatus is that the mean gap between the transducer and the specimen must be within specified limits which vary from one probe to another, of the available set. This requires in term that the flatness falls within those limits, which in the event prevent us from using a specimen from

which residual stresses were not relieved, although it was of particular interest, because it was not sufficiently flat.

This problem can be avoided by modifying the construction of the transducer holder unit to make the transducer 'float' in the sense that the distance between the face of the probe and the specimen can be varied. Then the mean gap can be kept constant automatically, using the d.c. signal which is proportional to the mean distance between the specimen and the transducer in a control loop.

The radius of curvature of a specimen which can be monitored depends on the design of the 'floating' arrangement.

But since the face of the probe must be parallel to the detected surface, a minimum radius of curvature of a specimen is determined by the finite size of the transducer selected.

We have explored in brief several proposed courses of further developing the experimental apparatus to improve its versatility as a research aid and offer some industrial applications. The discussion shows that the potentialities inherent in the rig extend beyond the scope of the project and advocate studying them in greater detail.

V. References.

1. Ikuo Mizutani.
   Reduction of Vertical Vibration at a Point on Ship Stern.
   J. of Japan Shipbuild. & Marine Eng. p.23 1967

2. R.D. Adams.
   Effect of a Hidamet Insert on the Resonant Vibration of
   a Flat, Square plate in Air and in Water.
   The Inst. of Sound and Vib. Research, University of Southampton.
   T.R. No. 10 1968

3.
   Mechanical Vibration Transmission in the 'Mariner 69' Spacecraft.
   California Inst. of Tech. Interim Report AX£-368523 1967

4. M. Heckl
   Measurements of Absorption Coefficients on Plates.
   J. Acoust. Soc. Am Vol. 34/6 p.803 1962

5. R.H. Lyon, E. Eichler.
   Random Vibration of Connected Structures.
   J. Acoust. Soc. Am. Vol. 36/7 p.1344 1964

6. T.D. Scharton.
   Random Vibration of Coupled Oscillators and Coupled Structures.
   M.I.T. Doctoral Thesis 1965

7. T.D. Scharton, R.H. Lyon.
   Power Flow and Energy Sharing in Random Vibration.
   J. Acoust. Soc. Am. Vol. 43/6 p.1332 1968

8. E.E. Ungar, T.D. Scharton
   Analysis of Vibration Distribution in Complex Structures.
   Proc. 36th Symposium on Shock and Vibration. California. 1966

9. D.E. Newland
   Power Flow Between a Class of Coupled Oscillators.
   J. Acoust. Soc. Am. Vol. 43/3 p.553. 1968

10. A. Rosselli
The Transmission of Random Vibration Between Connected Plates.
Imperial College of Science, London. D.I.C. Thesis 1965

11. G.B. Warburton.
The Vibration of Rectangular Plates.
Proc. Inst. Mech. Eng. Vol. 168/12 p. 371 1954

12. C.D. Kennedy, C.D.P. Pancu.
Use of Vectors in Vibration Measurement and analysis.
J. Aero. Sciences Vol. 14/11 p.603 1947

13. J.W. Pendered, R.E.D. Bishop.
3 Papers on Resonance Testing.
J. Mech. Eng. Science Vol. 5/4 pp.343-385 1963

14. S. Timoshenko.
Vibration Problems in Engineering.
Van Nostrand 1955

15. R. Plunkett.
Experimental Measurement of Mechanical Impedance or Mobilit
J. App. Mechanics ASME Transaction Vol.21/3 p.250 1954

16. J.W. Dunn.
Measurement Techniques for the Analysis of Forced Structural Vibration.
Proc. Inst. Mech. Eng. Vol. 182/38 p.47 1968

17. U. Shapiro.
Transmission of Noise Between Connected Structures.
Imperial College of Science, London. D.I.C. Thesis 1958

18. M.C. Junger.
Structure-Borne Noise. p.368
Proc. of the Symposium on Naval Structural Mechanics.
Stanford University. 1958

VI. List of symbols.

X	Transverse amplitude point response.
X_p	Theoretical point amplitude response of a plate.
α	Receptance.
$\emptyset$	Magnitude or notation of ratary coupling point response.
μ	Mass ratio.
Δf	Shift of modal frequency.
k	Stiffness factor.
l,w	Length and width of a plate.
m,n	Number of nodal lines counted in x and y directions respectively.
q	The generalised coordinate.
V	Volts.
o	Subscript denoting value measured at output.
x	Subscript denoting transverse motion.
ω	Circular frequency.

A	Area under bending waveform.
a,b	Subscript denoting the separate plates 1 and 2 respectively.
c	Subscript denoting coupling.
C	Damping coefficient.
F	Amplitude of disturbing force.
f	Circular frequency.
h,l	Higher and lower frequencies corresponding to half power point.
in	Subscript denoting point of forcing.
m,t	Subscript denoting measured and theoretical values.
n	Subscript denoting resonant.
M	Mass.
N	Normalising factor.
Q	Magnification factor.
r	Radius, or subscript denoting radius of scanning.
(r,θ)	Notation of a bending waveform.
S_d	Factor of error due to drift.
S_{fr}	Factor of error due to flanking energy.
S_m	Factor of difference between measured and calculated response ratio.
S_r	Factor of error due to poor agreement between bending waveforms.
T	Energy stored in a vibrating element.
ΔT	Energy dissipated in a vibrating element.

List of illustrations.

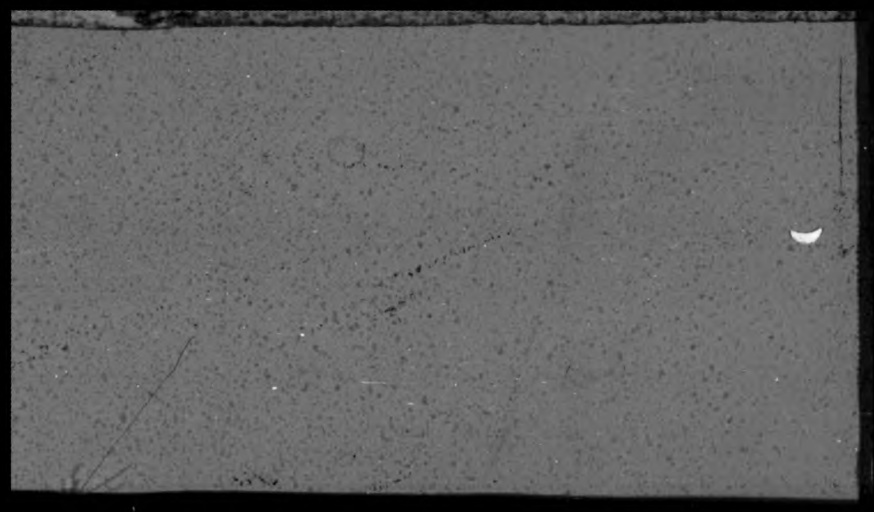

245 82

END